MIMO Wireless Communications with Limited Feedback

A DISSERTATION
SUBMITTED TO THE FACULTY OF THE GRADUATE SCHOOL
OF THE UNIVERSITY OF MINNESOTA
BY

Niranjay Ravindran

IN PARTIAL FULFILLMENT OF THE REQUIREMENTS
FOR THE DEGREE OF
Doctor of Philosophy

Professor Nihar Jindal, Advisor

September, 2012

Acknowledgements

I am grateful to my advisor, Professor Nihar Jindal, for his unwavering support and for showing endless patience during my time as a graduate student. I would also like to thank and acknowledge my research collaborators Joseph Blomer, Giuseppe Caire, Howard Huang, Mari Kobayashi and Peng Wu, with whom many of the results presented in this dissertation were jointly developed.

Professor Georgios Giannakis and Professor Tom Luo gave me an introduction to the field that I enjoyed very much, I am thankful for those crucial semesters of education. I am grateful for the efforts of Professor Maury Bramson and am glad to have developed an appreciation for probability *theory*. The support of Professor Anand Gopinath and Professor William Robbins during my final years as a student was invaluable to me, I would like to thank them for giving me the opportunity to explore my interests in engineering education. Finally, I would like to thank Debashish Burman, Balasubramanian Gopalakrishnan, Juyul Lee and Omar Mehanna, each for uniquely enriching my experience as a graduate student.

Abstract

In this dissertation, we investigate the effects of having imperfect channel state information due to limited training and feedback resources in multi-user systems with multiple antennas. We find that while the achievable rate is highly sensitive to the quality of channel training and feedback, the rate gap relative to the rate achievable with perfect channel information can be uniformly bounded for all values of signal-to-noise ratio, with proper design of the feedback link to acquire accurate channel information, that is, the multiplexing gain can be preserved. Further, when a large number of users are present in a system, we find the strong requirement for accurate channel information remains, contrary to many transmission strategies that are commonly proposed for this regime. We conclude that given a limited feedback budget, it is desirable to first use resources to acquire highly accurate channel information, and only then allocate resources to exploit multi-user diversity. We also obtain results characterizing the statistics of random subspace quantization, which we use to compute the reduction in feedback overhead possible when this form of quantization is used. Finally, we consider open-loop multi-hop ad hoc networks with multiple antennas and opportunistic routing, and investigate using multiple antennas to optimize the spatial reuse, per-hop length and per-hop rate to maximize end-to-end performance.

Contents

List of Tables

List of Figures

Chapter 1

Introduction

Multi-user multiple-input multiple-output (MIMO) communication is very powerful and has recently been the subject of intense research. In particular, a transmitter equipped with N_t antennas can serve up to N_t receivers (or users) simultaneously using the same frequency band. Thus, the presence of multiple antennas potentially allows for an additional dimension over which the rate of communication can be increased, in addition to frequency and time. The above result holds even if each receiver has only a single antenna, making it an attractive method to increase the capacity of a communication channel (either to support higher data rate per user, or equivalently, to serve more users at the same time, potentially incurring only the cost of installing an additional antenna at the transmitter). Such a model is relevant in many applications, such as the cellular downlink from a base station (BS) to user terminals (UTs) or cellular phones.

However, knowledge of the wireless channel from the BS to each UT is required at the BS in order to fully exploit the gains offered by MIMO. For example, when no channel state information (CSI) is available at the BS, the multi-user MIMO benefit is completely lost and point-to-point MIMO becomes optimal, that is, only a single user can be served for a given time and frequency band. This follows from the fact that serving multiple users simultaneously results in each user receiving data that may be intended for other users, which interferes with the data it is supposed to receive. However, if the BS has CSI, various methods exist that allow the BS to account for this interference, and this effectively creates N_t independent channels, one to each user, which in turn allows for N_t times the communication data rate that would be possible

when only a single user is served (assuming a high signal-to-noise ratio). Thus, the importance of acquiring CSI is matter of a factor of N_t, in terms of the communication rate.

We refer to channel state information at the transmitter, which in our framework is the BS, as CSIT. Similarly, we refer to channel state information at the receiver, which in our framework is the user terminal, as CSIR. Under the assumption of perfect CSIT and CSIR, a combination of single-user Gaussian codes, linear beamforming and "Dirty-Paper Coding" (DPC) [1] is known to achieve the capacity of the MIMO downlink channel [2, 3, 4, 5, 6], and when the number of base station antennas is larger than the number of antennas at each terminal, this capacity of the MIMO downlink channel is significantly larger than the rates achievable with point-to-point (single-user) MIMO techniques [2, 7, 8].

Unfortunately, acquiring accurate CSI is a challenging and resource-consuming task in time-varying wireless systems, since the channel varies with time and will need to be continuously tracked. Information obtained about the channel is inevitably imperfect. It is therefore critical to understand what communication rates are achievable under realistic CSI assumptions, and in particular, to understand the sensitivity of achievable rates to imperfections in CSI. In systems without channel reciprocity (such as frequency-division duplexed systems), the BS obtains CSI only through channel feedback from users, that is, only the user terminal is in a position to observe the wireless channel from the BS to its receiving antenna, and hence would need to observe this information and feed it back to the BS. Since the channel is time-varying, this process of observation of the channel by each user (referred to as "training") and feedback to the BS would need to be done periodically, and the resources spent on observation and feedback essentially amounts to overhead (that is, it does not contribute to the actual useful data rate). Hence, the resources available for this task are typically limited. The main goals of this work are:

- To model various sources of error in acquiring CSI at the BS for MIMO downlink systems
- To analyze the effect of these imperfections on the achievable communication rate

- To use these results and design practical systems that maximize the communication rate

It has been shown that *linear beamforming*, where the BS transmits linear combinations of the data to each UT, performs quite close to capacity when combined with user selection [9, 10], again under the simplifying assumption of perfect CSI. This is a relatively low-complexity strategy of relevance in practical scenarios, and for most of the chapters that follow, we focus on Zero-Forcing (ZF) linear beamforming, and compute achievable rates under the effect of imperfect CSI.

We divide our analysis into systems that have limited number of users (Chapter 2), of the order of the number of BS antennas N_t, and systems where a larger number of users are potentially available (Chapter 3). The former model applies to systems where a small number of users have been selected *a priori* based on, for example, scheduling priorities, and as such, the advantage of multi-user diversity is not exploited. In the latter case, we consider the situation when when there are enough users available in the system and multi-user diversity can indeed be exploited, but total feedback and training resources are limited.

For each case, we derive bounds on the rate achievable, and derive sufficient conditions on the training and feedback such that the system achieves the same *multiplexing gain* as the optimal capacity-achieving scheme under perfect CSI assumptions. The multiplexing gain is defined as the ratio of the achievable rate to the system signal-to-noise ratio (SNR), as the SNR goes to infinity, also commonly referred to as the "pre-log factor", or "degrees of freedom", so achieving full multiplexing gain amounts to mainting a constant rate gap relative to the rate achievable with perfect CSI. For a multi-user MIMO system with N_t antennas at the BS, the multiplexing gain is ideally N_t with perfect CSI at the BS, and 1 when there is no CSI available at the BS. Our general conclusion is that the full multiplexing gain of N_t is, in fact, achievable with simple pilot-based channel estimation and feedback schemes that consume a relatively small fraction of the system capacity, that is, we show that a well-designed training and feedback system can achieve maximum multiplexing gain despite the imperfections in CSI.

For the case when a large number of users are available in each cell, the BS has the opportunity to decide which users to serve for a given time/frequency, selecting

up to N_t users to serve at once from among a greater user pool. This allows the BS to only serve users with "good" wireless channels at a given moment, and due to the time-varying nature of wireless channels, different users will be served at different times. This exploitation of the randomness of wireless channels of different users to improve the total system data rate is referred to as *multi-user diversity*. We extend our analysis to include the possibility of exploiting multi-user diversity, and come to the conclusion that acquiring accurate CSI is far more important than exploiting multi-user diversity, when system feedback resources are limited.

We also extend our results to the case when users have access to multiple antennas (that is, multiple antennas at the UT) in Chapter 4, and investigate the advantages of exploiting this fact, comparing the achievable rate with limited feedback resources to various other feedback and transmission strategies. We show that exploiting multiple receive antennas can significantly reduce the total feedback overhead in a system, while achieving the same communication rate (or equivalently, a higher communication rate for the same feedback overhead).

Finally, we consider MIMO ad hoc networks where a transmitter and receiver may be separated by large distances, and data has to be "routed" through intermediate relays before reaching the receiver. Transmissions in such a network are uncoordinated, and the channels evolve rapidly making CSI feedback very difficult. We analyze the effect of exploiting multiple antennas in these situations where the transmitter does not (and cannot) have direct access to CSI, and show that the product of the distance a data packet can travel (progress), the data rate and the density of transmitters, abbreviated as PRD (progress-rate-density), can be increased linearly with the number of antennas.

Chapter 2

MIMO Limited Feedback with Limited Number of Users Per Cell

In this chapter, we consider the case when there are K user terminals (or UTs) acting as receivers, and a single base station (BS) with N_t antennas acting as the transmitter. The results presented in this chapter appear in [11, 12, 13]. We will use the terms user terminal and user interchangeably in the sections to follow. This models a typical cellular downlink scenario, where there are a number of mobile terminals per cell in a cellular network connecting to a single BS transmitter. We initially assume that each UT has a single antenna each and that there are $K = N_t$ UTs in the cell, but later relax these assumptions in Chapters 3 and 4.

We consider the errors introduced in CSI acquisition, first at the user terminals due to errors in observing the downlink channel (referred to as the training phase), then due to errors in feed back of this observed CSI from the UTs to the BS, and finally the errors introduced during a second round of downlink training, where the BS informs each UT of the signal and interference coefficients they can expect. We characterize the rates achievable after the training and feedback process in terms of the resources (i.e., channel symbols) used for training and feedback, and the channel feedback technique. In contrast to prior work in this area [14, 15, 16, 17, 18], this work considers and quantifies

the combined effect of downlink training as well as limited feedback.

We particularize our results to cases when unquantized (analog) and quantized (digital) channel state feedback schemes are used, and show that digital feedback can be superior in many cases. Also, we show that by proper design of the digital feedback link, errors in the feedback have a minor effect even if simple uncoded modulation is used on the feedback channel, which contrasts the conventional wisdom that errors in the feedback link are catastrophic.

2.1 Prior Work on Limited Feedback with Limited Number of Users

Several previous and concurrent works have treated training and channel feedback for point-to-pont (single-user) MIMO systems (see for example [19, 20, 21, 22, 23, 24, 25]) and for MIMO broadcast channels (see, for example, [14, 26, 27, 15, 16, 28, 29]). This work, however, considers the non-negligable effect of the UTs having imperfect CSIR obtained via downlink training, which degrades the quality of the information fed back to the BS, and hence, the CSIT. Further, we explicitly consider transmission from each UT to the BS over a noisy feedback channel, which allows us to meaningfully measure the uplink resources dedicated to channel feedback and also allows for a comparison between analog (unquantized) and digital (quantized) feedback.

Prior work such as [30][31][32] have used a worst-case uncorrelated noise argument to show that imperfect CSI, at worst, leads to the introduction of additional Gaussian noise and thus the achievable rate is lower bounded by the mutual information with ideal channel state information and reduced SNR. In our case, however, this same argument yields a largely uncomputable quantity and a further step must be taken that yields a tractable lower bound in terms of the rate difference between the ideal and actual cases, rather than in terms of a signal-to-noise ratio penalty.

Perhaps the most striking fact about this second aspect is that the full multiplexing gain of the ideal MIMO broadcast channel can be achieved with simple pilot-based channel estimation and feedback schemes that consume a relatively small fraction of the system capacity. Indeed, a fundamental property of the MIMO broadcast channel is that the quality of the CSIT must increase with signal-to-noise ratio (SNR), regardless

of what coding strategy is used, in order for the full multiplexing gain to be achievable [33, 34]. Under the reasonable assumption that the uplink channel quality is in some sense proportional to the downlink channel, our work shows that this requirement can be met using a *fixed* number of downlink and uplink channel symbols (i.e., system resources used for training and feedback need not increase with SNR).

2.2 Training and Feedback

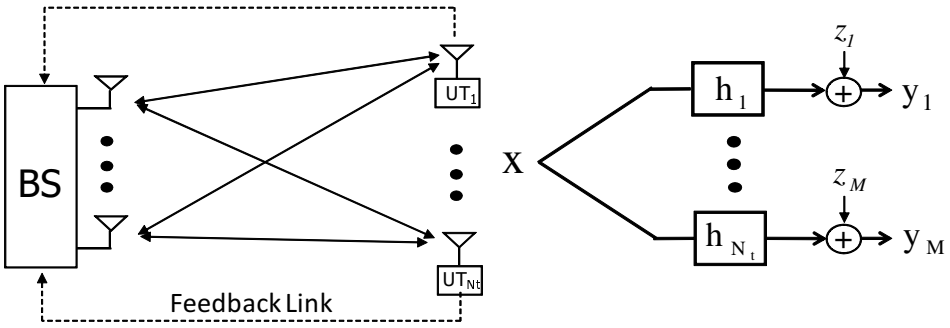

Figure 2.1: Feedback of channel information in a MIMO downlink system

We consider a multi-input multi-output (MIMO) Gaussian broadcast channel modeling the downlink of a system where a Base Station (BS) has N_t antennas and K User Terminals (UTs) have one antenna each, as depicated in Figure 2.1. A channel "use" of such a channel is described by

$$y_k = \mathbf{h}_k^{\mathsf{H}}\mathbf{x} + z_k, \quad k = 1, \ldots, K \tag{2.1}$$

where y_k is the complex number representing the signal received at UT k, $z_k \sim \mathcal{CN}(0, N_0)$ (the real and imaginary parts of $\mathbf{z}_k$ are independent and Gaussian distributed with mean 0 and variance N_0) is the corresponding Additive White Gaussian Noise (AWGN) added as the wireless signal propagates through the channel, $\mathbf{h}_k \in \mathbb{C}^{N_t}$ is the vector of complex channel coefficients from the k-th UT antenna to the BS antenna array (the superscript H refers to the Hermitian, or conjugate transpose) and $\mathbf{x}$ is the vector of complex symbols transmitted by the BS. The $j-^{\text{th}}$ element of $\mathbf{h}_k$ represents the multiplicative factor

affecting the signal transmitted from the BS to the $j-^{\text{th}}$ UT. The signal transmitted by the BS is subject to the average power constraint $\mathbb{E}\left[|\mathbf{x}|^2\right] \leq P$. Since the transmitted power is P and the AWGN variance is N_0, we refer to the quantity P/N_0 as the signal-to-noise ratio, or SNR. In some cases, we consider different situations which have different signal-to-noise ratios, often a multiple of SNR. We reserve the use of SNR to represent the quantity P/N_0, and will explicitly refer to other signal-to-noise ratios using corresponding formulas.

The channel *state*, given by the collection of all channel vectors $\mathbf{H} = [\mathbf{h}_1, \ldots, \mathbf{h}_K] \in \mathbb{C}^{N_t \times K}$, varies in time according to a block-fading model [35], where $\mathbf{H}$ is constant over each *frame* of length T channel uses, and evolves from frame to frame according to an ergodic, stationary, spatially white, jointly Gaussian process, where the entries of $\mathbf{H}$ are Gaussian i.i.d. with elements $\sim \mathcal{CN}(0,1)$. The above model represents Rayleigh "block" Fading, which applies when the signal transmitted by the BS is scattered by a large number of objects distributed uniformly around each UT, and there is no direct Line-of-Sight (LOS) path from the BS to UT (we examine LOS channels specifically in Section 2.6.2). Knowledge of $\mathbf{H}$ at the BS is referred to as the CSIT. Since $\mathbf{H}$ remains constant over a "block" of time, $\mathbf{h}_k$ can be "observed" by each UT and then fed back to the BS at the start of each time block. The BS can then use this information to transmit data to the UTs for the rest of the duration of the time block.

It should be noticed that the rate lower bounds given in the following sections should be multiplied by the factor $(1 - \Delta/T)$, where Δ denotes the total number of channel uses for each frame that has been dedicated to training and feedback. This factor is neglected in the results that follow since it is common to all rate bounds and since $\Delta \ll T$ in a typical slowly-fading system scenario. However, in the general case where Δ is not necessarily small with respect to T, the amount of training and feedback should be optimized by taking this multiplicative factor into account. Based on the bounds presented here, this system optimization is carried out in the follow-up works [36, 37, 38].

Because of simplicity and robustness to non-perfect CSIT, simple *linear precoding* or *linear beamforming* schemes with standard Gaussian coding have been extensively considered. Here, the transmit signal is formed as $\mathbf{x} = \mathbf{V}\mathbf{u}$, where $\mathbf{u} \in \mathbb{C}^K$ is the vector consisting the K data symbols that is to be transmitted by the BS to each of the K UTs. Thus the signal transmitted $\mathbf{x}$ is actually a linear transformation of the actual

data vector $\mathbf{u}$, where $\mathbf{V} \in \mathbb{C}^{N_t \times K}$ is referred to as the *linear beamforming* matrix. $\mathbf{u}$ is assumed to contain the symbols from K independently generated Gaussian codewords. In particular, for $K \leq N_t$, the Zero-Forcing (ZF) beamforming technique chooses the k-th column $\mathbf{v}_k$ of $\mathbf{V}$ to be a unit vector orthogonal to the subspace $\mathcal{S}_k = \text{span}\{\mathbf{h}_j : j \neq k\}$.

Our focus is on the achievable *ergodic* rates under ZF linear beamforming. In this case, the achievable rate-sum is given by

$$\max_{\sum_k \mathbb{E}[\mathcal{P}_k(\mathbf{H})] \leq P} \sum_{k=1}^{K} \mathbb{E}\left[\log_2\left(1 + \frac{|\mathbf{h}_k^{\mathsf{H}}\mathbf{v}_k|^2 \mathcal{P}_k(\mathbf{H})}{N_0}\right)\right]. \tag{2.2}$$

The choice of values $\mathcal{P}_k(\mathbf{H})$ satisfying $\sum_k \mathbb{E}[\mathcal{P}_k(\mathbf{H})] \leq P$ represents the power allocated to each of the K data streams, where P is the total transmit power allowed to the BS. This allocation is obtained by waterfilling over the set of channel gains $\{|\mathbf{h}_k\mathbf{v}_k|^2 : k = 1, \ldots, K\}$ for maximum ergodic rate. Performance can further be improved by using a *user scheduling* algorithm to select in each frame an *active* user subset not larger than N_t (if $K > N_t$, such selection has to be performed if ZF is used). Schemes for user scheduling have been extensively discussed, for example in [9, 29, 10, 39].

Our focus for Chapter 2, is on the case $K = N_t$ with uniform power allocation across users and frames: $\mathcal{P}_k(\mathbf{H}) = \frac{P}{N_t}$ (each UT gets an equal slice of the transmit power), and without user selection, in which case the per-user ergodic rate is

$$R_k^{\text{ZF}}(P) = \mathbb{E}\left[\log_2\left(1 + \frac{|\mathbf{h}_k^{\mathsf{H}}\mathbf{v}_k|^2 P}{N_0 M}\right)\right]. \tag{2.3}$$

The above restriction is dictated by a few reasons. Note that the maximum multiplexing gain is N_t for all $K \geq N_t$, that is, even though we might have more than N_t users, the maximum multiplicative factor we can have as $\mathsf{SNR} \to \infty$ for the rate is N_t, since we have only N_t antennas available at the BS and can hence effectively transmit only N_t independent data streams at once. Therefore, the case $K = N_t$ suffices to capture the fundamental aspects of the problem (particularly at high SNR). We consider $K > N_t$ in Chapter 3 however, and investigate the effect of $K > N_t$ separately to show that the dependence on CSI quality is roughly the same even when user selection with $K > N_t$ is performed.

Because $\mathbf{h}_k$ is spatially white and $\mathbf{v}_k$ is selected independent of $\mathbf{h}_k$ (by the ZF procedure), it follows that $\mathbf{h}_k^{\mathsf{H}}\mathbf{v}_k$ is $\sim \mathcal{CN}(0, 1)$. As a result, R_k^{ZF} is the ergodic capacity

of a point-to-point channel in Rayleigh fading with average SNR equal to $\frac{P}{N_0 N_t}$, and thus can be written in closed form as [40]

$$R_k^{\mathrm{ZF}} = \exp\left(\frac{N_t}{\mathsf{SNR}}\right) \mathrm{E}_i\left(1, \frac{N_t}{\mathsf{SNR}}\right) \tag{2.4}$$

where $\mathrm{E_i}(n,x) = \int_1^\infty \frac{e^{-xt}}{t^n} dt,\ x > 0$ [41]. Note that R_k^{ZG} does not depend on k, that is, all users have the same rate since we have assumed that all users are statistically identical. Hence, we will drop the suffix k and use R^{ZG} to denote this rate. In the remainder of this chapter, R^{ZF} serves as a benchmark against which we compare the achievable rates with imperfect CSI, and we will often refer to the "rate gap", that is, the extent to which the achievable rate is less than the benchmark rate R^{ZG}.

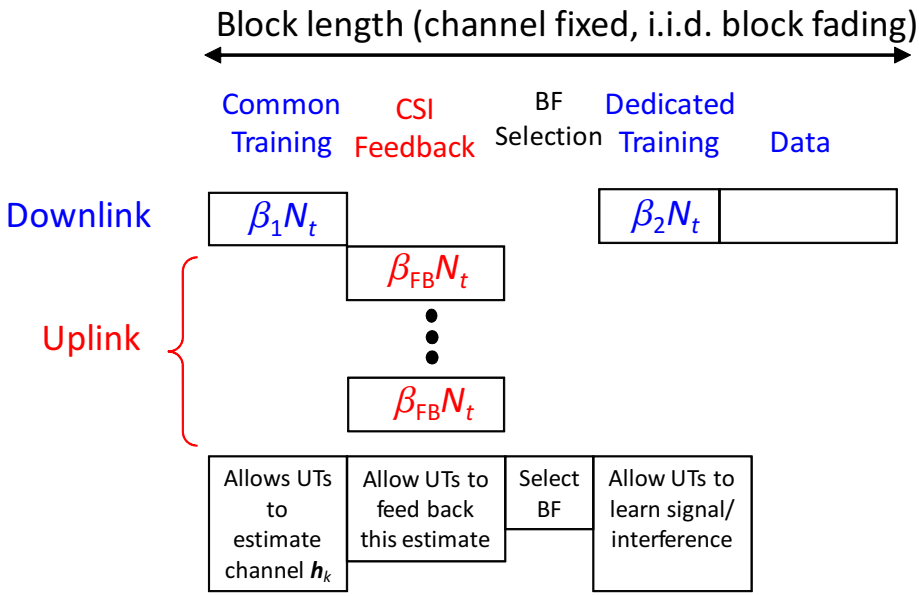

Figure 2.2: Channel estimation and feedback model

We assume that each UT estimates its channel vector from *downlink training symbols* and then feeds this information back to the BS. This scenario, referred to as "closed-loop" CSIT estimation, is relevant when the uplink and downlink channels are not identical (such as in a Frequency-Division Duplexed, or FDD, system), and the BS can only learn of the downlink channel through feedback. Our basic model is depicted in Fig. 2.2 and consists of the following phases:

1. **Common Training**: The BS transmits $\beta_1 N_t$ shared "pilots" (for a choice of $\beta_1 \geq 1$ pilot symbols per antenna) on the downlink. If β_1 is an integer, pilot symbols can be orthogonal in time, i.e., β_1 pilots are successively transmitted from each of the N_t BS antennas for a total of $\beta_1 N - t$ channel uses. More generally, it is sufficient for $\beta_1 N - t$ to be an integer and to use a unitary $N_t \times \beta_1 N_t$ spreading matrix as described in [27]; in either case the effective received signal-to-noise ratio is $\beta_1 \frac{P}{N_0}$ (or $\beta_1 \mathsf{SNR}$). Clearly, higher the value of β_1 (which corresponds to using more training pilots), higher the effective signal-to-noise ratio for the common training phase.

   Each UT k receives the signal represented by the complex vector $\mathbf{s}_k$ for the common training phase, given as follows:

$$\mathbf{s}_k = \sqrt{\beta_1 P}\ \mathbf{h}_k + \mathbf{z}_k. \tag{2.5}$$

   Here, $\mathbf{z}_k \sim \mathcal{CN}(0, N_0\mathbf{I})$ (complex white Gaussian with covariance matrix $N_0\mathbf{I}, \mathbf{I}$ being the $N_t \times N_t$ identity matrix) represents the noise in the downlink channel. The Minimum Mean-squared Error (MMSE) estimate $\widetilde{\mathbf{h}}_k$ of $\mathbf{h}_k$ given the observation $\mathbf{s}_k$ is given by [42]:

$$\widetilde{\mathbf{h}}_k = \mathbb{E}[\mathbf{h}_k \mathbf{s}_k^{\mathsf{H}}]\mathbb{E}[\mathbf{s}_k \mathbf{s}_k^{\mathsf{H}}]^{-1}\mathbf{s}_k = \frac{\sqrt{\beta_1 P}}{N_0 + \beta_1 P}\mathbf{s}_k \tag{2.6}$$

   The channel $\mathbf{h}_k$ can be written in terms of the estimate $\widetilde{\mathbf{h}}_k$ and the estimation noise, denoted by, $\mathbf{n}_k$ as:

$$\mathbf{h}_k = \widetilde{\mathbf{h}}_k + \mathbf{n}_k, \tag{2.7}$$

   where $\mathbf{n}_k$ is independent of the estimate and is Gaussian with covariance $\sigma_1^2\mathbf{I}$ where

$$\sigma_1^2 \quad = \quad \frac{1}{1 + \beta_1 \mathsf{SNR}} \tag{2.8}$$

2. **Channel State Feedback**: Each UT feeds back its channel estimate $\widetilde{\mathbf{h}}_k$ to the BS immediately after completion of the common training phase. We use $\widehat{\mathbf{H}} = [\widehat{\mathbf{h}}_1, \ldots, \widehat{\mathbf{h}}_K] \in \mathbb{C}^{N_t \times K}$ to denote the (imperfect) CSIT available at the BS corresponding to true channel state $\mathbf{H}$. The feedback is thus a mapping, possibly probabilistic, from $\widetilde{\mathbf{h}}_k$ to $\widehat{\mathbf{h}}_k$, or alternatively from $\mathbf{h}_k$ to $\widehat{\mathbf{h}}_k$ (where the second

interpretation follows from the representation (2.7)). For now we leave the feedback scheme unspecified to allow development of general achievability bounds in Section 2.3.1, and particularize to specific feedback schemes in Sections 2.3.2 and 2.3.3.

In general, we measure the *amount* of feedback by the number of feedback symbols, as opposed to the more commonly used "feedback bits". That is, we assume each UT transmits its feedback over $\beta_{\text{fb}} N_t$ feedback channel symbols. This characterization will allow us a more general framework to study feedback, which we will later particularize to the more commonly used "feedback bits" in Section 2.3.3.

3. **Beamformer Selection**: The BS selects the beamforming vectors by treating the estimated CSIT $\widehat{\mathbf{H}}$ as if it was the true channel (we refer to this approach as "naive" ZF beamforming). Following the ZF recipe, $\widehat{\mathbf{v}}_k$ is a unit vector orthogonal to the subspace $\mathcal{S}_k = \text{span}\{\widehat{\mathbf{h}}_j : j \neq k\}$. We use the notation $\widehat{\mathbf{V}} = [\widehat{\mathbf{v}}_1, \ldots, \widehat{\mathbf{v}}_K]$. Since $K = N_t$ and the BS channel estimates $\widehat{\mathbf{h}}_1, \ldots, \widehat{\mathbf{h}}_{N_t}$ are independent, the subspace $\mathcal{S}_k$ is $N_t - 1$ dimensional (with probability one) and is independent of $\widehat{\mathbf{h}}_k$. The beamforming vector $\widehat{\mathbf{v}}_k$ is chosen in the one-dimensional nullspace of $\mathcal{S}_k$; as a result $\widehat{\mathbf{v}}_k$ is statistically independent of the channel estimate $\widehat{\mathbf{h}}_k$ and of the true channel vector $\mathbf{h}_k$.

4. **Dedicated Training**: Each UT does not know the choice of the beamformers $\{\widehat{\mathbf{v}}_k\}$, as they are functions of the channel state information $\{\widehat{\mathbf{h}}_1, \ldots, \widehat{\mathbf{h}}_K\}$ at the BS, and UT k only knows $\widetilde{\mathbf{h}}_k$ or, at best, $\widehat{\mathbf{h}}_k$ (if error-free digital feedback is used). Hence, each UT is unaware of the multiplicative factors affecting both of the data symbol it is supposed to receive, as well as the multiplicative factors affecting the data symbols destined to other UTs. Hence, we would need an additional round of downlink training after the BS has computed the beamforming vectors so that each UT can "learn" these factors. Let the set of the coefficients affecting the signal received by UT k be denoted by

$$\mathcal{A}_k \triangleq \{a_{k,j} : j = 1, \ldots, N_t\}$$

where $a_{k,j} = \mathbf{h}_k^{\mathsf{H}} \widehat{\mathbf{v}}_j$ is the multiplicative factor between the k-th channel and the j-th beamforming vector, that is, for $k \neq j$, this represents the interference at

UT k due to the data transmitted to UT j (which will be zero if there are no feedback and training errors, by the ZF procedure), and for $k = j$, this represents the multiplicative factor affecting the data for UT k. The received signal at the k-th UT is given by

$$\begin{aligned} y_k = \mathbf{h}_k^{\mathsf{H}} \widehat{\mathbf{V}} \mathbf{u} + z_k &= a_{k,k} u_k + \sum_{j \neq k} a_{k,j} u_j + z_k \\ &= a_{k,k} u_k + I_k + z_k \end{aligned} \tag{2.9}$$

where the sum of the data components received at UT k, but is data for UT $j \neq k$, is refereed to as the *interference* at UT k. Hence, each UT receives not only its own data, corrupted by a multiplicative factor and AWGN, but also the interfering signals transmitted to the other UTs, each corrupted by a multiplicative factor as well (if the CSIT is perfect, under the ZF scheme, $a_{k,j}$ will be 0 for $j \neq k$). In the above expression, I_k is the total interference at UT k given by:

$$I_k = \sum_{j \neq k} a_{k,j} u_j. \tag{2.10}$$

The dedicated training is intended to allow the estimation of the coefficients in $\mathcal{A}_k$ at each UT k. This is accomplished by transmitting β_2 orthogonal training symbols along each of the beamforming vectors on the downlink, thus requiring a total of $\beta_2 N_t$ downlink channel uses. The relevant observation model for the estimation of $\mathcal{A}_k$ is given by

$$r_{k,j} = \sqrt{\beta_2 P}\ a_{k,j} + z_{k,j}, \quad j = 1, \ldots, N_t \tag{2.11}$$

We now denote the full set of observations available to UT k as:

$$\mathcal{R}_k \triangleq \{r_{k,j} : j = 1, \ldots, N_t\}.$$

In particular, we shall consider explicitly the case where UT k estimates its useful signal coefficient using linear MMSE estimation based on $r_{k,k}$, i.e.,

$$\widehat{a}_{k,k} = \frac{\sqrt{\beta_2 P}}{N_0 + \beta_2 P} r_{k,k}. \tag{2.12}$$

Because $\widehat{\mathbf{v}}_k$ is a unit vector independent of $\mathbf{h}_k$, the useful signal coefficient $a_{k,k} = \mathbf{h}_k^{\mathsf{H}} \widehat{\mathbf{v}}_k$ is complex Gaussian with unit variance. As a result we have the representation

$$a_{k,k} = \widehat{a}_{k,k} + f_k \tag{2.13}$$

where f_k and $\widehat{a}_{k,k}$ are independent and Gaussian with variance σ_2^2 and $1-\sigma_2^2$, respectively, with

$$\sigma_2^2 = \frac{1}{1+\beta_2 \mathsf{SNR}}. \tag{2.14}$$

5. **Data Transmission**: Finally, after the dedicated downlink training phase, the BS sends the coded data symbols $u_1, \ldots, u_K$ for the rest of the frame duration. The effective channel output for this phase is therefore given by the sequence of corresponding channel output symbols y_k given by (2.9), and by the observation of the dedicated training phase $\mathcal{R}_k$ given by (2.11).

   When considering the *ergodic* rates achievable by the proposed scheme, we implicitly assume that coding is performed over a long sequence of frames, each frame comprising a common training phase, channel state feedback phase, dedicated training phase and data transmission.

In the following sections, we quantify the rate gap upper bound for different feedback strategies under the assumption that the feedback channel is an unfaded AWGN channel with the same transmit power and AWGN variance as the downlink, i.e., P and N_0, respectively, and that the UTs access the channel orthogonally. Each UT uses $\beta_{\mathrm{fb}} N_t$ feedback channel symbols, and therefore the total number of feedback channel uses is $\beta_{\mathrm{fb}} N_t^2$.

2.3 Analytical Results

2.3.1 Upper and Lower Bounds on the Achievable Rate

We assume that the user codes are independently generated according to an i.i.d. Gaussian distribution, i.e., the input symbols are $u_k \sim \mathcal{CN}(0, \mathsf{SNR})$. The remainder of this section is dedicated to deriving upper and lower bounds on the mutual information achieved by such Gaussian inputs, indicated by $R_k \triangleq I(u_k; y_k, \mathcal{R}_k)$, where $I_k(\cdot)$ is the mutual information.

The following lower bound is obtained by using techniques similar to those in [30, 32, 31].

Theorem 2.3.1 *The achievable rate for ZF beamforming with Gaussian inputs and CSI training and feedback as described in Section 2.2 can be bounded from below by:*

$$R_k \geq \mathbb{E}\left[\log_2\left(1+\frac{|\widehat{a}_{k,k}|^2\mathsf{SNR}/(N_t)}{1+\sigma_2^2\mathsf{SNR}/(N_t)+\mathbb{E}\left[|I_k|^2|\widehat{a}_{k,k}\right]/N_0}\right)\right] \tag{2.15}$$

Proof: See Section 2.6.3. □

The second moment of the conditional interference term $\mathbb{E}\left[|I_k|^2|\widehat{a}_{k,k}\right]$ in (2.15) may be difficult to compute even by Monte Carlo simulation, due to the complicated dependency of I_k on $\widehat{a}_{k,k}$ (this dependence is unknown even if the dedicated training is perfect, i.e., $\widehat{a}_{k,k} = a_{k,k}$). However, we will not need to compute this explicitly, as discussed in forthcoming sections.

A very useful measure is the difference between R_k and R_k^{ZF}, that is, the achievable rate with ZF beamforming and ideal CSI defined in (2.3). The rate gap is defined as follows

$$\Delta R \triangleq R_k^{\mathrm{ZF}} - R_k, \tag{2.16}$$

and is upper bounded in the following theorem.

Theorem 2.3.2 *The rate gap incurred by ZF beamforming with training and feedback as described in Section 2.2 with respect to ideal ZF with equal power allocation is upper-bounded by:*

$$\Delta R \leq \log_2\left(1+\sigma_2^2\,\frac{\mathsf{SNR}}{N_t}+\frac{\mathbb{E}[|I_k|^2]}{N_0}\right) \tag{2.17}$$

Proof: See Section 2.6.4. □

For clarity of notation, we denote the right-hand-side of the above equation, referred to as the rate gap upper bound, as $\overline{\Delta R}$:

$$\overline{\Delta R} \triangleq \log_2\left(1+\sigma_2^2\,\frac{\mathsf{SNR}}{N_t}+\frac{\mathbb{E}\left[|I_k|^2\right]}{N_0}\right) \tag{2.18}$$

$$= \log_2\left(1+\frac{\mathsf{SNR}}{N_t}\left(\sigma_2^2\;+\sum_{j\neq k}\mathbb{E}\left[|\mathbf{h}_k^{\mathsf{H}}\widehat{\mathbf{v}}_j|^2\right]\right)\right) \tag{2.19}$$

where the latter follows from a simple calculation of $\mathbb{E}[|I_k|^2]$. The term σ_2^2 depends only on dedicated training; on the other hand, $\mathbb{E}\left[|\mathbf{h}_k^{\mathsf{H}}\widehat{\mathbf{v}}_j|^2\right]$ is determined by the mismatch between $\mathbf{h}_k$ and the BS estimate $\widehat{\mathbf{h}}_k$ (because $\widehat{\mathbf{v}}_j$ is chosen orthogonal to $\widehat{\mathbf{h}}_k$ rather than $\mathbf{h}_k$) and therefore depends on the common training and feedback phases.

Interestingly, the rate gap upper bound captures the dependence on the two phases of training and on the channel state feedback through the downlink useful signal coefficient estimation variance σ_2^2 and the residual interference variance $\mathbb{E}[|I_k|^2]$. Because $I_k = \sum_{j \neq k} a_{k,j} u_j$ with the u_j's chosen independently as $\mathcal{CN}(0, P/N_t)$, we have:

$$\mathbb{E}[|I_k|^2] = \frac{P}{N_t} \sum_{j \neq k} \mathbb{E}\left[|a_{k,j}|^2\right] = \frac{P}{N_t} \sum_{j \neq k} \mathbb{E}\left[|\mathbf{h}_k^{\mathsf{H}} \widehat{\mathbf{v}}_j|^2\right]. \tag{2.20}$$

An obvious result of the rate gap upper bound is the following lower bound to R_k:

Corollary 2.3.3 *The achievable rate for ZF beamforming with Gaussian inputs and CSIT training and feedback as described in Section 2.2 can be bounded from below by:*

$$R_k \geq R_k^{\mathrm{ZF}} - \overline{\Delta R} \tag{2.21}$$

Because only the estimate of $a_{k,k}$ is used in the derivation, Corollary 2.3.3 is also a lower bound to $I(u_k; y_k, r_{k,k})$.

Notice that only the estimation of $a_{k,k}$ is relevant in the derivation of the bound of Corollary 2.3.3. Therefore, Corollary 2.3.3 also provides a bound to the achievable rate for a system where the dedicated training phase is used only to estimate the useful signal coefficients $a_{k,k}$ at each UT rather than the full set of interference coefficients $\mathcal{A}_k$.

A useful upper bound to R_k is reached by providing each UT k with exact knowledge of the interference coefficients $\mathcal{A}_k$. Thus, this is referred to as the "genie-aided upper-bound".

Theorem 2.3.4 *The achievable rate for ZF beamforming with Gaussian inputs and CSI training and feedback is upper bounded by the rate achievable when, after the beamforming matrix $\widehat{\mathbf{V}}$ is chosen, a genie provides the k-th UT with perfect knowledge of the coefficients $\mathcal{A}_k = \{a_{k,j} = \mathbf{h}_k^{\mathsf{H}} \widehat{\mathbf{v}}_j : j = 1, \ldots, N_t\}$:*

$$R_k \leq \mathbb{E}\left[\log_2\left(1 + \frac{|a_{k,k}|^2 \frac{\mathsf{SNR}}{N_t}}{1 + \sum_{j \neq k} |a_{k,j}|^2 \frac{\mathsf{SNR}}{N_t}}\right)\right]. \tag{2.22}$$

Proof: Since $\mathcal{R}_k$ is a noisy version of $\mathcal{A}_k$, the data-processing inequality yields

$$R_k = I(u_k; y_k, \mathcal{R}_k) \leq I(u_k; y_k, \mathcal{A}_k) \tag{2.23}$$

Because y_k conditioned on $\mathcal{A}_k$ is complex Gaussian with variance $N_0+\sum_{j=1}^{M}|a_{k,j}|^2P/N_t$ while y_k conditioned on $(\mathcal{A}_k, u_k)$ is complex Gaussian with variance $N_0+\sum_{j\neq k}|a_{k,j}|^2P/N_t$, we immediately obtain (2.22). □

The practical relevance of Theorem 2.3.4 is two-fold: on one hand, (2.22) is easy to evaluate by Monte Carlo simulation. It is usually difficult if not impossible to obtain in closed form the joint distribution of the coefficients $\mathcal{A}_k$. On the other hand, this bound can be approached for large β_2, since in this case each UT can accurately estimate all interference coupling coefficients and not only the useful signal coefficient.

2.3.2 Analog Feedback

"Analog feedback" refers to transmission (on the feedback link) of the estimated downlink channel coefficients by each UT using unquantized quadrature-amplitude modulation [27, 29, 43, 44], that is, the estimated channel coefficients are transmitted directly. Specifically, each UT transmits on the feedback channel a scaled version of its common downlink training observation $\mathbf{s}_k$ defined in (2.5). This method is simple and does not require complex quantization and coding schemes, and might hence seem appealing in practice. The resulting feedback channel output (that is, what the BS observes during the feedback process) relative to UT k is given by:

$$\begin{aligned}\mathbf{g}_k &= \frac{\sqrt{\beta_{\mathrm{fb}}P}}{\sqrt{\beta_1 P+N_0}}\,\mathbf{s}_k+\widetilde{\mathbf{w}}_k && (2.24)\\ &= \frac{\sqrt{\beta_{\mathrm{fb}}\beta_1}P}{\sqrt{\beta_1 P+N_0}}\,\mathbf{h}_k+\frac{\sqrt{\beta_{\mathrm{fb}}P}}{\sqrt{\beta_1 P+N_0}}\,\mathbf{z}_k+\widetilde{\mathbf{w}}_k && (2.25)\\ &= \frac{\sqrt{\beta_{\mathrm{fb}}\beta_1}P}{\sqrt{\beta_1 P+N_0}}\,\mathbf{h}_k+\mathbf{w}_k && (2.26)\end{aligned}$$

where $\widetilde{\mathbf{w}}_k$ represents the AWGN noise on the uplink feedback channel (variance N_0) and $\mathbf{z}_k$ is the noise during the common training phase. The power scaling β_{fb} corresponds to the number of channel uses per channel coefficient (we require $\beta_{\mathrm{fb}}\geq 1$ so that each coefficient is transmitted at least once), assuming that transmission in the feedback channel has per-symbol power P (averaged over frames) and that the channel state vector is modulated by a $\beta_{\mathrm{fb}}N_t\times N_t$ unitary spreading matrix [27]. Because $\widetilde{\mathbf{w}}_k$ and $\mathbf{z}_k$ are each complex Gaussian with covariance $N_0\mathbf{I}$ and are independent, $\mathbf{w}_k$ is complex

Gaussian with covariance $\sigma_w^2\mathbf{I}$ with:

$$\sigma_w^2 = N_0\left(1+\frac{\beta_{\text{fb}}\mathsf{SNR}}{1+\beta_1\mathsf{SNR}}\right) \tag{2.27}$$

The BS computes the MMSE estimate of the channel vector $\mathbf{h}_k$ based on $\mathbf{g}_k$ as:

$$\widehat{\mathbf{h}}_k = \frac{\sqrt{\beta_{\text{fb}}\beta_1}P}{\sqrt{\beta_1 P+N_0}\,(\beta_{\text{fb}}P+N_0)}\;\mathbf{g}_k. \tag{2.28}$$

Using (2.26), the channel can be written in terms of the BS estimate and estimation error $\mathbf{e}_k$ as:

$$\mathbf{h}_k = \widehat{\mathbf{h}}_k + \mathbf{e}_k \tag{2.29}$$

where $\mathbf{e}_k$ is independent of the estimate and is Gaussian with covariance $\sigma_e^2\mathbf{I}$ with:

$$\sigma_e^2 = \frac{\sigma_w^2}{\sigma_w^2+\frac{\beta_{\text{fb}}\beta_1P^2}{\beta_1P+N_0}} \;=\; \frac{1}{1+\beta_{\text{fb}}\frac{P}{N_0}}+\frac{\beta_{\text{fb}}\frac{P}{N_0}}{(1+\beta_{\text{fb}}\frac{P}{N_0})(1+\beta_1\frac{P}{N_0})}. \tag{2.30}$$

This characterization of $(\mathbf{h}_k,\widehat{\mathbf{h}}_k)$ can be used to derive the rate gap upper bound for analog feedback.

Theorem 2.3.5 *If each UT feeds back its channel coefficients in analog fashion over $\beta_{\text{fb}}N_t$ channel uses of an AWGN uplink channel with $\mathsf{SNR}=\frac{P}{N_0}$, the rate gap relative to ZF with perfect CSIT ($R_{\text{ZF}}(P)$) is bounded from above by ("AF" standing for Analog Feedback):*

$$\overline{\Delta R}^{\text{AF}} = \log_2\left(1+\frac{\mathsf{SNR}}{N_t}\left(\frac{1}{1+\beta_2\mathsf{SNR}}+\frac{N_t-1}{1+\beta_{\text{fb}}\mathsf{SNR}}+\frac{(N_t-1)\beta_{\text{fb}}\mathsf{SNR}}{(1+\beta_{\text{fb}}\mathsf{SNR})(1+\beta_1\mathsf{SNR})}\right)\right) \tag{2.31}$$

Proof: See Section 2.6.5. □

Thus, the rate achievable with analog feedback is at least as great as $R_{\text{ZF}}(P)-\overline{\Delta R}^{\text{AF}}$. It is straightforward to see that $\overline{\Delta R}^{\text{AF}}$ can be further bounded from above as follows:

$$\overline{\Delta R}^{\text{AF}} \;\leq\; \log_2\left(1+\frac{1}{N_t\beta_2}+\frac{N_t-1}{N_t}\left(\frac{1}{\beta_1}+\frac{1}{\beta_{\text{fb}}}\right)\right). \tag{2.32}$$

Hence, the rate gap is *uniformly bounded* for all values of SNR, that is, the rate gap is at least a constant value less than R^{ZF}. Thus, the multiplexing gain is preserved, i.e., $\lim_{\mathsf{SNR}\to\infty}\frac{R_k}{\log_2 P}=1$), *in spite of* the imperfect CSI.

An intuitive understanding of this rate loss is obtained if one re-examines the UT received signal in the form used in Theorem 2.3.1:

$$y_k = \widehat{a}_{k,k} u_k + \underbrace{f_k u_k}_{\text{Self Noise}} + \underbrace{\sum_{j \neq k} (\mathbf{h}_k^{\mathsf{H}} \widehat{\mathbf{v}}_j) u_j}_{\text{Interference}} + \underbrace{z_k}_{\text{Noise}} \tag{2.33}$$

The imperfect channel state information (at the UT and BS) effectively increases the noise from the thermal noise level N_0 to the sum of the thermal noise, self-noise, and interference power, and the rate gap upper bound $\overline{\Delta R}^{\mathrm{AF}}$ is precisely the logarithm of the ratio of the effective noise to the thermal noise power.

In many systems, the uplink SNR is smaller than the downlink SNR because UT's transmit with reduced power (compared to the BS). If the uplink SNR is $\Gamma \frac{P}{N_0}$ rather than $\frac{P}{N_0}$, $\overline{\Delta R}^{\mathrm{AF}}$ is equal to the expression in Theorem 2.3.5 with β_{fb} replaced with $\Gamma \beta_{\mathrm{fb}}$. This does not change the multiplexing gain, but can have a significant effect on the rate gap.

2.3.3 Digital Feedback and Quantization with Error-Free Feedback

We now consider "digital" feedback, where the estimated channel vector is quantized at each UT and represented by B bits. The packet of B bits is fed back by each UT to the BS. Hence, each UT and the BS have an agreed upon codebook, where each UT selects the channel quantization that is "closest" to the estimated channel vector by some metric, and then feeds the B-bit index back to the BS to identify the "closest" quantization vector in the codebook.

We begin by computing the rate gap upper bound in terms of *bits*, and later in the section relate this to feedback *channel uses*. Following [21, 20, 19, 14], we consider a specific scheme for channel state quantization based on a quantization codebook $\mathcal{C} = \{\mathbf{p}_1, \ldots, \mathbf{p}_{2^B}\}$ of unit-norm vectors in $\mathbb{C}^{N_t}$. The quantization $\widehat{\mathbf{h}}_k$ of the estimated channel vector $\widetilde{\mathbf{h}}_k$ is found according to the decision rule:

$$\widehat{\mathbf{h}}_k = \underset{\mathbf{p} \in \mathcal{C}}{\arg\max} \ |\widetilde{\mathbf{h}}_k^{\mathsf{H}} \mathbf{p}|^2 \tag{2.34}$$

and thus $\widehat{\mathbf{h}}_k$ is the quantization vector forming the minimum angle with $\widetilde{\mathbf{h}}_k$. Thus, we use the angle between the quantized vector and the vector to be quantized as our

quantization metric (to be minimized). This is relevant for a beamforming method such as ZF, which requires knowledge of the subspace of various channel vectors taken together, and hence requires knowledge of the *direction* of each channel vector. The corresponding B-bits quantization index is fed back to the BS. Because $\widehat{\mathbf{h}}_k$ is unit-norm, no channel magnitude information is conveyed.

In [24, 14] it is shown that for a random ensemble of quantization codebooks referred to as *Random Vector Quantization* (RVQ). There are a number of reasons motivating our use of RVQ here. First, note that RVQ is quite close to optimal vector quantization, particularly for moderate to large values of B. In [14] it is shown that the expected distortion (i.e., square of the sine of the angle between channel and quantization) of RVQ is no more than $\frac{N_t}{N_t-1}$ times larger than the distortion achieved with optimal vector quantization. Second, the isotropic and random nature of the ensemble of codebooks allows for analytical tractability. Finally, because the statistics of RVQ are known in closed form, RVQ can be exactly emulated by drawing only one scalar random variable and one random vector as described in [45]. For large B this is considerably simpler than actually performing brute-force quantization. This allows for a vastly more simple simulation method where the quantized vectors are obtained by generating 2^B quantization vectors independently and uniformly distributed on the unit sphere in $\mathbb{C}^{N_t}$ (see [14] and references therein). In this case, the average (angular) distortion is given by:

$$\begin{aligned} \mathbb{E}\left[\sin^2\left(\widetilde{\mathbf{h}}_k, \widehat{\mathbf{h}}_k\right)\right] &= 2^B \beta\left(2^B, \frac{N_t}{N_t-1}\right) && (2.35) \\ &\leq 2^{-\frac{B}{N_t-1}}. && (2.36) \end{aligned}$$

where $\beta(\cdot)$ is the beta function and $\sin^2\left(\widetilde{\mathbf{h}}_k, \widehat{\mathbf{h}}_k\right) = 1 - \frac{|\widetilde{\mathbf{h}}_k^{\mathsf{H}} \widehat{\mathbf{h}}_k|^2}{\|\widetilde{\mathbf{h}}_k\|^2}$. For this particular quantization scheme, we can compute the rate gap upper bound:

Theorem 2.3.6 *If each UT quantizes its channel to B bits (using RVQ) and conveys these bits in an error-free fashion to the BS, the rate gap upper bound is given by ("DF" standing for Digital Feedback):*

$$\overline{\Delta R}^{\mathrm{DF}} = \log_2\left(1 + \frac{\mathsf{SNR}}{N_t}\left(\frac{1}{1+\beta_2 \mathsf{SNR}} + \frac{N_t}{1+\beta_1 \mathsf{SNR}}\left[\frac{N_t-1}{N_t} + \beta_1 \mathsf{SNR} 2^B \beta\left(2^B, \frac{N_t}{N_t-1}\right)\right]\right)\right)$$

Proof: See Section 2.6.6. □

Using (2.35), the rate gap upper bound can be further upper bounded as:

$$\overline{\Delta R}^{\mathrm{DF}} \quad \leq \quad \log_2 \left(1 + \frac{1}{N_t \beta_2} + \frac{N_t - 1}{N_t} \, \frac{1}{\beta_1} + (\mathsf{SNR}) \, 2^{-\frac{B}{N_t - 1}} \right). \tag{2.37}$$

Comparing this to the rate gap in the analog feedback case (2.32), we notice that the dependence on β_1 and β_2 is precisely the same for both analog and digital feedback.

If $B = \alpha(N_t - 1) \log_2 \mathsf{SNR}$ for some $\alpha > 0$, that is, the number of bits B is a linear multiple of SNR represented in decibels ($\mathsf{SNR}_{\mathrm{dB}} = 10 \log_{10} \mathsf{SNR}$), then (2.37) becomes:

$$\overline{\Delta R}^{\mathrm{DF}} \quad \leq \quad \log_2 \left(1 + \frac{1}{N_t \beta_2} + \frac{N_t - 1}{N_t} \, \frac{1}{\beta_1} + (\mathsf{SNR})^{1-\alpha} \right). \tag{2.38}$$

If $\alpha \geq 1$, this quantity is uniformly bounded for all values of SNR, and thus the full multiplexing gain is achieved, similar to the analog feedback case. Furthermore, we find that for $\alpha > 1$, the effect of channel feedback completely vanishes as $\mathsf{SNR} \to \infty$, while if $\alpha < 1$ then $\overline{\Delta R}^{\mathrm{DF}}$ increases as $(1 - \alpha) \log_2 \mathsf{SNR}$, and by [14, Theorem 4], we have that the multiplexing gain is only $\alpha < 1$.

The case of perfect CSIR is again obtained by letting $\beta_1, \beta_2 \to \infty$, and from (2.37) we obtain

$$\Delta R^{\mathrm{DF}}_{\mathrm{CSIR}} \leq \log_2 \left(1 + \mathsf{SNR} \; 2^{-\frac{B}{N_t - 1}} \right) \tag{2.39}$$

which recovers the result in [14, Theorem 1].

The next step is translating the rate gap upper bound so that it is in terms of feedback symbols rather than bits, which will allow us a fair and general framework to compare different feedback schemes. For the time being, we shall make the unrealistic assumption that the feedback link can operate error-free at capacity, i.e., it can reliably transmit $\log_2(1 + \mathsf{SNR})$ bits per symbol.[1]

The analog feedback considered before provides a noisy version of the channel vector norm in addition to its direction. Although this information is irrelevant for the ZF beamforming considered here, it might be useful in some user selection algorithms such as those proposed in [9, 29, 10, 39]. In contrast, digital feedback based on unit-norm quantization vectors provides no norm information. Thus, for fair comparison, we assume that $\beta_{\mathrm{fb}} N_t$ feedback symbols in the analog feedback scheme correspond to

[1] This assumption is unrealistic in the context of this model because the feedback channel coding block length is very small and because the need for very fast feedback (essentially delay-free) prevents grouping blocks of channel coefficients and using larger coding block length.

$\beta_{\text{fb}}(N_t - 1)$ feedback symbols for the digital feedback scheme; i.e., a system using digital feedback could use one feedback symbol to transmit channel norm information. An alternative justification for this is to notice that the analog feedback system could be modified to operate in $\beta_{\text{fb}}(N_t - 1)$ channel symbols by transmitting only the $N_t - 1$ *relative* phases and amplitudes of the channel coefficients, since the absolute norm and phase are irrelevant to the ZF beamforming considered here.

Under this assumption, the number of feedback bits per mobile is $B = \beta_{\text{fb}}(N_t - 1)\log_2(1 + \mathsf{SNR})$. Plugging this into (2.37) gives:

$$\overline{\Delta R}^{\text{DF}} \leq \log_2\left(1 + \frac{1}{N_t\beta_2} + \frac{N_t - 1}{N_t}\,\frac{1}{\beta_1} + \frac{\mathsf{SNR}}{(1+\mathsf{SNR})^{\beta_{\text{fb}}}}\right) \tag{2.40}$$

Similar to analog feedback, if $\beta_{\text{fb}} \geq 1$ then the rate gap is uniformly bounded for all SNR and full multiplexing gain is preserved. However, it should be noticed that for β_{fb} strictly larger than 1, digital feedback yields a term $(\mathsf{SNR})^{1-\beta_{\text{fb}}}$ that vanishes as $\mathsf{SNR} \to \infty$. This should be contrasted with the constant term $\frac{1}{\beta_{\text{fb}}}$ for the case of analog feedback (which does not vanish).

Further, in the case of perfect CSIR, the lower bound in Corollary 2.3.3, the genie-aided upper bound in Theorem 2.3.4, and the benchmark R_k^{ZF}, all coincide (in the sense that the absolute difference between them go to zero) at asymptotically high SNR for digital feedback, provided that $B = \alpha(N_t - 1)\log_2\frac{P}{N_0}$ with $\alpha > 1$. This provides a sufficient condition using digital feedback to ensure a vanishing rate gap for high SNR.

2.3.4 Digital Feedback and Quantization with Feedback Errors

We now remove the optimistic assumption that the digital feedback channel can operate error-free at capacity. In general, coding for the CSIT feedback channel should be regarded as a joint source-channel coding problem, made particularly interesting by the non-standard distortion measure and by the fact that a very short block length is required. A thorough discussion of this subject is out of the scope of this work and is the matter of current investigation (see for example [46, 47]). Here, we restrict ourselves to the detailed analysis of a particularly simple scheme based on uncoded QAM. Perhaps surprisingly, this scheme is *sufficient* to achieve a vanishing rate gap in the high SNR region, for an appropriate choice of the system parameters.

In the proposed scheme, the UTs perform quantization using RVQ and transmit the feedback bits using plain uncoded QAM. The quantization bits are randomly mapped onto the QAM symbols (i.e., no intelligent bit-labeling or mapping is used). Therefore, even a single erroneous feedback bit from UT k makes the BS's CSIT vector $\widehat{\mathbf{h}}_k$ essentially useless. Also, no particular error detection strategy is used and thus the BS computes the beamforming matrix on the basis of the received feedback, although this may be in error.

We again let $\beta_{\text{fb}}(N_t-1)$ denote the number of channel uses to transmit the feedback bits (per UT). Interestingly, even for this very simple scheme there is a non-trivial tradeoff between quantization distortion and channel errors. In order to maintain a bounded rate gap, the number of feedback bits must be scaled at least as $(N_t-1)\log_2(1+\mathsf{SNR}) \approx (N_t-1)\log_2 \mathsf{SNR}$. Therefore, we consider sending $B = \alpha(N_t-1)\log_2 \mathsf{SNR}$ bits for $1 \le \alpha \le \beta_{\text{fb}}$ in $\beta_{\text{fb}}(N_t-1)$ channel uses, which corresponds to $\frac{\alpha}{\beta_{\text{fb}}}\log_2 \mathsf{SNR}$ bits per QAM symbol.

The symbol error rate for square QAM with q constellation points is bounded by [48]:

$$P_s = 1 - \left(1 - 2\left(1 - \frac{1}{\sqrt{q}}\right) Q\left(\frac{3\mathsf{SNR}}{q-1}\right)\right)^2 \le 2\exp\left(-\frac{3}{2}\frac{\mathsf{SNR}}{q-1}\right). \tag{2.41}$$

where $Q(x) = \int_x^\infty \frac{1}{\sqrt{2\pi}} e^{-t^2/2} dt$ is the Gaussian probability tail function. Using the fact that $q = \mathsf{SNR}^{\frac{\alpha}{\beta_{\text{fb}}}}$, we obtain the upper bound

$$P_s \;\le\; 2\exp\left(-\frac{3}{2}\left(\mathsf{SNR}\right)^{1-\frac{\alpha}{\beta_{\text{fb}}}}\right) \tag{2.42}$$

If $\alpha = \beta_{\text{fb}}$, which corresponds to signaling at capacity with uncoded modulation, P_s does not decrease with SNR and system performance is very poor. However, for $\alpha < \beta_{\text{fb}}$, which corresponds to transmitting at a fraction of capacity, $P_s \to 0$ as $\mathsf{SNR} \to \infty$. The error probability of the entire feedback message (transmitted in $\beta_{\text{fb}}(N_t-1)$ QAM symbols) is given by

$$P_{e,\text{fb}} \;=\; 1 - (1-P_s)^{\beta_{\text{fb}}(N_t-1)} \le \beta_{\text{fb}}(N_t-1)P_s, \tag{2.43}$$

where the inequality follows from the union bound. Note the tradeoff between distortion and feedback error: α large yields finer quantization but larger $P_{e,\text{fb}}$, while α small provides poorer quantization but smaller $P_{e,\text{fb}}$.

Theorem 2.3.7 *If each UT quantizes its estimated channel using $B = \alpha(N_t-1)\log_2 \mathsf{SNR}$ bits (using RVQ), and transmits on the feedback link using $\beta_{\mathrm{fb}}(N_t-1)$ channel uses with uncoded QAM modulation, the resulting rate gap can be upperbounded by*

$$\overline{\Delta R}^{\text{DF-Errors}} \quad \leq \quad \log\left(1+\frac{1}{N_t\beta_2}+(1-P_{e,\mathrm{fb}})\left(\mathsf{SNR}^{1-\alpha}+\frac{N_t-1}{N_t}\,\frac{1}{\beta_1}\right)+\mathsf{SNR}P_{e,\mathrm{fb}}\right)$$

where $P_{e,\mathrm{fb}}$ is given by (2.42) and (2.43).

Proof: See Section 2.6.7. □

If $1 < \alpha < \beta_{\mathrm{fb}}$, then the effect of feedback vanishes as $\mathsf{SNR} \to \infty$, somewhat similar to the case of error-free feedback. This is because the feedback error probability decays exponentially as $\mathsf{SNR}^{1-\frac{\alpha}{\beta_{\mathrm{fb}}}}$, so that the term $\mathsf{SNR}P_{e,\mathrm{fb}}$ vanishes as $\mathsf{SNR} \to \infty$ for all $\alpha < \beta_{\mathrm{fb}}$, while obviously $SNR^{1-\alpha}$ vanishes for all $\alpha > 1$.

A number of simple improvements are possible. For example, each UT may estimate its interference coefficients $\{a_{k,j} : j \neq k\}$ from the dedicated training phase, and decide if its feedback message was correctly received or was received in error by setting a threshold on the interference power: if the interference power is $\approx (N_t-1)\mathsf{SNR}$, then it is likely that a feedback error occurred. If, on the contrary, it is $\approx 2^{-B/(N_t-1)}\mathsf{SNR}$, then it is likely that the feedback message was correctly received. Interestingly, for $B = \alpha(N_t-1)\log_2 \mathsf{SNR}$ with $\alpha > 1$, detecting feedback error events becomes easier and easier as SNR increases and/or as the number of antennas N_t increases. In brief, for a large number of antennas any terminal whose feedback message was received in error is completely drowned into interference and should be able to detect this event with high probability. Assuming that the UTs can perfectly detect their own feedback error events as described above, then they can simply discard the frames corresponding to feedback errors. The resulting achievable rate in this case is lowerbounded by

$$R_k^{\text{DF-Errors-Detect}} \quad \geq \quad (1-P_{e,\mathrm{fb}})\left[R_k^{\mathrm{ZF}}-\log\left(1+\frac{1}{N_t\beta_2}+\frac{N_t-1}{N_t}\frac{1}{\beta_1}+\mathsf{SNR}^{1-\alpha}\right)\right] \tag{2.44}$$

in light of (2.40) (after replacing α instead of β_{fb}) and of Corollary 2.3.3. Note that this rate lies between the achievable rate lower bound obtained via the rate gap in Theorem 2.3.7 and the genie-aided upper bound from Theorem 2.3.4.

We notice here that the naive ZF strategy examined in this work is *robust to feedback errors* in the following sense: the residual interference experienced by a given UT depends only on that particular UT feedback error probability. Therefore, a small number of users with poor feedback channel quality (very high feedback error probability) does not destroy the overall system performance. This observation goes against the conventional wisdom that feedback errors are "catastrophic".

2.4 Comparison of Feedback Strategies

Based upon the bounds developed in the previous subsections as well as the genie-aided upper bounds (computed using Monte Carlo simulation) we can now compare analog, error-free digital, and QAM-based digital feedback. Because the effect of downlink and common training is effectively the same for all feedback strategies, we pursue this comparison under the assumption of perfect CSIR, i.e., perfect common and dedicated training corresponding to $\beta_1 = \beta_2 \to \infty$. From (2.32) and (2.40) we have:

$$\Delta R_{\text{CSIR}}^{\text{AF}} \leq \log\left(1 + \frac{1}{\beta_{\text{fb}}}\right) \tag{2.45}$$

$$\Delta R_{\text{CSIR}}^{\text{DF}} \leq \log\left(1 + \frac{\mathsf{SNR}}{(1+\mathsf{SNR})^{\beta_{\text{fb}}}}\right) \tag{2.46}$$

If $\beta_{\text{fb}} = 1$ then analog and error-free digital feedback both achieve essentially the same rate gap of 1 bit per channel user (per UT). However, if $\beta_{\text{fb}} > 1$, the rate gap for quantized feedback vanishes for $\mathsf{SNR} \to \infty$. This conclusion finds an appealing interpretation in the context of rate-distortion theory. It is well-known (see for example [49] and references therein) that "analog transmission" (the source signal is input directly to the channel after suitable power scaling) is an optimal strategy to send an i.i.d. Gaussian source over a AWGN channel with the same bandwidth under quadratic distortion. In our case, the source vector is $\mathbf{h}_k$ (Gaussian and i.i.d.) and the feedback channel is AWGN with with SNR SNR. Hence, the fact that analog feedback cannot be essentially outperformed for $\beta_{\text{fb}} = 1$ is expected. However, it is also well-known that if the channel bandwidth is larger than the source bandwidth (which corresponds to the case where a block of N_t source coefficients are transmitted over $\beta_{\text{fb}} N_t$ channel uses with $\beta_{\text{fb}} > 1$),

then analog transmission is strictly suboptimal with respect to a digital scheme operating at the rate-distortion bound, because the distortion with analog transmission is $O(\mathsf{SNR}^{-1})$ whereas it is $O(\mathsf{SNR}^{-\beta_{\mathrm{fb}}})$ for digital transmission.

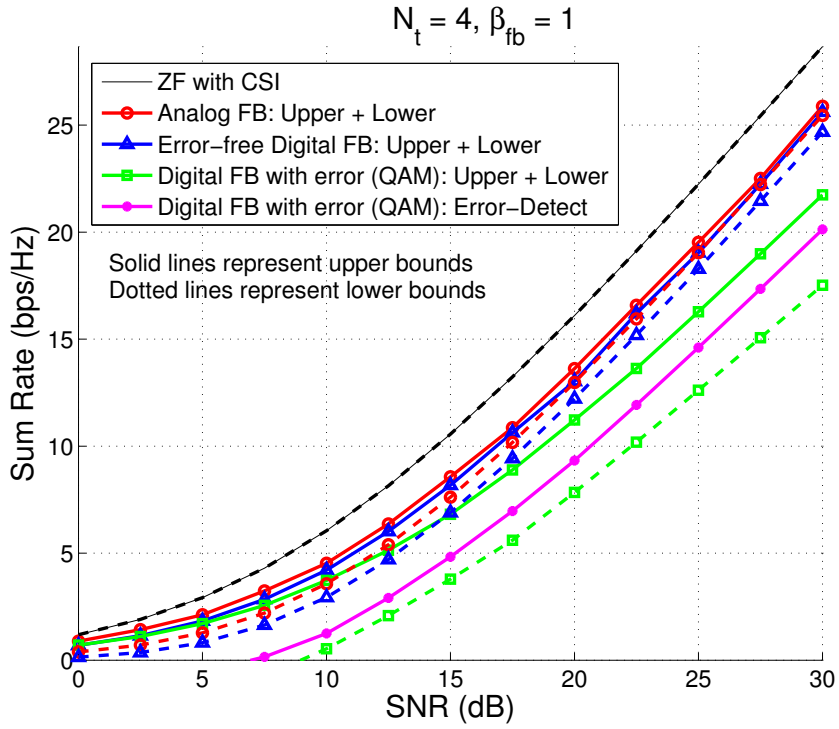

Figure 2.3: Rate bounds for analog and error-free/QAM digital feedback, $\beta_{\mathrm{fb}} = 1$

This conclusion is confirmed by the numerical results shown in Figures 2.3 and 2.4. In Figure 2.3 the lower and genie-aided upper bounds are plotted for analog feedback, digital feedback without error, and digital feedback with error (QAM) versus SNR for an $N_t = 4$ system with $\beta_{\mathrm{fb}} = 1$. For digital feedback with error, the error detection bound in (2.44) is also included. The analog and error-free digital feedback schemes perform virtually identically and achieve a rate approximately 3 dB away from the perfect channel state information benchmark. Note also that the gap between the upper and lower bounds is not very large. For digital feedback with uncoded QAM [2]

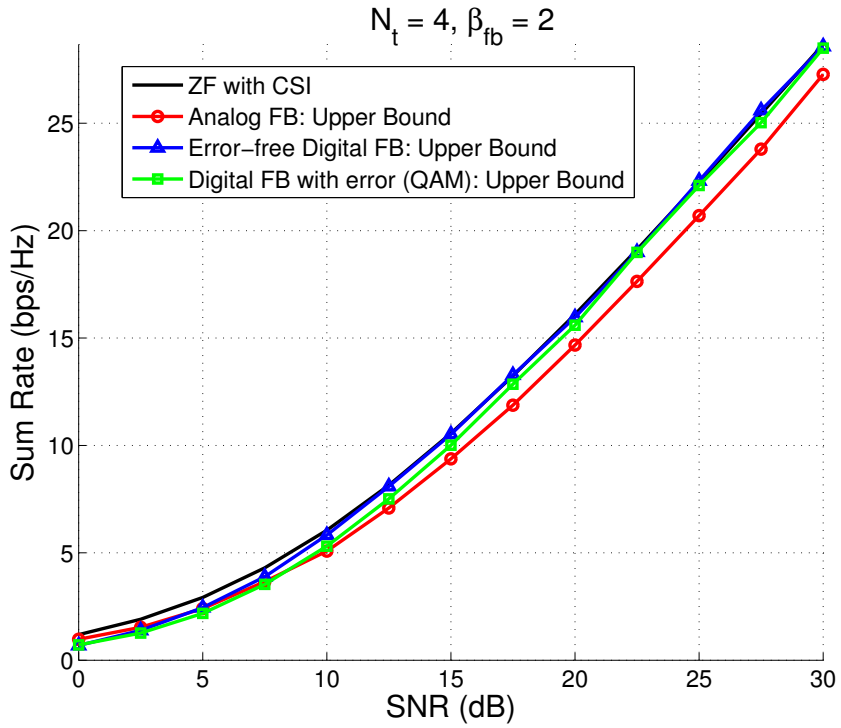

Figure 2.4: Rate bounds for analog and error-free/QAM digital feedback, $\beta_{\text{fb}} = 2$

, however, there is a substantial gap between the upper and lower bounds.[3] In Figure 2.4 only the genie-aided upper bounds are plotted (because the lower and upper are nearly identical and thus are difficult to distinguish) for the same setting with $\beta_{\text{fb}} = 2$. We see that digital feedback with uncoded QAM outperforms analog feedback above approximately 5 dB, and that the rate with digital feedback (with or without errors) converges to the ideal rate as predicted earlier. This figure confirms that the effect of feedback vanishes when digital feedback is used, with or without errors, and $\beta_{\text{fb}} > 1$. Finally, in Figure 2.5 the bounds are plotted as a function of β_{fb} for fixed $\mathsf{SNR} = 10$ dB and $\mathsf{SNR} = 20$ dB (that is, $\mathsf{SNR} = 10, 100$, respectively). When $\beta_{\text{fb}} \approx 1$

[2] These results are obtained by optimizing the value of $1 \leq \alpha \leq \beta_{\text{fb}}$ for each SNR. We refer to this as "envelope", that is, the plotted curve is the pointwise maximum of the rate vs. SNR curves for all α.

[3] Feedback errors make the residual interference behave as an impulsive noise: it has very large variance with small probability $P_{e,\text{fb}}$. Detecting errors and discarding corresponding frames yields significant improvements. Using this knowledge for the lower bound (2.44), avoids the large "Jensen's penalty" incurred by the upper bound Theorem 2.3.7

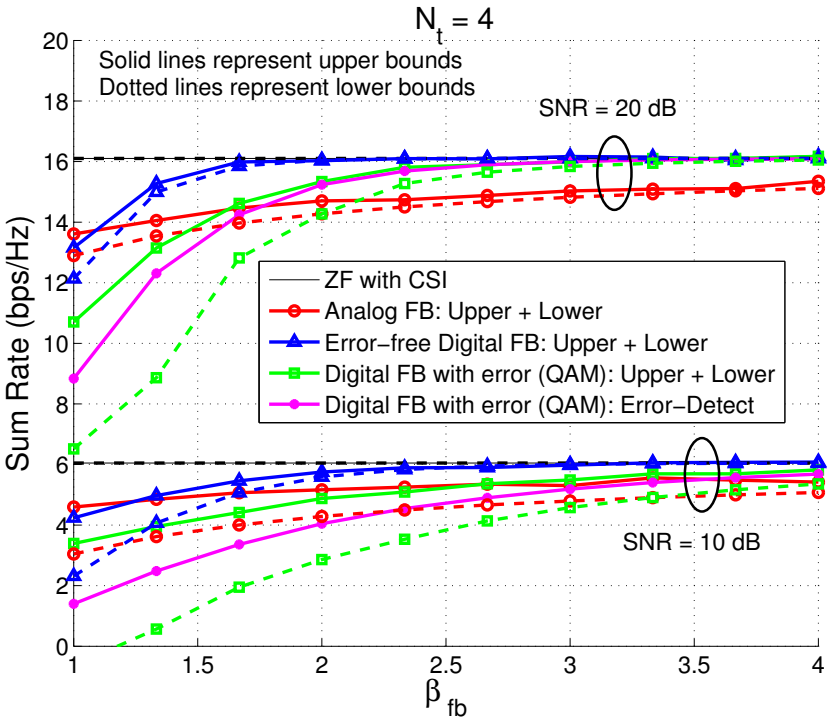

Figure 2.5: Rate bounds for analog and error-free/QAM digital feedback vs. β_{fb}

analog and error-free digital feedback are nearly equivalent, but as β_{fb} is increased the rate with error-free digital quickly approaches the perfect channel state information rate. When feedback errors are introduced, digital feedback does eventually outperform analog and also approaches the ideal rate, but a larger β_{fb} is required. It is also worth noticing that as the SNR is increased, the value of β_{fb} at which digital (with or without errors) begins to outperform analog decreases toward 1: this is to expected based upon the fact that the effect of feedback vanishes as $\mathsf{SNR} \to \infty$ for any $\beta_{\text{fb}} > 1$ for digital, whereas it does not for analog feedback.

It is worth noting that the same basic conclusion, i.e., that digital feedback (with or without errors) outperforms analog for sufficiently large β_{fb}, also holds in the presence imperfect CSIR. However, because imperfect CSIR leads to a residual term in the rate gap expression that does not vanish (even for large SNR), the absolute difference between digital and analog feedback is reduced.

2.5 Summary of Results for Limited Number of Users

This work presents a comprehensive and rigorous analysis of the achievable performance of ZF beamforming under pilot-based channel estimation and explicit channel state feedback. We considered what we believe are the most relevant system aspects. In particular, the often neglected effect of explicit channel estimation at the UTs is taken into account, including both common training and dedicated training phases. As for the feedback, our closed-form bounds allow for a detailed comparison of analog and digital feedback schemes, of digital feedback decoding errors, and of feedback delay.

Our results build on prior work, but generalize many results and models. We have focused on the case of FDD, but our results easily extend to TDD systems with channel reciprocity, as described in Section 2.6.1. It is perhaps important to point out here that our results show that, even in the case of FDD, a system with explicit CSIT feedback can be implemented, where the number of training and feedback channel uses scales linearly with the number of BS antennas, and eventually with the downlink throughput.

The throughput of the system analyzed here can be improved via the use of combined beamforming and user selection/scheduling. Simulation results show that a system with $K = 10$ and $N_t = 4$, with a greedy scheduling as proposed in [10, 29], achieves a very small gap with respect to the optimal dirty-paper coding and perfect CSIT case with the same parameters. Although a clean closed-form analytical characterization of a system with beamforming and user selection based on imperfect channel state information appears to be difficult, other results [50] indicate that the dependence on CSIT quality when user selection is performed is roughly the same as the equal-power/no selection scenario analyzed here.

2.6 Supplementary Materials and Proofs

2.6.1 Rate Gap for Time-Division Duplex MIMO Systems

In the preceding results, we have assumed that the uplink and downlink channels are not identical, thus necessitating feedback. However, it is easy to see that if the uplink and downlink channels were identical, such as in a Time-Division Duplex (TDD) system, assuming that each UT transmits β_{TDD} pilots (a single pilot trains all M BS antennas)

in an orthogonal manner corresponds, this corresponds exactly to a system with non-identical uplink/downlink with "perfect" feedback ($\beta_{\text{fb}} \to \infty$) and $\beta_1 = \beta_{\text{TDD}}$. Thus, as a byproduct of our analysis in Theorem 2.3.5, we obtain a result for TDD open loop (i.e., no feedback) CSIT estimation:

$$\begin{aligned} \overline{\Delta R}^{\text{TDD}} &= \log\left[1 + \frac{\mathsf{SNR}}{N_t}\left(\frac{1}{1+\beta_2\mathsf{SNR}} + \frac{N_t - 1}{1+\beta_{\text{TDD}}\mathsf{SNR}}\right)\right] && (2.47) \\ &\leq \log\left(1 + \frac{1}{N_t\beta_2} + \frac{N_t - 1}{N_t}\frac{1}{\beta_{\text{TDD}}}\right). && (2.48) \end{aligned}$$

Note that Dedicated training is necessary even in TDD systems because UTs do not know the channels of other UTs and thus are not aware of the beamforming vectors used by the BS. Hence, for TDD, a total of $N_t\beta_{\text{TDD}}$ uplink training symbols and $N_t\beta_2$ downlink (dedicated) training symbols are needed.

2.6.2 Feedback Requirement for Line-of-Sight Channels

We now investigate the feedback requirements for the case when $\mathbf{h}_k$ represents a Line-of-Sight (LOS) channel, as opposed to a Rayleigh fading (complex Gaussian) channel, and show that the feedback requirements can be considerably smaller. These results appeared in [51]. The LOS model is applicable when the signal transmitted from the BS is directly received by the UT, and is much larger than any components received after scattering and reflection of the transmitted signal. With a one dimensional antenna array at the BS with antenna spacing d, we have:

$$\mathbf{h}_k = \begin{bmatrix} 1 \\ e^{-i\frac{2\pi d}{\lambda}\sin(\theta_k)} \\ \vdots \\ e^{-i(M-1)\frac{2\pi d}{\lambda}\sin(\theta_i)} \end{bmatrix} \tag{2.49}$$

where λ is the communication signal wavelength and θ_k is the angle of departure measured with respect to the antenna array boresight direction. The users are all assumed to be at a constant equal distance from the transmitter following some distribution. We assume a model similar to the i.i.d. block fading model of previous sections: the positions of the users, and hence the θ_k's, are assumed to take a value for a certain time block, independent of previous values or each other.

We are mainly interested in quantifying how the feedback requirement would change for the LOS channel, relative to what we have discussed in preceding sections, and hence make certain simplifying assumptions. In particular, we neglect the effects of downlink pilot training, so each of the UTs is assumed to have perfect and instantaneous knowledge of its own channel. The channel to each UT, in any case, can be fully specified by the parameter θ_k, since λ and d are fixed known quantities, and so channel estimation at the UT would reduce to estimation of the angle, which is relatively easy to do compared to the estimation of the Rayleigh fading $\mathbf{h}_k$ vector considered in previous sections, and will hence have a relatively small estimation error. We also focus on digital feedback and assume that the feedback channel is error-free. We analyze the case when $K = N_t$, as we have done in preceding sections, but provide numerical results for $K > N_t$ as well.

In this case, the problem of quantizing $\mathbf{h}_k$ to $\widehat{\mathbf{h}_k}$ reduces to the problem of quantizing the real number θ_k at each UT k. For simplicity, we will assume that each UT quantizes $\sin(\theta_k)$ uniformly using B bits over the range of possible values and feeds this back to the transmitter i.e. $\sin(\theta_k)$) is quantized to $\widehat{w_k}$ where:

$$|\sin(\theta_k) - \widehat{w_k}| = |\delta| \leq \frac{r}{2^{B+1}} \tag{2.50}$$

where r is the range of values over which $\sin(\theta_k)$ is quantized (the range r is divided into 2^B "bins", and the real number $\sin(\theta_k)$ is quantized to the closest bin with rounding). Then, $\hat{w_k}$ is used to construct the quantized channel vector $\widehat{\mathbf{h}_k}$ at the BS:

$$\widehat{\mathbf{h}_k} = \begin{bmatrix} 1 \\ e^{-i\frac{2\pi d}{\lambda}\widehat{w}_k} \\ \vdots \\ e^{-i(M-1)\frac{2\pi d}{\lambda}\widehat{w}_k} \end{bmatrix} \tag{2.51}$$

We will assume "naive" Zero-Forcing beamforming as we did in the preceding sections, which dictates that the beamforming vectors $\widehat{\mathbf{v}}_k$ (for $k = 1, \ldots, N_t$) are selected based on $\widehat{\mathbf{h}}_k$, as described in the beamformer selection step in Section 2.2. Following a procedure similar that in to Section 2.3, we have that the rate gap for LOS channels is

bounded from above by:

$$\begin{aligned}
\overline{\Delta R^{\mathrm{LOS}}} &= \mathbb{E}\left[\log_2\left(1+\frac{\mathsf{SNR}}{N_t}\left|\mathbf{h}_k^{\mathsf{H}}\mathbf{v}_k\right|^2\right)\right]-\mathbb{E}\left[\log_2\left(1+\frac{\mathsf{SNR}}{N_t}\sum_{j=1}^{N_t}\left|\mathbf{h}_k^{\mathsf{H}}\widehat{\mathbf{v}}_j\right|^2\right)\right] \\
&\quad +\mathbb{E}\left[\log_2\left(1+\frac{\mathsf{SNR}}{N_t}\sum_{j=1,j\neq k}^{N_t}\left|\mathbf{h}_k^{\mathsf{H}}\widehat{\mathbf{v}}_j\right|^2\right)\right] \\
&\overset{(a)}{\leq} \mathbb{E}\left[\log_2\left(1+\frac{\mathsf{SNR}}{N_t}\left|\mathbf{h}_k^{\mathsf{H}}\widehat{\mathbf{v}}_k\right|^2\right)\right]-\mathbb{E}\left[\log_2\left(1+\frac{\mathsf{SNR}}{N_t}\left|\mathbf{h}_k^{\mathsf{H}}\widehat{\mathbf{v}}_k\right|^2\right)\right] \\
&\quad +\mathbb{E}\left[\log_2\left(1+\frac{\mathsf{SNR}}{N_t}\sum_{j=1,j\neq k}^{N_t}\left|\mathbf{h}_k^{\mathsf{H}}\widehat{\mathbf{v}}_j\right|^2\right)\right] \\
&\overset{(b)}{\approx} \mathbb{E}\left[\log_2\left(1+\frac{\mathsf{SNR}}{N_t}\sum_{j=1,j\neq k}^{N_t}\left|\mathbf{h}_k^{\mathsf{H}}\widehat{\mathbf{v}}_k\right|^2\right)\right] \qquad (2.52)
\end{aligned}$$

where (a) follows by neglecting the interference terms w.r.t. the signal component, and (b) follows from the fact that when the quantizations are very good, the angles formed between $\mathbf{h}_k, \mathbf{v}_k$ and $\mathbf{h}_k, \widehat{\mathbf{v}}_k$ are nearly the same.

Now,

$$\begin{aligned}
||\mathbf{h}_k||^2 = N_t &\geq \frac{\left|\mathbf{h}_k^{\mathsf{H}}\widehat{\mathbf{h}}_k\right|^2}{||\widehat{\mathbf{h}}_k||^2}+\left|\mathbf{h}_k^{\mathsf{H}}\widehat{\mathbf{v}}_j\right|^2 \\
\Rightarrow \left|\mathbf{h}_k^{\mathsf{H}}\widehat{\mathbf{v}}_j\right|^2 &\leq N_t\left(1-\cos^2\angle\left(\mathbf{h}_k,\widehat{\mathbf{h}}_k\right)\right) \qquad (2.53)
\end{aligned}$$

for any $j \neq k$, and

$$\begin{aligned}
\cos^2\angle\left(\mathbf{h}_k,\widehat{\mathbf{h}}_k\right) &= \frac{1}{N_t^2}\left|\sum_{k=0}^{N_t-1} e^{ik\frac{2\pi d}{\lambda}\ (sin(\theta_k)-\hat{w_k})}\right|^2 \\
&= \frac{1}{N_t^2}\left|\frac{\sin\left(\frac{N_t\pi d}{\lambda}\delta\right)}{\sin\left(\frac{\pi d}{\lambda}\delta\right)}e^{i\frac{(N_t-1)\pi d}{\lambda}\delta}\right|^2 \\
&\overset{(a)}{=} \frac{1}{N_t^2}\frac{\sin^2\left(\frac{N_t\pi d}{\lambda}\delta\right)}{\sin^2\left(\frac{\pi d}{\lambda}\delta\right)} \qquad (2.54) \\
&\overset{(b)}{\approx} 1-\frac{(N_t^2-1)}{3}\pi^2\frac{d^2}{\lambda^2}\delta^2 \\
&\geq 1-\frac{(N_t^2-1)}{12}\pi^2\frac{d^2}{\lambda^2}r^2 2^{-2B} \qquad (2.55)
\end{aligned}$$

where (a) follows by evaluating the sum of the series of exponentials [52] and (b) is obtained by a second order Taylor's expansion about $\delta = 0$, and the bound follows from (2.50).

Using (2.55) and (2.53) in (2.52), the rate gap can be bounded by a function of the number of feedback bits per user.

Corollary 2.6.1 *The rate gap upper bound with LOS channels is given by:*

$$\overline{\Delta R^{\mathrm{LOS}}} \;\approx\; \log_2\left(1 + \mathsf{SNR}\; C(N_t, d, \lambda, r)\; 2^{-2B}\;\right) \tag{2.56}$$

where $C(N_t, d, \lambda, r) = \frac{(N_t-1)(N_t^2-1)\pi^2 d^2 r^2}{12\lambda^2}$.

The above is an approximation due to the fact that we have made the assumption that the angular error is small (that is, δ is small), and have used the second order Taylor's series expansion about zero to replace $\sin^2(\cdot)$. However, for reasonably sized codebooks of interest (reasonable B), δ^2 will be very small, making this approximation very accurate.

The rate loss appears to be an increasing function of SNR and (2.56) suggests that increasing B as SNR increases will bound the rate loss by a constant. In order to maintain a rate gap of no more than $\log_2(b)$ (bps/Hz) per user, the (approximate) sufficient number of bits can be found by inverting expression (2.56) and solving for B.

$$B \;\approx\; \frac{1}{6}\mathsf{SNR}_{\mathrm{dB}} + \frac{1}{2}\log_2\left(C(N_t, d, \lambda, r)\right) - \frac{1}{2}\log_2(b-1) \tag{2.57}$$

To maintain an SNR loss of at most 3dB between the rates under finite rate feedback and perfect CSIT, $b = 2$:

$$B \;\approx\; \frac{1}{6}\mathsf{SNR}_{dB} + \frac{1}{2}\log_2\left(\frac{(N_t-1)(N_t^2-1)\pi^2}{12}\right) \tag{2.58}$$

where d is selected to have a $\frac{\lambda}{2}$ spacing between antenna elements and θ_k ranges from 0 to 2π i.e. $\sin(\theta_k)$ ranges from -1 to 1 to give $r = 2$. Interestingly, the number of bits must be scaled linearly with the SNR as we saw in the case with Rayleigh fading in preceding sections, but the dependence on the number of antenna elements N_t is much less pronounced, and there is no linear dependence on N_t.

Simulations for a system with $N_t = 4$ transmit antennas and $\frac{\lambda}{2}$ antenna placement with θ_k distributed uniformly in $[0, 2\pi]$ are shown in the Figure 2.6. All users are thus

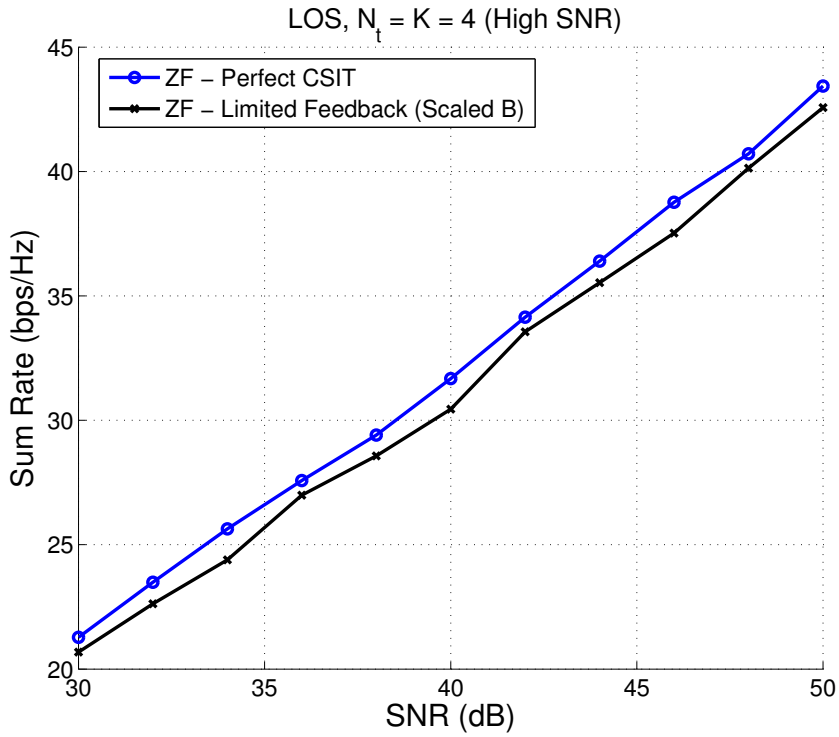

Figure 2.6: Sum rate for LOS channels with $N_t = 4$

distributed uniformly on a circle of fixed radius about the transmitter. The number of bits per user is determined by (2.58) to maintain an SNR gap of 3dB. The number of bits required are found to be quite small (only 7 bits even at 30dB). However, if there are only $K = N_t = 4$ users in the system, the probability of the channels of two or more users having the same quantization is quite large (without more users). At high SNR however (due to large B), it is possible to beamform to all of the $K = N_t$ users, and hence these cases are considered.

The SNR gap is found to be 0.7 dB instead of 3 dB, as (2.56) is a conservative bound. Nevertheless, a constant gap is indeed maintained between the perfect CSIT rate and the rate with CSI feedback by scaling the bits as per (2.58). Simulations suggest that using one less bit than that suggested by (2.58) is typically sufficient.

Figure 2.7 shows the numerically computed achievable rates curves for the same situation as above as a function of N_t (at high SNR). $K = N_t$ users in the system

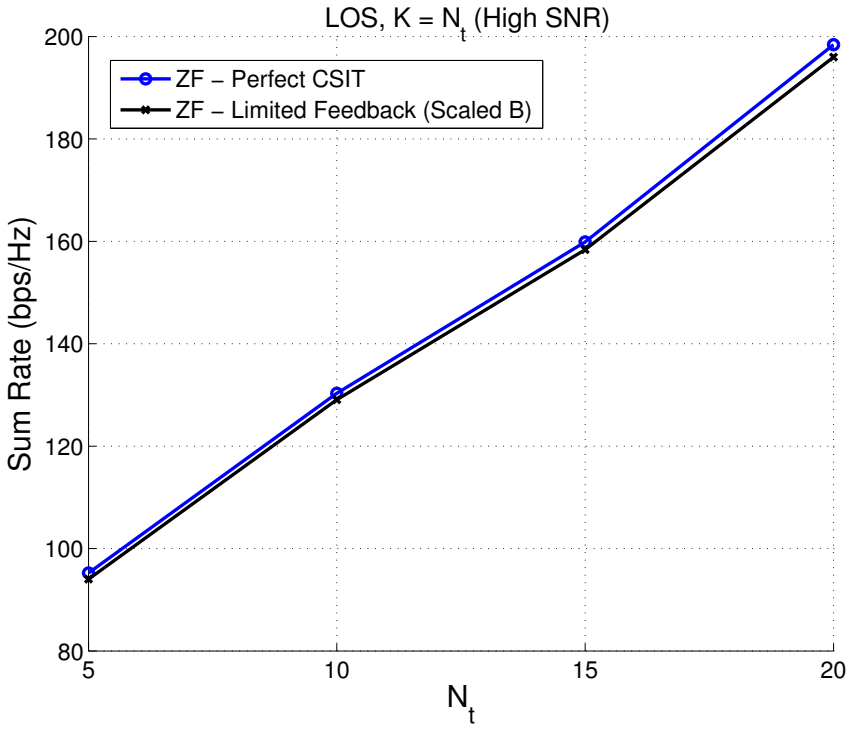

Figure 2.7: Sum rate for LOS channels for various N_t

are assumed and the SNR is chosen to be high enough to allow for the N_t different channels to be quantized to different codewords with high probability. The number of bits required varies only as $\mathrm{O}(\log(N_t))$ from (2.58), and varies no more than a bit from $M = N_t$ to $N_t = 20$. This is in contrast to the results seen in preceding sections, where we required that $B \sim \alpha N_t$, that is, a linear increase in the number of bits with the number of antennas to maintain a constant rate gap. This can be attributed to the fact that it is much easier to quantize the LOS channel, due to the channel being entirely specified by the parameter θ_k.

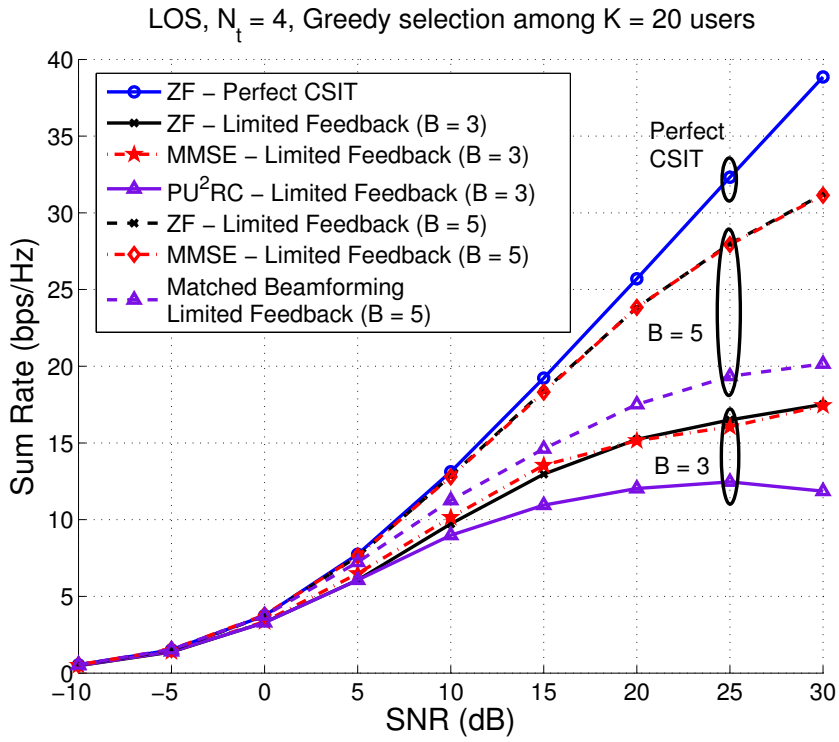

Figure 2.8: Sum rate for LOS channels with Greedy User Selection, fixed B

Figures 2.8 and 2.9 compare ZF, MMSE Beamforming[53], and the more conventional "matched" beamforming. The three schemes each require the beamforming vectors to be selected as:

$$\text{ZF beamforming}: \quad \mathbf{V} = \hat{\mathbf{H}}(\hat{\mathbf{H}}^H\hat{\mathbf{H}})^\dagger \tag{2.59}$$

$$\text{MMSE beamforming}: \quad \mathbf{V} = \hat{\mathbf{H}}(\hat{\mathbf{H}}^H\hat{\mathbf{H}} + \frac{n}{\text{SNR}}\mathbf{I}_n)^\dagger \tag{2.60}$$

$$\text{Matched beamforming}: \quad \mathbf{v}_{\pi(k)} = \hat{\mathbf{h}}_{\pi(k)} \tag{2.61}$$

where $\hat{\mathbf{H}} = [\hat{\mathbf{h}}_{\pi(1)}, \hat{\mathbf{h}}_{\pi(2)}, \ldots, \hat{\mathbf{h}}_{\pi(n)}]$ and $\mathbf{V} = [\tilde{\mathbf{v}}_{\pi(1)}, \tilde{\mathbf{v}}_{\pi(2)}, \ldots, \tilde{\mathbf{v}}_{\pi(n)}]$, $\mathbf{v}_{\pi(k)} = \frac{\tilde{\mathbf{v}}_{\pi(k)}}{||\tilde{\mathbf{v}}_{\pi(k)}||}$, $k = 1, \ldots, n$. Although our analysis was for $K = N_t$, we consider $K = 20 > N_t$ in the numerical results to model a more practical scenario. In this case, a subset of the 20 users are selected by the BS, namely n users denoted by $(\pi(1), \pi(2), \ldots, \pi(n))$, with the selection made based on a greedy algorithm [10], using quantized information at the BS.

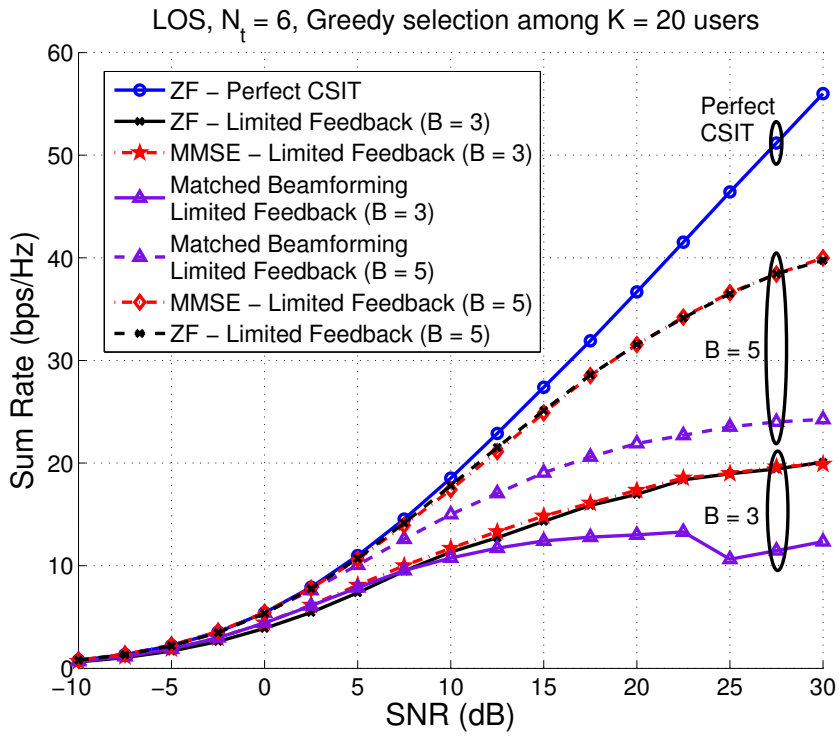

Figure 2.9: Sum rate for LOS channels with Greedy User Selection, scaled B

Figure 2.8 compares perfect CSIT and limited feedback with fixed number of bits ($B = 3, 5$). Keeping the number of bits fixed is seen to result in an increasing gap between the rate curves, resulting in failure to capture the full multiplexing gain. Figure 2.9 includes bit scaling as per (2.58), with a minimum of one bit used for feedback. The gap at low SNR in Figure 2.9 is due to the fact that only a single bit of feedback is used at low SNR, which makes it difficult to get N_t different users with different quantizations of their respective θ_k. The performance of ZF and MMSE with user selection is found to be nearly the same, with MMSE performing marginally better at lower SNR values (as expected by design of the MMSE beamformers). The SNR offset between ZF with perfect CSIT and limited feedback is bounded by about 1.3 dB (as opposed to 3 dB due to the conservative design). The sum rate with conventional beamforming does not scale with SNR as the system becomes interference limited.

These results reinforce our conclusions from the preceding sections, that is, feedback

information is important and must be utilized to remove interference (using ZF or MMSE beamforming, for example), and with proper design of the feedback link, the rate gap can be bounded by a constant, and hence the multiplexing gain is preserved. For LOS channels, we see that the dependence of B on the number of antennas N_t is much less when compared to Rayleigh fading, but the dependence on SNR remains similar.

2.6.3 Proof of Theorem 2.3.1

The proof is closely inspired by that of Lemma B.0.1 of [31]. First, notice that since $\widehat{a}_{k,k}$ is a function of $\mathcal{R}_k$, by the data-processing inequality we have that

$$I(u_k; y_k, \mathcal{R}_k) \geq I(u_k; y_k, \widehat{a}_{k,k})$$

Then, because $I(u_k; y_k, \widehat{a}_{k,k}) = h(u_k) - h(u_k|y_k, \widehat{a}_{k,k})$ and $h(u_k) = \log\left(\pi e \frac{P}{N_t}\right)$, a lower bound on mutual information is derived by upper bounding $h(u_k|y_k, \widehat{a}_{k,k})$ as follows:

$$\begin{aligned} h(u_k|y_k, \widehat{a}_{k,k}) &\overset{(a)}{=} h(u_k - \alpha\ y_k|y_k, \widehat{a}_{k,k}) \\ &\overset{(b)}{\leq} h(u_k - \alpha\ y_k|\widehat{a}_{k,k}) \\ &\overset{(c)}{\leq} \mathbb{E}\left[\log\left(\pi e \cdot \mathbb{E}\left[|u_k - \alpha\ y_k|^2|\widehat{a}_{k,k}\right]\right)\right] \end{aligned} \tag{2.62}$$

where (a) holds for any deterministic function α of y_k and $\widehat{a}_{k,k}$, (b) follows from the fact that conditioning reduces entropy and (c) follows by the fact that differential entropy is maximized by a Gaussian RV with the same second moment. Substituting (2.13) in (2.9) we have

$$y_k = (\widehat{a}_{k,k} + f_k)u_k + I_k + z_k \tag{2.63}$$

where $\widehat{a}_{k,k}u_k$ and $f_k u_k + I_k + z_k$ are *uncorrelated* and zero-mean, even if we condition on $\widehat{a}_{k,k}$, because $\widehat{a}_{k,k}, f_k, u_1, \ldots, u_K, z_k$ are independent, zero-mean Gaussian's. Thus, we have

$$\mathbb{E}\left[|y_k|^2\ |\widehat{a}_{k,k}\right] = |\widehat{a}_{k,k}|^2\mathbb{E}[|u_k|^2] + \sigma_2^2\ \mathbb{E}[|u_k|^2] + \mathbb{E}\left[|I_k|^2|\widehat{a}_{k,k}\right] + N_0, \tag{2.64}$$

Choosing α that minimizes $\mathbb{E}\left[|u_k - \alpha\ y_k|^2|\widehat{a}_{k,k}\right]$ tightens the bound. This corresponds to setting $\alpha\ y_k$ equal to the linear MMSE estimate of u_k given y_k and $\widehat{a}_{k,k}$, i.e.,

$$\alpha = \frac{\mathbb{E}\left[u_k y_k^*\ |\ \widehat{a}_{k,k}\right]}{\mathbb{E}\left[|y_k|^2\ |\ \widehat{a}_{k,k}\right]} = \frac{\mathbb{E}[|u_k|^2]\widehat{a}_{k,k}^*}{\mathbb{E}\left[|y_k|^2\ |\ \widehat{a}_{k,k}\right]} \tag{2.65}$$

Using (2.64), the corresponding MMSE is given by

$$\mathbb{E}\left[|u_k - \alpha\ y_k|^2 |\widehat{a}_{k,k}\right] = \mathbb{E}\left[|u_k|^2\right]\left(1 - \frac{\mathbb{E}[|u_k|^2]|\widehat{a}_{k,k}|^2}{\mathbb{E}\left[|y_k|^2 \mid \widehat{a}_{k,k}\right]}\right) \tag{2.66}$$

$$= \frac{P}{N_t}\frac{1 + \sigma_2^2\frac{\mathsf{SNR}}{N_t} + \mathbb{E}\left[|I_k|^2|\widehat{a}_{k,k}\right]/N_0}{|\widehat{a}_{k,k}|^2\frac{\mathsf{SNR}}{N_t} + 1 + \sigma_2^2\frac{\mathsf{SNR}}{N_t} + \mathbb{E}\left[|I_k|^2|\widehat{a}_{k,k}\right]/N_0} \tag{2.67}$$

Replacing (2.67) into (2.62) and using $h(u_k) = \log\left(\pi e \frac{P}{N_t}\right)$, we obtain (2.15).

2.6.4 Proof of Theorem 2.3.2

Using the lower bound on R_k from Theorem 2.3.1 we have:

$$\begin{aligned}
\Delta R &\leq \mathbb{E}\left[\log\left(1 + \frac{|\mathbf{h}^{\mathsf{H}}\mathbf{v}_k|^2\mathsf{SNR}}{N_t}\right)\right] - \mathbb{E}\left[\log\left(1 + \frac{|\widehat{a}_{k,k}|^2\mathsf{SNR}/(N_t)}{1 + \sigma_2^2\mathsf{SNR}/(N_t) + \mathbb{E}\left[|I_k|^2|\widehat{a}_{k,k}\right]/N_0}\right)\right] \\
&\overset{(a)}{\leq} \mathbb{E}\left[\log\left(1 + \frac{|\mathbf{h}^{\mathsf{H}}\mathbf{v}_k|^2\mathsf{SNR}}{N_t}\right)\right] - \mathbb{E}\left[\log\left(1 + \frac{\mathsf{SNR}}{N_t}\left(|\widehat{a}_{k,k}|^2 + \sigma_2^2\right)\right)\right] \\
&\qquad + \mathbb{E}\left[\log\left(1 + \sigma_2^2\frac{\mathsf{SNR}}{N_t} + \frac{\mathbb{E}\left[|I_k|^2|\widehat{a}_{k,k}\right]}{N_0}\right)\right] \\
&\overset{(b)}{\leq} \mathbb{E}\left[\log\left(1 + \sigma_2^2\frac{\mathsf{SNR}}{N_t} + \frac{\mathbb{E}\left[|I_k|^2|\widehat{a}_{k,k}\right]}{N_0}\right)\right] \qquad (2.68) \\
&\overset{(c)}{\leq} \log\left(1 + \sigma_2^2\frac{\mathsf{SNR}}{N_t} + \frac{\mathbb{E}[|I_k|^2]}{N_0}\right) \qquad (2.69)
\end{aligned}$$

where (a) follows by dropping the non-negative term $\mathbb{E}\left[|I_k|^2|\widehat{a}_{k,k}\right]/N_0$. Using the fact that $\mathbf{h}_k$ is spatially white and $\mathbf{v}_k$ is selected independent of $\mathbf{h}_k$ (by the ZF procedure), it follows that $\mathbf{h}_k^{\mathsf{H}}\mathbf{v}_k$ is $\sim \mathcal{CN}(0,1)$ and $\widehat{a}_{k,k} \sim \mathcal{CN}(0, 1-\sigma_2^2)$. Direct application of Lemma 2.6.2, which is provided below, with $A = \mathsf{SNR}/N_t$, $\lambda = \sigma_2^2$ and $X = |\mathbf{h}_k^{\mathsf{H}}\mathbf{v}_k|^2$, thus proves (b). Finally, (c) follows from the concavity of $\log(\cdot)$ and Jensen's inequality.

Lemma 2.6.2 *If X is a non-negative random variable with $\mathbb{E}[X] = 1$, for any $A > 0$ and any $0 \leq \lambda \leq 1$:*

$$\mathbb{E}\left[\log\left(1 + XA\right)\right] \leq \mathbb{E}\left[\log\left(1 + (\lambda + (1-\lambda)X)\,A\right)\right]. \tag{2.70}$$

Proof: For all $0 \leq z \leq 1$, define the function

$$\psi(z) = \mathbb{E}\left[\log\left(1 + zA + (1-z)XA\right)\right]. \tag{2.71}$$

Then (2.70) is equivalent to the inequality $\psi(0) \leq \psi(\lambda)$. By the concavity of $\log(\cdot)$ and Jensen's inequality we have

$$\psi(z) \quad \leq \quad \log\left(1 + zA + (1-z)\mathbb{E}\left[X\right]A\right) = \psi(1). \tag{2.72}$$

In particular, $\psi(0) \leq \psi(1)$. Moreover, $\psi(z)$ is an expectation of the composition of a concave function and a linear function of z, and is hence concave [54]. Thus, the concave function $\psi(z)$ for $z \in [0,1]$ lies above the line joining the points $(0, \psi(0))$ and $(1, \psi(1))$. Hence, we have $\psi(0) \leq \psi(\lambda)$ for $\lambda \in [0,1]$, which proves (2.70). □

2.6.5 Proof of Theorem 2.3.5

Using (2.19), to compute $\overline{\Delta R}^{\mathrm{AF}}$ we only need to find $\mathbb{E}\left[|\mathbf{h}_k^{\mathsf{H}}\widehat{\mathbf{v}}_j|^2\right]$:

$$\begin{aligned}
\mathbb{E}\left[|\mathbf{h}_k^{\mathsf{H}}\widehat{\mathbf{v}}_j|^2\right] &\overset{(a)}{=} \mathbb{E}\left[|\widehat{\mathbf{h}}_k^{\mathsf{H}}\widehat{\mathbf{v}}_j + \mathbf{e}_k^{\mathsf{H}}\widehat{\mathbf{v}}_j|^2\right] \\
&\overset{(b)}{=} \mathbb{E}\left[|\mathbf{e}_k^{\mathsf{H}}\widehat{\mathbf{v}}_j|^2\right] \\
&\overset{(c)}{=} \mathbb{E}\left[\widehat{\mathbf{v}}_j^{\mathsf{H}}\mathbb{E}[\mathbf{e}_k\mathbf{e}_k^{\mathsf{H}}]\widehat{\mathbf{v}}_j\right] \\
&\overset{(d)}{=} \sigma_e^2
\end{aligned} \tag{2.73}$$

where (a) follows from (2.29), (b) follows from the fact that $\widehat{\mathbf{h}}_k^{\mathsf{H}}\widehat{\mathbf{v}}_j = 0 \;\forall\; j \neq k$ by naive ZF, (c) is obtained from the independence of $\mathbf{e}_k$ and $\widehat{\mathbf{v}}_j$ ($\widehat{\mathbf{v}}_j$ is a deterministic function of $\{\widehat{\mathbf{h}}_i\}_{i\neq j}$), and (d) follows from $\mathbb{E}[\mathbf{e}_k\mathbf{e}_k^{\mathsf{H}}] = \sigma_e^2\mathbf{I}$ and $\|\widehat{\mathbf{v}}_j\| = 1$.

2.6.6 Proof of Theorem 2.3.6

To compute the rate gap upper bound, we determine $\mathbb{E}\left[|\mathbf{h}_k^{\mathsf{H}}\widehat{\mathbf{v}}_j|^2\right]$ by writing the channel in terms of the UT channel estimate (which is quantized) and the UT estimation error: $\mathbf{h}_k = \widetilde{\mathbf{h}}_k + \mathbf{n}_k$ from (2.7). This yields:

$$\begin{aligned}
\mathbb{E}\left[|\mathbf{h}_k^{\mathsf{H}}\widehat{\mathbf{v}}_j|^2\right] &\overset{(a)}{=} \mathbb{E}\left[|\widetilde{\mathbf{h}}_k^{\mathsf{H}}\widehat{\mathbf{v}}_j|^2\right] + \mathbb{E}\left[|\mathbf{n}_k^{\mathsf{H}}\widehat{\mathbf{v}}_j|^2\right] \\
&\overset{(b)}{=} \mathbb{E}\left[\|\widetilde{\mathbf{h}}_k\|^2\right]\mathbb{E}\left[\frac{|\widetilde{\mathbf{h}}_k^{\mathsf{H}}\widehat{\mathbf{v}}_j|^2}{\|\widetilde{\mathbf{h}}_k\|^2}\right] + \mathbb{E}\left[|\mathbf{n}_k^{\mathsf{H}}\widehat{\mathbf{v}}_j|^2\right] \\
&\overset{(c)}{=} \frac{\mathbb{E}\left[\|\widetilde{\mathbf{h}}_k\|^2\right]}{N_t - 1}\, 2^B\beta\left(2^B, \frac{N_t}{N_t-1}\right) + \mathbb{E}\left[\widehat{\mathbf{v}}_j^{\mathsf{H}}\mathbb{E}[\mathbf{n}_k\mathbf{n}_k^{\mathsf{H}}]\widehat{\mathbf{v}}_j\right] \\
&\overset{(d)}{=} \frac{N_t}{N_t-1}\frac{\beta_1 P}{N_0 + \beta_1 P}\, 2^B\beta\left(2^B, \frac{N_t}{N_t-1}\right) + \sigma_1^2
\end{aligned} \tag{2.74}$$

where (a) is obtained from the representation $\mathbf{h}_k = \widetilde{\mathbf{h}}_k + \mathbf{n}_k$ and the fact that $\mathbb{E}\left[\widetilde{\mathbf{h}}_k^{\mathsf{H}} \widehat{\mathbf{v}}_j \widehat{\mathbf{v}}_j^{\mathsf{H}} \mathbf{n}_k\right] = 0$ because $\mathbf{n}_k$ is zero-mean Gaussian and is independent of $\widetilde{\mathbf{h}}_k$ and $\widehat{\mathbf{v}}_j$, (b) from the independence of the channel norm and direction of $\widetilde{\mathbf{h}}_k$, (c) from (2.35) and from the property [14, Lemma 2] $\mathbb{E}\left[\frac{|\widetilde{\mathbf{h}}_k^{\mathsf{H}} \widehat{\mathbf{v}}_j|^2}{\|\widetilde{\mathbf{h}}_k\|^2}\right] = \frac{1}{N_t - 1}\mathbb{E}\left[\sin^2\left(\widetilde{\mathbf{h}}_k, \widehat{\mathbf{h}}_k\right)\right]$, and finally (d) by computing the expected norm of $\widetilde{\mathbf{h}}_k = \frac{\sqrt{\beta_1 P}}{N_0 + \beta_1 P}\mathbf{s}_k$ using $\mathbf{s}_k = \sqrt{\beta_1 P}\ \mathbf{h}_k + \mathbf{z}_k$. The final result follows by using the above result in the expression (2.17) for the rate gap.

2.6.7 Proof of Theorem 2.3.7

Using $P_{e,\text{fb}}$ to denote the error probability in the feedback link, we decompose the interference variance term as

$$\begin{aligned}
\mathbb{E}\left[|\mathbf{h}_k^{\mathsf{H}} \widehat{\mathbf{v}}_j|^2\right] &= (1 - P_{e,\text{fb}})\mathbb{E}[|\mathbf{h}_k^{\mathsf{H}} \widehat{\mathbf{v}}_j|^2 | \text{no fb. errors}] + P_{e,\text{fb}}\mathbb{E}[|\mathbf{h}_k^{\mathsf{H}} \widehat{\mathbf{v}}_j|^2 | \text{fb. errors}] \\
&\leq (1 - P_{e,\text{fb}}) \frac{N_t}{N_t - 1} \frac{\beta_1 P}{N_0 + \beta_1 P}\ 2^B \beta\left(2^B, \frac{N_t}{N_t - 1}\right) + \sigma_1^2 + P_{e,\text{fb}},
\end{aligned}$$

where $\mathbb{E}[|\mathbf{h}_k^{\mathsf{H}} \widehat{\mathbf{v}}_j|^2 | \text{no fb. errors}]$ is the same as in the error-free case and is thus given in (2.74) while for the case of feedback errors we trivially have $\mathbb{E}[|\mathbf{h}_k^{\mathsf{H}} \widehat{\mathbf{v}}_j|^2 | \text{fb. errors}] \leq 1$. The final result is reached by simply substituting $B = \alpha(N_t - 1)\log_2 \mathsf{SNR}$ and using the bound in the beta function (2.35).

Chapter 3

MIMO Limited Feedback with Many Users Per Cell

In this chapter, we relax the assumption that $K = N_t$ and consider the achievable rate when $K > N_t$ UTs are present in the system, the implications of which have been discussed in Chapter 1. The results presented in this chapter appear in [55, 56]. Although there has been considerable prior work on the MIMO downlink channel feedback there is a dichotomy between results on systems with a small number of receivers/users (of the order of N_t) and systems with many users. The throughput of systems with the number of users on the order of N_t, as we have seen in Chapter 2, is extremely sensitive to the accuracy of the CSI, and thus many feedback bits are needed from each user in order to achieve a large sum rate. At the other extreme, it has been shown that systems can achieve a very large sum rate even with very few feedback bits per user, in the asymptotic limit as the number of users is taken to infinity. For example, Random Beamforming (RBF) requires only $\log_2 N_t$ bits and one real number per user [17].

The presence of these two extremes leads to a natural question: how should a MIMO downlink system be designed such that feedback resources are most efficiently utilized to maximize sum rate? In order to answer this question, the *aggregate feedback load* in the system must be considered, instead of the conventional focus on the per-user feedback load.

An example helps illustrate the importance of this design question. Consider a

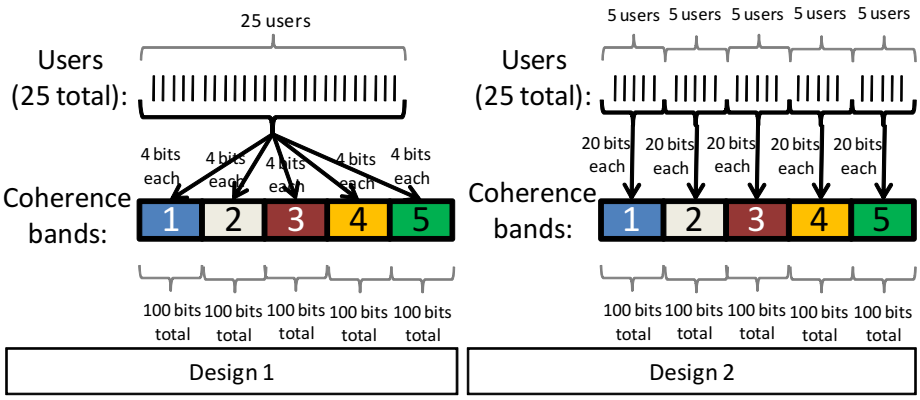

Figure 3.1: Two possible design strategies for a MIMO downlink system

MIMO downlink system with 25 users and 5 independent coherence bands (in frequency). One system design is to have all 25 users feed back 4 bits of quantized CSI for each of the 5 coherence bands, and then select, for each band, a subset of users for beamforming, as depicted by Design 1 in Figure 3.1. An alternative is Design 2, where the 25 users are divided into 5 arbitrary (or randomly assigned) groups of 5 users each, where each group is assigned a single band[1] . Each user then feeds back 20 bits of quantized CSI for its assigned band, and for each band a subset of the 5 eligible users is chosen for beamforming, in that band. Although both of the above designs use 100 bits of feedback per coherence band, it is not clear which design provides a larger sum rate.

Thereby motivated, in this work, we ask the following fundamental design question, which we do not believe has been sufficiently addressed by prior work: *Given a constraint on the aggregate number of feedback bits, is a larger system sum rate achieved by collecting a few feedback bits from a large number of users, or by collecting more bits from fewer users?*

Assuming an aggregate feedback load of T_{fb} bits (for a block of symbols over which the channel is constant), we consider a system where T_{fb}/B users quantize their channel

[1] This grouping is random or arbitrary, and the number of actual users is immaterial. This model also applies when users are grouped based on scheduling priorities, and hence the grouping process should not incur significant additional overhead. Alternatively, users can also be grouped based on their instantaneous channel, but this would introduce a random-access component to the feedback link and is not considered in the present work.

direction to B bits each and feed back these bits along with one real number (per user) representing the channel quality. The BS then selects, based upon the feedback received from the T_{fb}/B users, up to N_t users for transmission using multi-user beamforming. The parameter B, which is an offline design parameter, allows the system designer to choose the desired mix of multi-user diversity and CSI accuracy: a small value of B emphasizes multi-user diversity over CSI accuracy, whereas CSI is emphasized if a large value of B is chosen.

In a real system, this optimization can be interpreted as determining the appropriate grouping of mobiles in frequency and/or time, as illustrated in the earlier example. It is important to realize that the problem considered here is an *offline* optimization, meaning that the per-user feedback rate is decided beforehand for a given T_{fb}, SNR and N_t, and does not vary dynamically from one coherence block to another (i.e., B is a deterministic function of T_{fb}, SNR and N_t). Considering dynamic optimization would only further improve the performance and importance of this approach, but we only consider offline optimization in this work.

In the example introduced in Figure 3.1, $T_{\text{fb}} = 100$ bits and Design 1 has 25 users feeding back $B = 4$ bits of information each for each band, thereby offering the BS many users to select from (more multi-user diversity), albeit with limited CSI accuracy. On the other hand, Design 2 has 5 users feeding back information per band which reduces the multi-user diversity available, but each of the 5 users feed back $B = 20$ bits of information, which corresponds to much more accurate CSI. Assuming $N_t = 4$, $\mathsf{SNR} = 10$ dB, ZF beamforming and greedy user selection, Design 1 achieves a sum rate of 4.67 bps/Hz (per band), while Design 2 achieves a much higher sum rate of 9.97 bps/Hz. Clearly, choosing the wrong value of B can lead to a substantial sum rate loss.

By comparing the sum rates of different beamforming and user selection schemes at different values of B, we reach the following simple but striking conclusion: for almost any number of antennas N_t, average SNR, and feedback budget T_{fb}, *sum rate is maximized by choosing B (feedback bits per user) such that near-perfect CSI is obtained for each of the T_{fb}/B users that do feedback.* In other words, we find that accurate CSI is more valuable than multi-user diversity.

For the above comparison, we consider commonly proposed RBF-based strategies and ZF with greedy user selection, although we find that our basic result holds even

when other beamforming and user selection schemes are included. Further, we find that ZF generally outperforms RBF, which is rather surprising in the context of prior work on schemes with a very small per-user feedback load. For example, RBF achieves a sum rate that scales with the number of users in the same manner as the perfect-CSI sum rate [17]. Conventional wisdom has been that RBF could compensate for coarse feedback through multi-user diversity and outperform ZF if there were enough users. But on the contrary, we find that RBF achieves a significantly smaller sum rate than a ZF-based system with highly accurate CSI, when both systems have the same aggregate feedback load, T_{fb} bits. This is true even when T_{fb} is extremely large, in which case the number of users feeding back under RBF is also very large, and thus multi-user diversity is plentiful. Because much of our work is supported by numerical results, the associated MATLAB code has been made available online [57].

3.1 Prior Work on Limited Feedback with Many Users

While there already exists a large body of work focusing on ZF, RBF and Per unitary basis stream user and rate control (PU^{2}RC) [58][59] for the MIMO downlink, we believe that the questions considered in our work have not be addressed before, and are critical with respect to maximizing the sum rate. Prior work has compared ZF and PU^{2}RC assuming a fixed number of per-user feedback bits and users [59], and it is shown that for certain combinations of bits and users, PU^{2}RC outperforms ZF. As we shall see, our findings are quite different because we allow additional flexibility in terms of choosing the per-user feedback rate subject to a constraint on the aggregate feedback load. Comparisons with a fixed per-user feedback rate make sense for wireless standards that are currently being finalized and lack the flexibility to vary per-user feedback, however, we argue that this results in a significant loss in sum rate, and that future standards should certainly consider feedback from an aggregate rather than per-user perspective, with per-user feedback chosen optimally.

A closely related work is [60], where the tradeoff between multi-user diversity and accurate CSI is studied in the context of two-stage feedback. In the first stage all users feed back coarse estimates of their channel, based on which the transmitter runs a selection algorithm to select N_t users who feed back more accurate channel quantization

during the second feedback stage, and the split of the feedback budget between the two stages is optimized. Our work differs in that we consider only a *single stage* approach, and more importantly in that we optimize the number of users (randomly selected) who feed back accurate information rather than limiting this number to N_t. Indeed, this optimization is precisely why our approach shows such large gains over simple RBF or unoptimized ZF.

There has also been related work on systems with *channel-dependent* feedback, in which each user determines whether or not to feed back on the basis of its current channel condition (i.e., channel norm and quantization error) [59][61][62][63][64]. As a result, the BS does not *a priori* know who feeds back for each coherence block, and thus there is a random-access component to the feedback. Channel-dependent feedback intuitively appears to provide an advantage because only users with good channels feed back. Although some of this prior work has considered aggregate feedback load (c.f., [16]), that work has not considered optimization of B, the per-user feedback load, as we do here for channel-independent feedback. We are currently investigating the per-user optimization for channel-dependent feedback and our preliminary results actually reinforce the basic conclusions of the present work. However, this is beyond the scope of this work and we consider only channel-independent feedback here (meaning the users who do feed back are arbitrary in terms of their channel conditions).

3.2 Dealing with Large Number of Users

The channel model is as defined in Section 2, with the exception that we allow $K > N_t$ instead of requiring $K = N_t$. We mainly focus on digital feedback for this chapter, and the ignore effects of receive training in the feedback channel. We may use the results obtained in Chapter 2 to argue that our main conclusion will not be affected greatly by these assumptions, and we discuss this further in Section 3.6.

As described in Section 2.3.3, each UT quantizes the channel $\mathbf{h}_k$ to $\widehat{\mathbf{h}}_k$ using B bits. In addition, we assume that each user feeds back a single real number, which can be the channel norm or some other Channel Quality Indicator (CQI). The feed back of the CQI becomes important for $K > N_t$, as the BS may need to select only a subset of the K users for transmission, and may use the CQI information to make this selection.

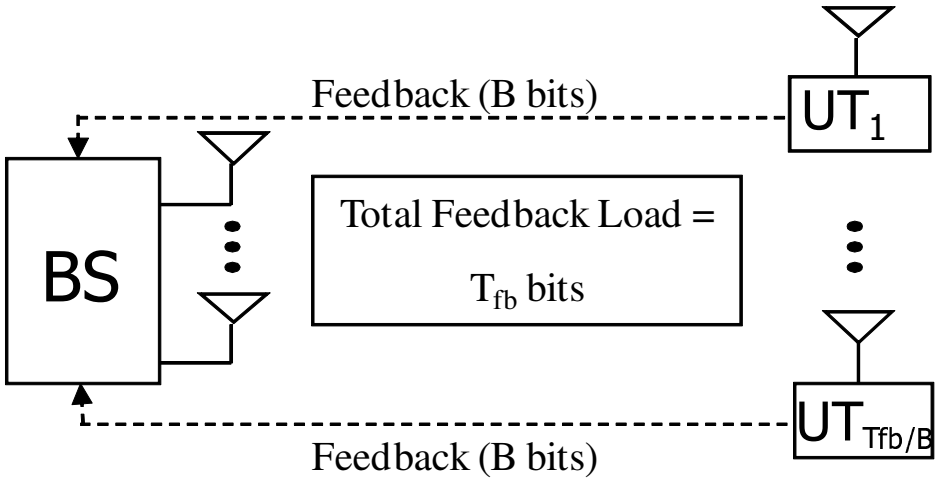

Figure 3.2: Feedback of CSI with many users

We assume that this CQI for each UT is known perfectly to the BS, i.e., it is not quantized, and thus CQI feedback is not included in the feedback budget; this effect of this simplification is discussed in Section 3.6.2.

For a total aggregate feedback load of T_{fb} bits, we are interested in the sum rate (of the different feedback/beamforming strategies described later in this section) when T_{fb}/B users feed back B bits each. The T_{fb}/B users who feed back are arbitrarily selected from a larger user set. Furthermore, in our block fading setting, only those users who feed back in a particular block/coherence time are considered for transmission in that block; in other words, we are limited to transmitting to a subset of only the T_{fb}/B users.

There are many schemes proposed for the MIMO downlink, and investigating all of these would be beyond the scope of this work. However, we believe that ZF and PU^{2}RC represent and capture the two basic ideas associated with most MIMO downlink strategies: that of exploiting accurate per-user CSI, and that of exploiting multi-user diversity, respectively. Further, ZF and PU^{2}RC have received a lot of attention in the research community, and we have therefore chosen to analyze these.

3.2.1 Zero-Forcing Beamforming with User Selection

We assume Zero-Forcing (ZF) beamforming with the channel norm $||\mathbf{h}_k||$ being fed back perfectly as the CQI. The BS then uses the greedy user selection algorithm described

in [10], adopted to imperfect CSI by treating the vector $||\mathbf{h}_k|| \cdot \widehat{\mathbf{h}}_k$ as if it were user k's true channel, with uniformly allocated power (the same assumption as Chapter 2).

We denote the indices of selected users by $\Pi(1), \ldots, \Pi(n)$, where $n \leq N_t$ is the number of users selected for transmission in any given frame. By the ZF criterion, the unit-norm beamforming vector $\widehat{\mathbf{v}}_{\Pi(k)}$ for user $\Pi(k)$ is chosen in the direction of the projection of $\widehat{\mathbf{h}}_{\Pi(k)}$ on the nullspace of $\{\widehat{\mathbf{h}}_{\Pi(j)}\}_{j \neq k}$. Although ZF beamforming is used, there is residual interference because the beamformers are based on imperfect CSI. The (post-selection) signal-to-interference-and-noise ratio (SINR) for selected user $\Pi(k)$ is

$$\mathsf{SINR}_{\Pi(k)} = \frac{\frac{\mathsf{SNR}}{n}||\mathbf{h}_{\Pi(k)}||^2 \cos^2 \angle(\mathbf{h}_{\Pi(k)}, \widehat{\mathbf{v}}_{\Pi(k)})}{1 + \frac{\mathsf{SNR}}{n}||\mathbf{h}_{\Pi(k)}||^2 \sum\limits_{j \neq k} \cos^2 \angle(\mathbf{h}_{\Pi(k)}, \widehat{\mathbf{v}}_{\Pi(j)})}, \tag{3.1}$$

and the corresponding sum rate is $\sum_{k=1}^{n} \log_2(1 + \mathsf{SINR}_{\Pi(k)})$.

$$R_{\mathrm{ZF}}\left(\mathsf{SNR}, N_t, \frac{T_{\mathrm{fb}}}{B}, B\right) = \mathbb{E}\sum_{k=1}^{n} \log_2\left(1 + \frac{\frac{\mathsf{SNR}}{n}||\mathbf{h}_{\Pi(k)}||^2 \cos^2\left(\angle(\mathbf{h}_{\Pi(k)}, \widehat{\mathbf{v}}_{\Pi(k)})\right)}{1 + \frac{\mathsf{SNR}}{n}||\mathbf{h}_{\Pi(k)}||^2 \sum\limits_{j \neq k} \cos^2\left(\angle(\mathbf{h}_{\Pi(k)}, \widehat{\mathbf{v}}_{\Pi(j)})\right)}\right) \tag{3.2}$$

For the sake of analysis and ease of simulation, we continue to assume random codebooks, as described in Section [24]. However, in Section 3.6.1, we show that our conclusions can be extended to other quantization schemes. In [65] it is shown that this sum rate with N_t randomly selected users is very sensitive to the CSI accuracy. With $N_t = 4$ and $\mathsf{SNR} = 10$ dB, for example, $B = 10$ corresponds to a sum rate loss of 4 bps/Hz (relative to perfect CSI) and 17 bits are required to reduce this loss to 1 bps/Hz.

3.2.2 Random Beamforming and PU2RC

Thus far, we have focused on analyzing ZF beamforming and a few variations of ZF. However, more options become attractive when we have $K > N_t$, especially from the perspective of having limited feedback resources. We consider here two alternatives to ZF that are conventionally considered to be attractive methods of beamforming for practical systems with many users. These alternatives are attractive to their very low computational complexity, and the fact that they can function well with a very small amount of per-user feedback, if there are a large number of users in the cell.

Random beamforming (RBF) was proposed in [17][66], wherein each user feeds back $\log_2 N_t$ bits along with one real number. In this case, there is a common quantization codebook $\mathcal{C}$ consisting of N_t orthogonal unit vectors and quantization is performed according to (2.34). In addition to the quantization index, each user feeds back a real number representing its SINR. If $\mathbf{w}_m$ $(1 \leq m \leq N_t)$ is the selected quantization vector for user k, then SINR_k is given by

$$\frac{\frac{\mathsf{SNR}}{N_t}|\mathbf{h}_k^{\mathsf{H}}\mathbf{w}_m|^2}{1+\frac{\mathsf{SNR}}{N_t}\sum\limits_{n\neq m}|\mathbf{h}_k^{\mathsf{H}}\mathbf{w}_n|^2} = \frac{||\mathbf{h}_k||^2\cos^2\angle\mathbf{h}_k,\mathbf{w}_m}{\frac{N_t}{\mathsf{SNR}}+||\mathbf{h}_k||^2\sin^2\angle\mathbf{h}_k,\mathbf{w}_m}. \tag{3.3}$$

After receiving the feedback, the BS selects the user with the largest SINR on each of the N_t beams $(\mathbf{w}_1,\ldots,\mathbf{w}_{N_t})$, and beamforming is performed along these same vectors.[2]

The main attraction here is that, since the beamforming vectors are decided beforehand, each user can accurately compute the SINR and feed this back to the BS, which consists of only a single real number. It is shown in [17] that this method achieves full multiplexing gain as the number of users K goes to infinity, and has a sum rate that converges in ratio to the maximum achievable rate as $K \to \infty$.

Per unitary basis stream user and rate control (PU^{2}RC), proposed in [58] (a more widely available description can be found in [59]), is a generalization of RBF in which there is a common quantization codebook $\mathcal{C}$ consisting of $2^{B-\log_2 N_t}$ 'sets' of orthogonal codebooks, where each orthogonal codebook consists of N_t orthogonal unit vectors, and thus a total of 2^B vectors. Quantization is again performed according to (2.34), and each user feeds back the same SINR statistic as in RBF. User selection is performed as follows: for each of the orthogonal sets the BS repeats the RBF user selection procedure and computes the sum rate (where the per-user rate is $\log_2(1+\mathsf{SINR})$), after which it selects the orthogonal set with the highest sum rate. If $B = \log_2 N_t$, there is only a single orthogonal set and the scheme reduces to ordinary RBF.

For each of the two strategies ZF and PU^{2}RC, we determine an optimal B that maximizes the respective sum rate and compare the resulting rates. PU^{2}RC and ZF differ in that the latter strategy involves a dedicated downlink training phase, while the former

[2] Because the SINR in (3.3) is monotonically decreasing in the sine of the angle between the channel and the quantized vector, quantizing according to (2.34) is equivalent to quantizing to the beam that maximizes SINR.

does not. Also, PU^{2}RC is restricted to selecting users within one of the orthogonal sets and thus has very low complexity, whereas the described ZF technique has no such restriction. We show, however, in Section 3.6.1, that our results hold even when ZF with selection strategies of comparable complexity is used.

3.3 Analysis of Beamforming Strategies

3.3.1 Analysis of Zero-Forcing Beamforming

Let $R_{\mathrm{ZF}}\left(\mathsf{SNR}, N_t, \frac{T_{\mathrm{fb}}}{B}, B\right)$ be the sum rate for a system using ZF with N_t antennas at the transmitter, signal-to-noise ratio SNR, and $\frac{T_{\mathrm{fb}}}{B}$ users each feeding back B bits. From Section 3.2.1, we have Equation 3.2, where the expectation is carried out over channels, as well as random codebooks. No closed form for this expression is known to exist, even in the case of perfect CSI, but this quantity can be easily computed via Monte Carlo simulation. We are interested in the number of feedback bits per user $B_{\mathrm{ZF}}^{\mathrm{OPT}}\left(\mathsf{SNR}, N_t, T_{\mathrm{fb}}\right)$ that maximizes this sum rate for a total feedback budget of T_{fb}:

$$B_{\mathrm{ZF}}^{\mathrm{OPT}}(\mathsf{SNR}, N_t, T_{\mathrm{fb}}) \triangleq \underset{\log_2 N_t \leq B \leq \frac{T_{\mathrm{fb}}}{N_t}}{\operatorname{argmax}} R_{\mathrm{ZF}}\left(\mathsf{SNR}, N_t, \frac{T_{\mathrm{fb}}}{B}, B\right).$$

Although this optimization is not analytically tractable, it is well behaved and can be meaningfully understood (further, Monte-Carlo simulations combined with a line-search can be used to numerically compute the optimal point).[3]

Consider first Figure 3.3, where the sum rate $R_{\mathrm{ZF}}\left(\mathsf{SNR}, N_t, \frac{T_{\mathrm{fb}}}{B}, B\right)$ is plotted versus B for 2 and 4-antenna systems for various values of SNR and T_{fb}. Based on this plot it is immediately evident that the sum rate increases very rapidly with B, and that the rate-maximizing $B_{\mathrm{ZF}}^{\mathrm{OPT}}$ is very large, e.g., in the range $15-20$ and $20-25$ for $N_t = 4$ at 5 and 10 dB, respectively. Both of these observations indicate a strong preference for accurate CSI over multi-user diversity.

The achievable sum rate with ZF and user selection is considered in [67], where the behavior of the sum rate is characterized by identifying three regimes: the *large user regime*, the *interference limited regime*, and the *high resolution regime*. When the

[3] The optimization can alternatively be posed in terms of the numbers of users who feedback, i.e., K users feedback T_{fb}/K bits each. However, it turns out to be much more insightful to consider this in terms of B, the feedback bits per user.

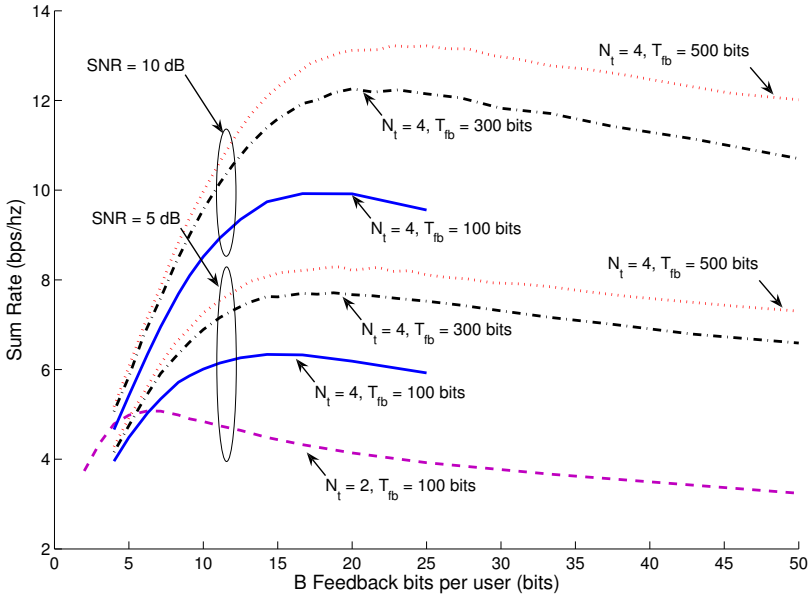

Figure 3.3: Sum rate Vs. Feedback load for Zero-forcing

number of users feeding back is large, i.e., T_{fb}/B is large, the system operates in the large user regime, and the rate achievable with SINR feedback is detailed in [67, Eq. (41)]. In that regime, the achievable rate increases with the quantity $2^B(T_{\text{fb}}/B)$, and thus increasing the per-user feedback by one bit is equivalent to maintaining the per-user feedback, but doubling the number of users. This effect is seen in Figure 3.4, where increasing the user pool from 10 to 100 results in a large increase in sum rate, but the rate grows very slowly with the number of users thereafter. For instance, the sum rate with 2000 users feeding back 15 bits each is the same as with 4000 users feeding back 14 bits each. Because $2^B(T_{\text{fb}}/B)$ is increasing in B (for $B > 2$), the sum rate is increasing in B within the large user regime when the aggregate feedback load is fixed, and thus it is sub-optimal to operate in the large user regime. As B increases, T_{fb}/B decreases, thus eventually driving the system away from the large user regime and into the high resolution regime. We will see shortly that it is similarly sub-optimal to remain in the interference limited regime as well, and hence it is important to understand the behavior of sum rate in the high resolution regime to truly understand the optimization problem.

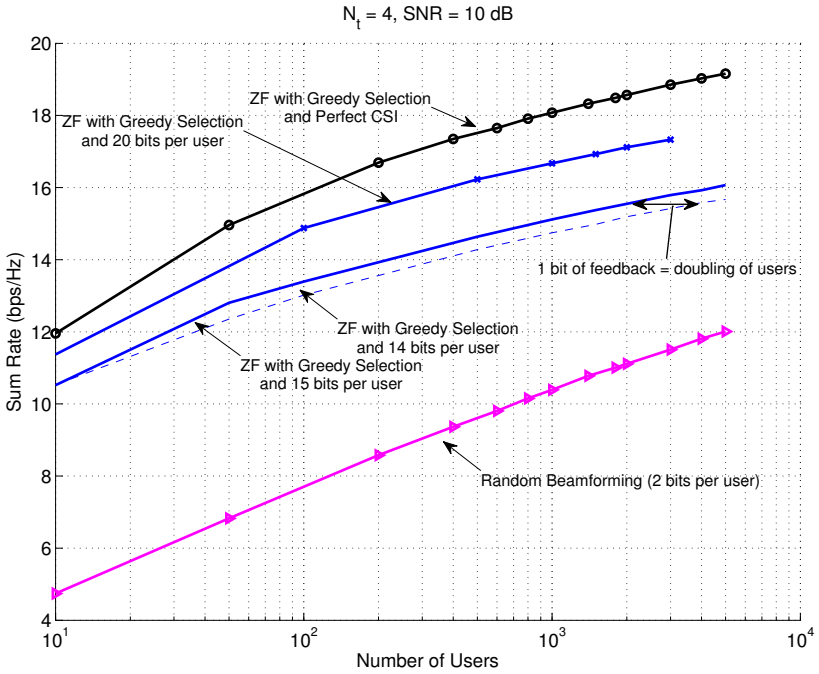

Figure 3.4: Sum rate Vs. Number of Users. Aggregate feedback is not held constant.

Unfortunately, the characterization of the sum rate for the high resolution regime presented in [67, Eq. (47)] is not accurate enough to capture the behavior for the purposes of our optimization (and results in a trivial optimal point). Thus, in order to more precisely understand this behavior, we introduce the following sum rate approximation, denoted by $\widetilde{R}_{\mathrm{ZF}}\left(\mathsf{SNR}, N_t, \frac{T_{\mathrm{fb}}}{B}, B\right)$, given by:

$$N_t \ \log_2\left[1+\frac{\left(\frac{\mathsf{SNR}}{N_t}\right)\log\left(\frac{T_{\mathrm{fb}}N_t}{B}\right)}{1+\left(\frac{\mathsf{SNR}}{N_t}\right)2^{-\frac{B}{N_t-1}}\log\left(\frac{T_{\mathrm{fb}}N_t}{B}\right)}\right], \tag{3.4}$$

where $R_{\mathrm{ZF}} \approx \widetilde{R}_{\mathrm{ZF}}$. This approximation is obtained from the expression for R_{ZF} in (3.2) by (a) assuming that the maximum number of users are selected (i.e., $n = N_t$), (b) replacing each $\cos^2\left(\angle(\mathbf{h}_{\Pi(k)}, \widehat{\mathbf{v}}_{\Pi(j)})\right)$ in the SINR denominator with its expected value $2^{-\frac{B}{N_t-1}}/(N_t-1)$ [65, Lemma 2], and (c) approximating the $\cos^2\left(\angle(\mathbf{h}_{\Pi(k)}, \widehat{\mathbf{v}}_{\Pi(k)})\right)$ term in the SINR numerator with unity. Further, $||\mathbf{h}_{\Pi(k)}||^2$ is treated as the largest channel norm among $\frac{T_{\mathrm{fb}}}{B}$ users, which stochastically dominates the maximum of $T_{\mathrm{fb}}N_t/B$ random

variables with $\Gamma(1,1)$ distribution, the latter having an expected value which behaves as $\log(T_{\text{fb}}N_t/B)$, for large T_{fb}.

The approximation (3.4) is not meant to accurately capture the sum rate, but rather to capture the effect of B, and we will see that this captured with reasonable accuracy. Further, when the number of users feeding back is large, $|\mathbf{h}_{\Pi(k)}^{\mathsf{H}}\widehat{\mathbf{v}}_{\Pi(k)}|^2$ indeed behaves like the logarithm of the number of users available for selection (see [67]) and (c) becomes valid with high probability. The value of n is difficult to characterize, but when the number of users feeding back is large, we generally expect to select N_t users (except, when the SNR is very small). Hence, (b) is merely Jensen's inequality, and (3.4) becomes a lower bound to the sum rate when the number of users is large, and SNR is large enough to warrant selection of N_t users.

We first use the approximation to explain the rapid sum rate increase with B. From (3.4) we see that increasing B by $N_t - 1$ bits reduces the interference power by a factor of 2. As long as the interference power is significantly larger than the noise power, this leads to (approximately) a 3 dB SINR increase and thus a N_t bps/Hz sum rate increase. When the system is interference limited, the two instances of 1 in (3.4) can be dropped, which gives $\widetilde{R}_{\text{ZF}}\left(\mathsf{SNR}, N_t, \frac{T_{\text{fb}}}{B}, B\right) \approx BN_t/(N_t-1)$, i.e., sum rate increases almost linearly with B for smaller values of B, consistent with Fig. 3.3, and the BS should take advantage of the maximum possible CSI accuracy that it can gather.

$$\widetilde{B}_{\text{ZF}}^{\text{OPT}}\left(\mathsf{SNR}, N_t, T_{\text{fb}}\right) \quad \sim \quad (N_t-1)\log_2\frac{\mathsf{SNR}}{N_t} + (N_t-1)\log_2\frac{L}{N_t} + (N_t-1)\log_2\log\frac{L\mathsf{SNR}}{N_t} \tag{3.5}$$

It is clear that accurate CSI is strongly preferred to multi-user diversity in the range of B for which sum rate increases roughly linearly with B. However, we see from Figure 3.3 that increasing B beyond a point actually decreases sum rate. To understand the desired combination of CSI and multi-user diversity at $B_{\text{ZF}}^{\text{OPT}}$, in Figure 3.5 the sum rate $R_{\text{ZF}}\left(\mathsf{SNR}, N_t, \frac{T_{\text{fb}}}{B}, B\right)$ as well as the perfect CSI sum rate for the same number of users (i.e., $\frac{T_{\text{fb}}}{B}$ users) $R_{\text{ZF}}\left(\mathsf{SNR}, N_t, \frac{T_{\text{fb}}}{B}, \infty\right)$ are plotted versus B for a system with $N_t = 4$, $T_{\text{fb}} = 300$ bits and $\mathsf{SNR} = 10$ dB. Motivated by [65, Theorem 1] (see Section 3.2.1

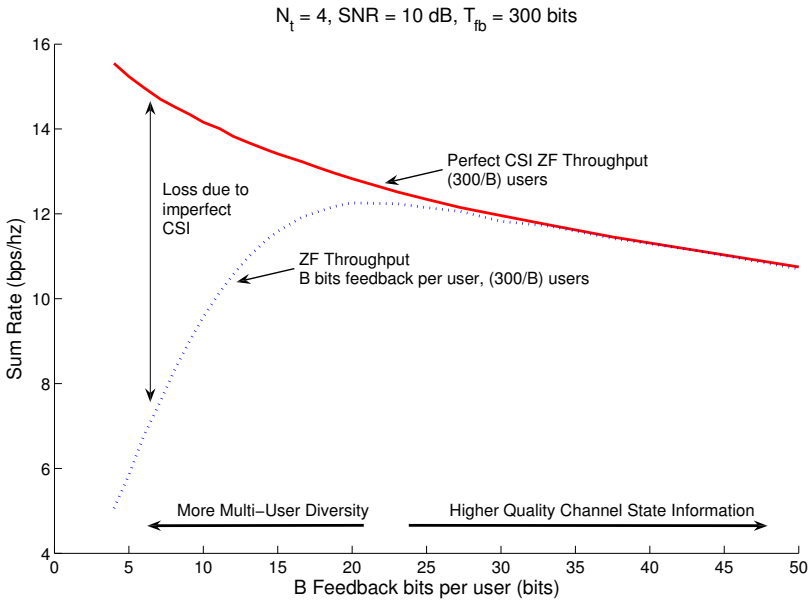

Figure 3.5: Sum rate Vs. Feedback load for Zero-forcing

for discussion), we approximate the sum rate by the perfect CSI sum rate minus a multi-user interference penalty term:

$$R_{\mathrm{ZF}}\left(\mathsf{SNR}, N_t, \frac{T_{\mathrm{fb}}}{B}, B\right) \approx R_{\mathrm{ZF}}\left(\mathsf{SNR}, N_t, \frac{T_{\mathrm{fb}}}{B}, \infty\right) - N_t \ \log_2\left(1 + \frac{\mathsf{SNR}}{N_t} 2^{-\frac{B}{N_t - 1}} \log \frac{T_{\mathrm{fb}} N_t}{B}\right) \tag{3.6}$$

This penalty term reasonably approximates the loss due to imperfect CSI which is indicated in Figure 3.5. In the figure we see that for $B \geq 25$ the sum rate curves for perfect and imperfect CSI essentially match and thus the penalty term in (3.6) is nearly zero. As a result, it clearly does not make sense to increase B beyond 25 because doing so reduces the number of users but does not provide a measurable CSI benefit. Keeping this in mind, the most interesting observation gleaned from Figure 3.5 is that $B_{\mathrm{ZF}}^{\mathrm{OPT}}$ corresponds to a point where the loss due to imperfect CSI is very small. In other words, it is optimal to operate at the point where effectively the maximum benefit of accurate CSI has been reaped.

Although $B_{\mathrm{ZF}}^{\mathrm{OPT}}$ is quite large for many parameter choices, it appears to not be

particularly dependent on the total feedback budget T_{fb}, but is very sensitive to (and increasing with) SNR and N_t. We explain this by computing the optimal B corresponding to (3.4), that is, $B_{\text{ZF}}^{\text{OPT}}(\mathsf{SNR}, N_t, T_{\text{fb}}) \approx \widetilde{B}_{\text{ZF}}^{\text{OPT}}(\mathsf{SNR}, N_t, T_{\text{fb}})$, where:

$$\widetilde{B}_{\text{ZF}}^{\text{OPT}}(\mathsf{SNR}, N_t, T_{\text{fb}}) \triangleq \underset{\log_2 N_t \leq B \leq \frac{T_{\text{fb}}}{N_t}}{\text{argmax}} \widetilde{R}_{\text{ZF}}\left(\mathsf{SNR}, N_t, \frac{T_{\text{fb}}}{B}, B\right).$$

The approximation is concave in B, and thus the following fixed point characterization of $\widetilde{B}_{\text{ZF}}^{\text{OPT}}$ is obtained by setting the derivative of $\widetilde{R}_{\text{ZF}}\left(\mathsf{SNR}, N_t, \frac{T_{\text{fb}}}{B}, B\right)$ to zero:

$$\frac{\mathsf{SNR}}{N_t} 2^{-\frac{\widetilde{B}_{\text{ZF}}^{\text{OPT}}}{N_t - 1}} \frac{\widetilde{B}_{\text{ZF}}^{\text{OPT}} \log 2}{N_t - 1} \left(\log \frac{T_{\text{fb}} N_t}{\widetilde{B}_{\text{ZF}}^{\text{OPT}}}\right)^2 = 1. \tag{3.7}$$

This quantity is easily computed numerically, but a more analytically convenient form is found by rewriting (3.7) as:

$$\widetilde{B}_{\text{ZF}}^{\text{OPT}}(\mathsf{SNR}, N_t, T_{\text{fb}}) = -\frac{N_t - 1}{\log 2} W_{-1}\left(-\frac{N_t}{\mathsf{SNR}} \frac{1}{L}\right) \tag{3.8}$$

where $L = \left(\log T_{\text{fb}} N_t / (\widetilde{B}_{\text{ZF}}^{\text{OPT}})\right)^2$ and $W_{-1}(\cdot)$ is branch -1 of the LambertW function [68].[4] Using the asymptotic expansion [68, Equation 4.19] for $W_{-1}(-x)$ and small $x > 0$ in (3.8), we have Equation 3.5.

By repeatedly applying the asymptotic expansion of $W_{-1}(\cdot)$ to the occurrences of L in (3.5), we have that $\widetilde{B}_{\text{ZF}}^{\text{OPT}}(\mathsf{SNR}, N_t, T_{\text{fb}})$ varies as $\text{O}(\log\log T_{\text{fb}})$, $(N_t - 1)\log_2 \mathsf{SNR} + O(\log\log N_t)$ and $(N_t - 1)\log_2(\mathsf{SNR}/N_t) + O(\log\log\log \mathsf{SNR})$ for large T_{fb}, N_t and SNR, respectively. These scaling results are consistent with the scaling results without user selection or optimization of B, presented in [65].

In Figures 3.6 and 3.7, $B_{\text{ZF}}^{\text{OPT}}(\mathsf{SNR}, N_t, T_{\text{fb}})$ and the approximation $\widetilde{B}_{\text{ZF}}^{\text{OPT}}(\mathsf{SNR}, N_t, T_{\text{fb}})$ are plotted versus T_{fb} and SNR_{dB}, respectively (we restrict ourselves to values of feedback bits such that the number of users feeding back is an integer). In both figures we see that the approximation is quite accurate, and that the behavior agrees with the scaling relationships described previously.

[4] In order for the LambertW function to produce a real value, the argument should be larger than $-\frac{1}{e}$. This condition is satisfied for operating points of interest.

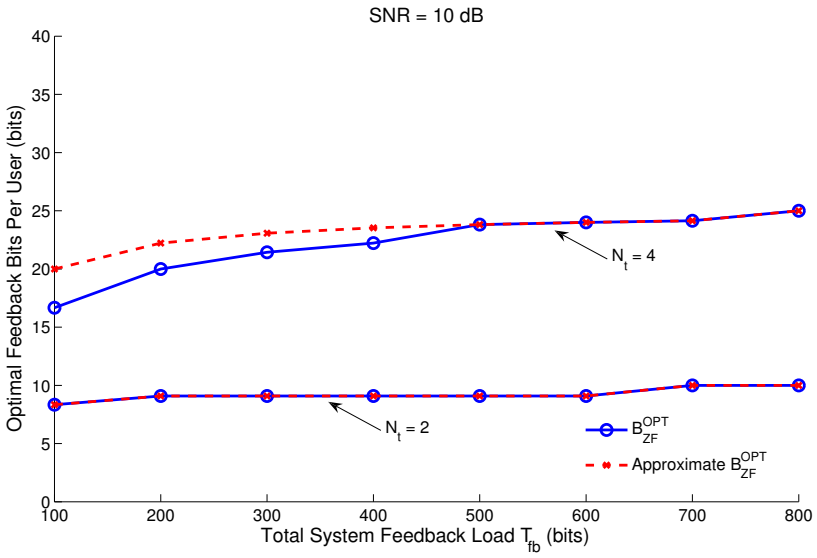

Figure 3.6: Behavior of $B_{\mathrm{ZF}}^{\mathrm{OPT}}(\mathsf{SNR}, N_t, T_{\mathrm{fb}})$ with T_{fb}

3.3.2 Analysis of Random Beamforming and PU2RC Beamforming

Per unitary basis stream user and rate control (PU^{2}RC) generalizes RBF to more than $\log_2 N_t$ feedback bits per user. A common quantization codebook, consisting of $2^B/N_t$ 'sets' of N_t orthogonal vectors each, is utilized by each user. A user finds the best of the 2^B quantization vectors, according to (2.34), and feeds back the index of the set ($B - \log_2 N_t$ bits) and the index of the vector/beam in that set ($\log_2 N_t$ bits). Although the quantization codebooks for ZF and PU^{2}RC are slightly different, the key difference is in user selection. While ZF allows for selection of *any* subset of (up to) N_t users, the low-complexity PU^{2}RC procedure described in Section 3.2.2 constrains the BS to select a set of up to N_t users from one of the $2^B/N_t$ sets.

As a result of this difference, a very different conclusion is reached when we optimize the per-user feedback load B for PU^{2}RC: we find that $B = \log_2 N_t$ (i.e., RBF) is near-optimal and thus the optimization provides little advantage. Sum rate is plotted versus B (for PU^{2}RC) in Figure 3.8. Very different from ZF, the sum rate does not increase rapidly with B for small B, and it begins to decrease for even moderate values of B.

If B is too large, the number of orthogonal sets $2^B/N_t$ becomes comparable to the number of users T_{fb}/B and thus it is likely that there are fewer than N_t users on every

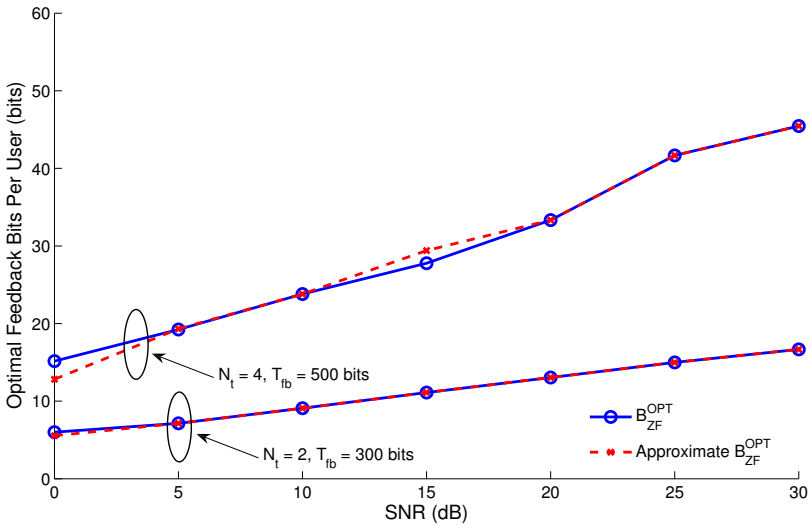

Figure 3.7: Behavior of $B_{\mathrm{ZF}}^{\mathrm{OPT}}(\mathsf{SNR}, N_t, T_{\mathrm{fb}})$ with SNR

set (there are on average $\frac{T_{\mathrm{fb}}N_t}{B2^B}$ users per set). For example, if $T_{\mathrm{fb}} = 500$ and $B = 8$, there are 2^6 orthogonal sets and 40 users and thus less than a user per set on average. Hence, the BS likely schedules much fewer than N_t users, thereby leading to a reduced sum rate. For moderate values of $B > \log_2 N_t$, there are a sufficient number of users per set but nonetheless this 'thinning' of users is the limiting factor. As B increases the quantization quality increases, but because there are only $\frac{T_{\mathrm{fb}}N_t}{B2^B}$ users per set (on average) the multi-user diversity (in each set) decreases sharply, so much so that the rate per set in fact decreases with B. (For ZF there is also a loss in multi-user diversity as B is increased, but the number of users is inversely proportional to B, whereas here it is inversely proportional to $B2^B$.) The BS does choose the best set (amongst the $2^B/N_t$ sets), but this is not enough to compensate for the decreasing per-set rate. Hence, we find that PU^{2}RC strongly prefers multi-user diversity.

3.4 Comparison of Beamforming Strategies

In Figure 3.9, the sum rates of ZF and PU^{2}RC (with randomly generated codebooks) are compared for various values of SNR, T_{fb} and N_t; for each strategy, B has been optimized

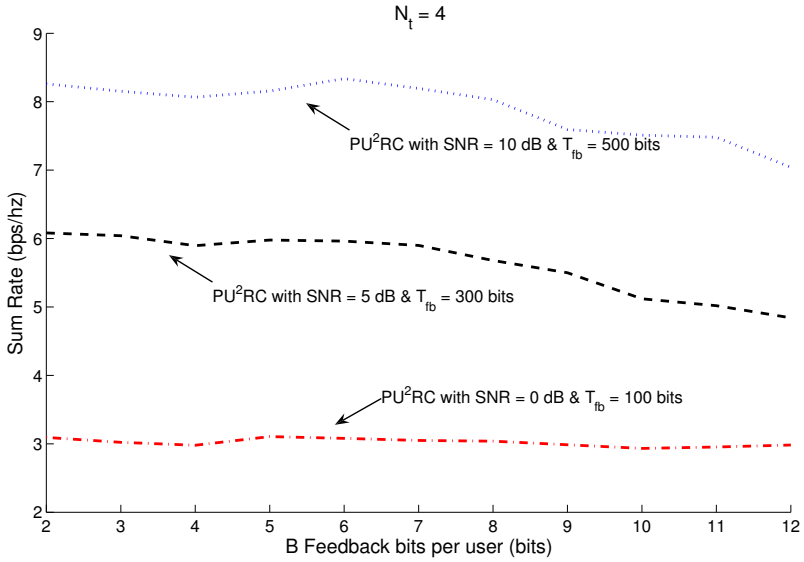

Figure 3.8: Sum rate vs B for PU^{2}RC with $N_t = 4$

separately as discussed in Sections 3.2.1 and 3.2.2, respectively. It is seen that ZF maintains a significant advantage over PU^{2}RC for $N_t = 4$. At small N_t, both schemes perform similarly, but ZF maintains an advantage. Also included, is the performance of RBF/PU^{2}RC with the following enhancements: (a) the BS may choose to schedule fewer than N_t beams (as proposed in [18]), (b) power is near-optimally (rather than uniformly) allocated across users using the iterative procedure proposed in [18], and (c) an optimal DFT-based codebook is designed, as suggested in [69]. Enhancements (a) and (b) require finer (if not perfect) knowledge of the channels and is hence an upper bound on what can be achieved with RBF/PU^{2}RC. In spite of these enhancements, we see that the performance of ZF is superior, and the advantage of ZF increases extremely rapidly with N_t and SNR. Note the contrast with [59], where an unoptimized ZF system is found inferior to PU^{2}RC.

As optimized PU^{2}RC performs essentially the same as RBF (Section 3.2.2), this large gap in sum rate can be explained by contrasting RBF and optimized ZF. From [17], we have that the SINR of the k^{th} user (on a particular beam) under RBF has CDF $1 - \frac{e^{-x\frac{N_t}{\mathsf{SNR}}}}{(x+1)^{N_t-1}}$. By basic results in order statistics, the expectation of the maximum

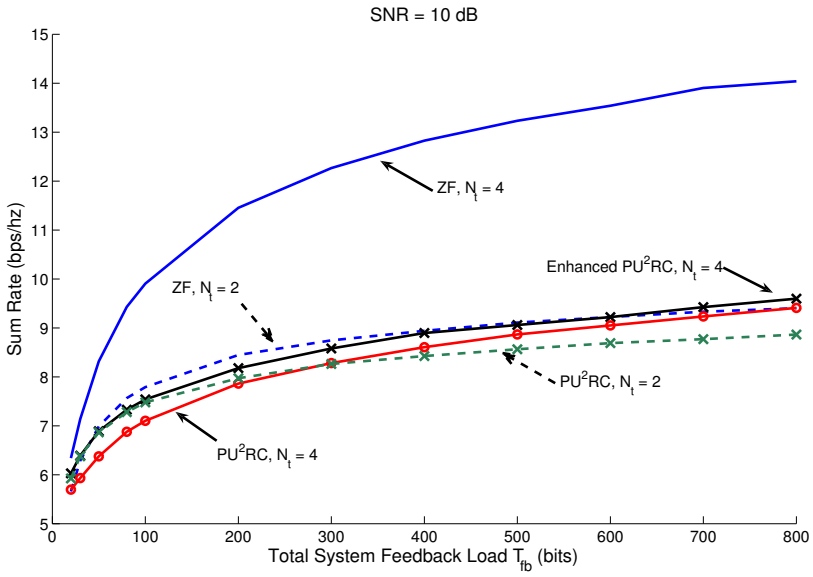

Figure 3.9: Sum rate of ZF vs. PU^{2}RC with optimized B

amongst K i.i.d. random variables is accurately approximated by the point at which the CDF equals $(K-1)/K$ [70]. Hence, in order to achieve a target SINR S, RBF requires about $K = \exp\left(\frac{SN_t}{\mathsf{SNR}}\right)(1+S)^{N_t-1}$ users. Setting $S = \frac{\mathsf{SNR}}{N_t}\log\frac{T_{\mathrm{ZF}}N_t}{B_{ZF}^{OPT}}$, which approximately describes the ZF SINR with a total feedback budget of T_{ZF} bits (while operating at near-perfect CSI, as described in Section 3.2.1), we see that RBF requires $K = \frac{T_{\mathrm{ZF}}N_t}{B_{ZF}^{OPT}}\left(1+\frac{\mathsf{SNR}}{N_t}\log\frac{T_{\mathrm{ZF}}N_t}{B_{ZF}^{OPT}}\right)^{N_t-1}$ users to match the rate achieved by optimized ZF. Equivalently, RBF requires $(\log_2 N_t)\frac{T_{\mathrm{ZF}}N_t}{B_{ZF}^{OPT}}\left(1+\frac{\mathsf{SNR}}{N_t}\log\frac{T_{\mathrm{ZF}}N_t}{B_{ZF}^{OPT}}\right)^{N_t-1}$ total bits to match the sum rate of optimized ZF with T_{ZF} bits. When $N_t = 4$, $\mathsf{SNR} = 5$ dB, RBF requires 5000 users (10000 total bits) in order to match the sum rate of ZF with only 300 bits. Clearly, it is impractical to consider RBF in such a setting, and the RBF bit requirement increases rapidly with T_{ZF}, N_t as well as SNR, making RBF increasingly impractical.

Although RBF uses a very small codebook, it may appear that this is compensated by the large number of users, as has been suggested in prior work [17], as it might be possible to select users that are well-aligned to one of the N_t quantization vectors/beamformers. To understand this, consider the *smallest* quantization error

amongst the $T_{\text{fb}}/\log_2 N_t$ users, which, due to independence of the channels, is effectively the same as the error of a single codebook of size $B = \log_2(T_{\text{fb}} N_t/\log_2 N_t)$. For example, with $N_t = 4$ and $T_{\text{fb}} = 300$ bits, the *best* quantization error is only as good as an 8-bit quantization. As we saw in Section 3.2.1, the sum rate is very sensitive to quantization error and multi-user diversity cannot compensate for this. Hence, the "large-user" advantage of RBF is never realized, even as T_{fb} grows.

3.5 Summary of Results for Many Users

In this chapter, we have considered the basic question of whether low-rate feedback/many user systems or high-rate feedback/limited user systems provide a larger sum rate in MIMO downlink channels. This question simplifies to a comparison between multi-user diversity (many users) and accurate channel information (high-rate feedback), and the surprising conclusion is that there is a very strong preference for accurate CSI. Multi-user diversity provides a throughput gain that is only double-logarithmic in the number of users who feed back, whereas the marginal benefit of increased per-user feedback is very large up to the point where the CSI is essentially perfect.

In closing, it is worth emphasizing that our results do not imply that multi-user diversity is inconsequential. On the contrary, multi-user diversity actually provides a significant benefit. However, the basic design insight is that feedback resources should first be used to obtain accurate CSI and only afterwards be used to exploit multi-user diversity. Given the increasing importance of multi-user MIMO in single-cell and multi-cell (i.e., network MIMO) settings, it seems that this point should be fully exploited in the design of future cellular systems.

3.6 Further Considerations

3.6.1 Complexity considerations

While comparing ZF and RBF, we have not explicitly compared the complexity requirements for implementing these two algorithms. Particularly, RBF is considered a popular choice for beamforming because (a) user selection can be performed with $O(N_t/\log N_t)$ complexity [17], compared to $O(N_t^3)$ complexity with ZF and greedy selection [10], and

(b) each user can quantize the channel with $O(N_t^2)$ complexity using a codebook that is uniform across users in the RBF scheme, compared to a worst-case exhaustive search of $O(N_t 2^{N_t})$ for an arbitrary vector codebook (these complexity calculations are expressed in terms of N_t, assuming T_{fb} and B grow linearly with N_t as per (3.5)). However, we show in this section that ZF-based selection and quantization methods that have complexity similar to RBF can still maintain the large advantage in sum rate.

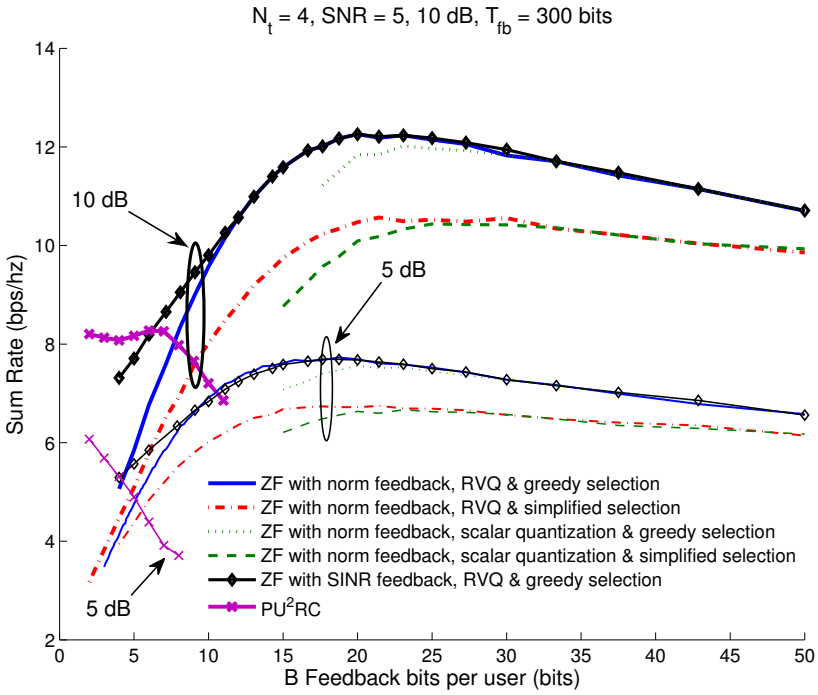

Figure 3.10: Sum rate of various user selection schemes with optimized B

We first consider the following "simplified" user selection algorithm for ZF while addressing (a): the BS computes the ZF rate while assuming that the users with the j largest channel norms are selected, for $j = 1, \ldots, N_t$, and then picks j that provides the largest sum rate. This simple algorithm involves just N_t sum rate computations. Figure 3.10 compares the sum rate for ZF with greedy and simplified selection, as well as RBF/PU^{2}RC. The selected user set with simplified selection is likely to have less orthogonal users than greedy selection and thus performs worse, but nonetheless is seen to outperform RBF/PU^{2}RC at the optimal operating point.

We address (b) using the the scalar quantization scheme proposed in [19] as an example, which independently quantizes the relative magnitudes and phases of each component of the channel vector with $O(N_t)$ complexity ($O(1)$ complexity per entry in the vector). From Figure 3.10, we see that scalar quantization provides a sum rate only slightly smaller than RVQ at the optimal point.[5] However, because CSI is strongly preferred to multi-user diversity, it is still worthwhile to operate at the "essentially perfect" CSI point, even with a suboptimal quantization codebook, and the performance with scalar quantization is still competitive. For large B, which is typically the preferred operating point, the same quantizer can be used by all users with small probability of the quantized vectors being the same, allowing for uniformity of codebooks across users. For small B, structured vector codebooks can be used (with low complexity due to the small size) to avoid quantizing different vectors to the same direction.

The simplified schemes presented here for ZF have slightly higher complexity at the BS and slightly lower complexity at the user terminal compared to RBF, and can be considered to be of similar complexity overall. We note that they may not be the best low-complexity algorithms, but they serve to illustrate that complexity considerations do not invalidate our main conclusion.

3.6.2 Channel Quality Indicator Feedback

Prior work has shown that CQI quantized to 3-4 bits (per user) is virtually the same as unquantized CQI [16][67], and we have hence thus far considered only quantization of the channel direction. However, if we account for CQI feedback in the budget, the actual per-user feedback is the B directional bits in addition to the CQI bits, meaning that by ignoring CQI bits we have artificially inflated the number of users. If the CQI bits are accounted for, strategies that utilize few directional bits become even less attractive, i.e., CQI bits make multi-user diversity more expensive, and thus our basic conclusion is unaffected. For example, with $N_t = 4$, $T_{\text{fb}} = 300$ bits and $\mathsf{SNR} = 10$ dB, ZF with unquantized CQI (i.e., not accounting for CQI feedback) is optimized with 13 users and $B = 23$, while ZF with CQI quantized to 4 bits per user is optimized with 10 users and

[5] The expected distortion of an idealized codebook that achieves the quantization upper bound in [71] is only a factor of $\frac{N_t-1}{N_t}$ smaller than with RVQ, and thus it is also not possible to greatly improve upon RVQ either.

$B = 26$, i.e., multi-user diversity is even less important in the latter case.

An alternative CQI is the expected SINR, as discussed in [67]: $\frac{||\mathbf{h}_k||^2 \cos^2\left(\angle(\mathbf{h}_k, \widehat{\mathbf{h}}_k)\right)}{\frac{N_t}{\mathsf{SNR}} + ||\mathbf{h}_k||^2 \sin^2\left(\angle(\mathbf{h}_k, \widehat{\mathbf{h}}_k)\right)}$, which is similar to the CQI in RBF/PU^{2}RC. This allows the BS to select users that have not only large channels, but also small quantization errors. However, as presented earlier, the system preferably operates in the high resolution regime, as described in [67], and the advantage of SINR feedback over channel norm feedback is minimal in this regime as the quantization error is small, and there is no real difference between the two CQI feedback schemes at the optimal point. This is seen in Figure 3.10.

3.6.3 Effect of Receiver Training

We have neglected the effects of downlink training in this chapter, but our results can be extended to account for these effects using the same framework as Chapter 2. The effect of the estimation error at the user changes our sum rate approximation to $\widetilde{R}_{\mathrm{ZF}}\left(\mathsf{SNR}/(1 + \phi\frac{N_t}{N_t - 1}\mathsf{SNR}), N_t, \frac{T_{\mathrm{fb}}}{B}, B\right)$, where the term $\phi = (1 + \beta\ \mathsf{SNR})^{-1}$ is the additional multi-user interference due to downlink training. Hence, all results discussed in this chapter continue to apply, although with a downward shift in system SNR to account for the effect of receiver training.

3.6.4 Beamforming to a Single User

In this section, we consider the case when the BS is constrained to beamform to only a single user, i.e., we impose the constraint that only one user be selected. Each user quantizes its channel direction using B bits and feeds back its quantization index, or equivalently $\widehat{\mathbf{h}}_k$, along with the received signal-to-noise ratio for beamforming along the direction $\widehat{\mathbf{h}}_k$: $\mathsf{SNR}\ |\mathbf{h}_k^{\mathsf{H}}\widehat{\mathbf{h}}_k|^2 = \mathsf{SNR}\ ||\mathbf{h}_k||^2 \cos^2 \angle(\mathbf{h}_k, \widehat{\mathbf{h}}_k)$. The BS then selects the user k^* with the largest such post-beamforming SNR:

$$k^* = \underset{1 \le k \le \frac{T_{\mathrm{fb}}}{B}}{\operatorname{argmax}}\ \mathsf{SNR}\ ||\mathbf{h}_k||^2 \cos^2\left(\angle(\mathbf{h}_k, \widehat{\mathbf{h}}_k)\right). \tag{3.9}$$

Let $R_{\mathrm{SUBF}}\left(\mathsf{SNR}, N_t, \frac{T_{\mathrm{fb}}}{B}, B\right)$ be the average rate achieved with signal-to-noise ratio

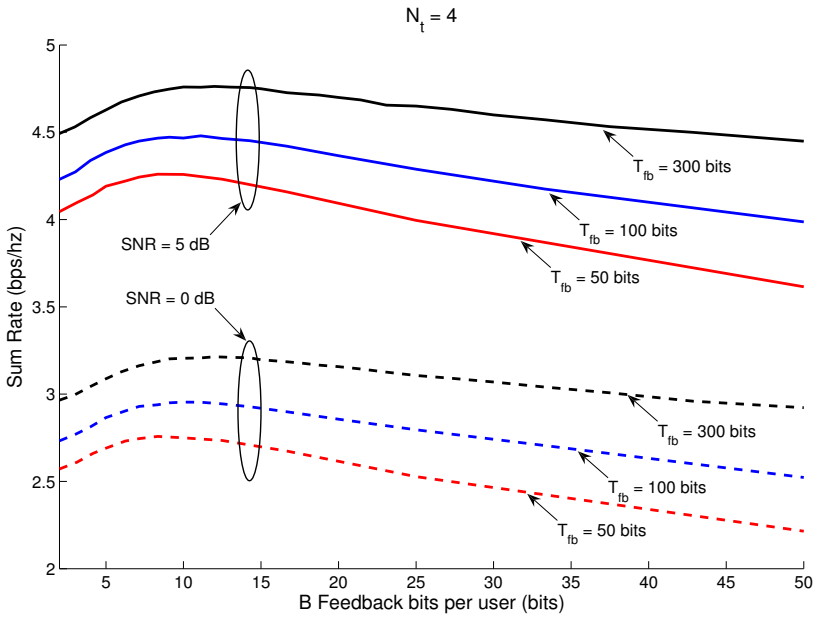

Figure 3.11: Sum rate for single-user beamforming

SNR, N_t antennas at the BS and T_{fb}/B users feeding back B bits each:

$$R_{\text{SUBF}}\left(\text{SNR}, N_t, \frac{T_{\text{fb}}}{B}, B\right) = \mathbb{E}\left[\log_2\left(1+\text{SNR}\max_{1\le k\le\frac{T_{\text{fb}}}{B}}\left(||\mathbf{h}_k||^2\cos^2\left(\angle(\mathbf{h}_k,\widehat{\mathbf{h}}_k)\right)\right)\right)\right] \quad (3.10)$$

$$\approx \log_2\left[1+\text{SNR}\left(\log\frac{T_{\text{fb}}N_t}{B}-2^{-\frac{B}{N_t-1}}\log\left(T_{\text{fb}}N_t\right)\right)\right]. \quad (3.11)$$

Ideally, $1 \le B \le T_{\text{fb}}$ is chosen to maximize (3.10), but for analytical tractability, we choose $B = \widetilde{B}^{\text{OPT}}_{\text{SUBF}}$ that maximizes (3.11), an approximation to (3.10) (the derivation of which is omitted), where

$$\widetilde{B}^{\text{OPT}}_{\text{SUBF}}\left(\text{SNR}, N_t, \frac{T_{\text{fb}}}{B}\right) = -\frac{(N_t-1)}{\log 2}W_{-1}\left(-\frac{1}{\log\left(T_{\text{fb}}N_t\right)}\right) \quad (3.12)$$

$$\sim (N_t-1)\log_2\log\left(T_{\text{fb}}N_t\right)+O(\log\log(N_t\log T_{\text{fb}})), \quad (3.13)$$

is truncated to be between 1 and T_{fb}. $W_{-1}(\cdot)$ is branch -1 of the LambertW function and (3.13) is obtained through asymptotic expansion [68]. Note that the optimal number

of bits scale roughly linearly with N_t, provided T_{fb} is sufficiently large, and double logarithmically with T_{fb}.

Figure 3.11 depicts the behavior of rate with B for a 4 antenna system at 0 and 5 dB. Although there clearly is a peak for all of the curves, very different from multi-user beamforming, the sum rate is not particularly sensitive to B and thus using the optimizing B provides only a small rate advantage.[6]

Multi-user beamforming systems are extremely sensitive to CSI because the interference power depends critically on the CSI; for single-user beamforming there is no interference and thus the dependence upon CSI is much weaker.

[6] The opportunistic beamforming (OBF) strategy proposed in [66] is equivalent to the system considered here with a *single* quantization vector; i.e., $B = 0$. This option is not explored by our optimization, but it is easy to confirm that an optimized single-user beamforming system outperforms OBF when CQI feedback is accounted for.

Chapter 4

MIMO Limited Feedback with Multiple Receive Antennas

In this chapter, we consider the case when each UT has $N_r > 1$ antennas, as opposed to a single antenna. These results appear in [72, 73]. In terms of the preceding chapters, the assumption of $N_r > 1$ amounts to allowing N_r antennas to occur together at the same user terminal, instead of being distributed as N_r separate single-antenna user terminals. The fact that N_r of these antennas is present at the same user terminal raises the question of whether this can be exploited to any advantage. For example, will the presence of multiple receive antennas reduce the feedback requirement while maintaining the same sum rate?

Block Diagonalization (BD) [74, 75] is a linear beamforming scheme similar to ZF, in that it involves transmission of N_t spatial beams by the BS, but the beams are selected such that the signals received at different receivers, but not necessarily at the different antenna elements of a particular receiver, are de-coupled. For example, if there are $N_t/2$ receivers with two antennas each, then two beams are aimed at each of the receivers. If ZF is used, an independent and (ideally) de-coupled data stream is received on each of the antennas present at the user terminals. If BD is used, the streams for different receivers do not (ideally) interfere, but the two streams intended for a particular receiver are generally not aligned with its two antennas and thus post-multiplication by a rotation matrix (to align the streams) is generally required before decoding.

In [45], an antenna combining method is proposed to reduce the feedback requirements needed while maintaining the same sum rate. However, in this chapter, we will show that using Block Diagonalization (BD) and quantizing the *subspace* spanned by the columns of the channel matrix at each user terminal, and feeding this subspace information back to the BS, proves advantageous in terms of sum rate (or equivalently, the feedback requirement is reduced while maintaining the same sum rate).

4.1 Dealing with Multiple Receive Antennas

4.1.1 System Model

We consider the same system as Chapter 2, with the exception that each of the K UTs have N_r antennas, instead of just a single antenna. The BS has N_t antennas as before. The downlink channel is described then as:

$$\mathbf{y}_k = \mathbf{H}_k^{\mathsf{H}}\mathbf{x} + \mathbf{n}_k, \quad k = 1, \ldots, K \tag{4.1}$$

where $\mathbf{y}_k$ is the signal received by the $k-^{\text{th}}$ UT. The $j-^{\text{th}}$ entry of $\mathbf{y}_k$ represents the signal received by the $j-^{\text{th}}$ antenna of UT k, where $1 \leq k \leq K$ and $1 \leq j \leq N_r$. This is similar to (2.1), with the exception that $\mathbf{y}_k$ and $\mathbf{n}_k$ are vectors in $\mathbb{C}^{N_r}$ instead of simply a complex number. Moreover, the channel is represented by the matrix $\mathbf{H}_k \in \mathbb{C}^{N_t \times N_r}$, where the $(i,j)-^{\text{th}}$ entry of $\mathbf{H}_k$ represents the multiplicative factor affecting the signal from the $i-^{\text{th}}$ transmit antenna to the $j-^{\text{th}}$ receive antenna at the $k-^{\text{th}}$ UT. Assuming Rayleigh fading and AWGN, we have that $\mathbf{H}_k$ has entries that are i.i.e. complex Gaussian with mean zero and variance 1, and $\mathbf{n}_k$ has entries that are i.i.d. complex Gaussian with mean zero and variance N_0. We assume a transmit power constraint of P, so that so that $E[||\mathbf{x}||^2] \leq P$ giving $\mathsf{SNR} = P/N_0$, which is the same as preceding sections. We assume uniform power allocation, that is, each UT is allocated an equal slice of power, so the signal transmitted to each user is P/n, if n users are selected for transmission to for a given frame.

We neglect the effects of receiver training, but as described in Section 3.6.3, these effects can be incorporated using the same framework presented in Chapter 2. We focus, instead, on digital feedback and the feedback requirement with multiple UT antennas, and compare this to the feedback nt when UTs have a single antenna each.

4.1.2 Block Diagonalization

The Block Diagonalization (BD) strategy, when perfect CSI is available at the transmitter, involves linear precoding that suppresses the interference at each user due to all other users (but does not suppress interference due to different antennas for the same user). If $\mathbf{u}_k \in \mathbb{C}^{N_r \times 1}$ contains the N_r complex (data) symbols intended for the $k-^{\text{th}}$ $(1 \leq k \leq K)$ user, then $\mathbf{V}_k \in \mathbb{C}^{N_t \times N_r}$ is the beamforming matrix and the transmitted vector is given by:

$$\mathbf{x} = \sum_{k=1}^{K} \mathbf{V}_k \mathbf{u}_k. \tag{4.2}$$

This is similar to the linear beamforming strategies presented in Chapters 2 and 3, that is, the transmitted signal is a linear combination of the data symbols. The only difference is that we consider beamforming matrices $\mathbf{V}_k$ rather than vectors $\mathbf{v}_k$, since we have $N_r > 1$.

The received signal at the $k-^{\text{th}}$ UT is given by:

$$\mathbf{y}_k = \mathbf{H}_k^{\mathsf{H}} \mathbf{V}_k \mathbf{u}_k + \sum_{j=1, j \neq k}^{K} \mathbf{H}_k^{\mathsf{H}} \mathbf{V}_j \mathbf{u}_j + \mathbf{n}_k \tag{4.3}$$

The $\sum_{j=1, j \neq k}^{K} \mathbf{H}_k^{\mathsf{H}} \mathbf{V}_j \mathbf{u}_j$ term represents the multi-user interference at user k. In order to maintain the power constraint, it is assumed that $\mathbf{V}_k^{\mathsf{H}} \mathbf{V}_k = \mathbf{I}$ (that is, the beamforming matrices are unitary, analogous to the constraint that the beamforming vectors from Chapters 2 and 3 are unit-norm) and $E\left[||\mathbf{u}_k||^2\right] = \frac{P}{N_t}$, for $k = 1, \ldots, K$.

Following the BD procedure, each $\mathbf{V}_k$ is chosen such that $\mathbf{H}_j^{\mathsf{H}} \mathbf{V}_k$ is $\mathbf{0}$, $\forall k \neq j$. This amounts to determining an orthonormal basis for the left null space of the matrix formed by stacking all $\{\mathbf{H}_j\}_{j \neq k}$ matrices together. This reduces the interference terms in equation (4.4) to zero at each UT. This is different from ZF in that each complex symbol to be transmitted to the $i-^{\text{th}}$ antenna (among the receive N_r antennas) of the $k-^{\text{th}}$ user is precoded by a vector that is orthogonal to all the columns of $\mathbf{H}_j, j \neq k$, as well as orthogonal to all but the $i-^{\text{th}}$ column of $\mathbf{H}_k$. That is, with ZF, each UT ideally sees an effective "diagonal" channel matrix, so that the signal to each of the N_r antennas are decoupled. However, with BD, as the name suggests, each UT ideally sees a "block diagonal" channel matrix, where the signals to other UTs $j \neq k$ are decoupled, but the signals to N_r antennas at UT k are still coupled.

Note that in order to produce a feasible set of matrices $\mathbf{V}_k$ with the above constraint, we will require $K = N_t/N_r$ (with $K \geq 2$). We assume that this is the case, that is, we assume that the aggregate number of receive antennas equals the number of transmit antennas; as a result it is not necessary to select a subset of users for transmission.

4.1.3 Quantizing Subspaces

As we saw in the preceding chapters, zero interference can only be achieved with perfect CSIT, that is, knowledge of $\{\mathbf{H}_k\}_{k=1}^K$ at the BS. In the case of limited feedback, only a quantized version $\mathbf{H}_k$, namely $\widehat{\mathbf{H}}_k$, is available at the BS, where each UT uses B bits to quantize $\mathbf{H}_k$ to $\widehat{\mathbf{H}}_k$. We can then perform "naive" BD, analogous to the naive ZF strategy assumed in preceding chapters, where $\widehat{\mathbf{H}}_1, \ldots, \widehat{\mathbf{H}}_K$ are treated as the true channels while performing BD. To distinguish these beamforming matrices from those selected with perfect CSIT, we denote these matrices as $\widehat{\mathbf{V}}_1, \ldots, \widehat{\mathbf{V}}_K$, where each $\widehat{\mathbf{V}}_k$ is chosen such that $\widehat{\mathbf{H}}_j^{\mathsf{H}} \widehat{\mathbf{V}}_k = \mathbf{0}\ \forall k \neq j$. Thus, $\mathbf{H}_j^H \widehat{\mathbf{V}}_k \neq 0$ in general, which leads to residual interference terms and a loss in sum rate. The received signal in the case of limited feedback can thus be written as:

$$\mathbf{y}_k = \mathbf{H}_k^{\mathsf{H}} \widehat{\mathbf{V}}_k \mathbf{u}_k + \sum_{j=1, j\neq k}^{K} \mathbf{H}_k^{\mathsf{H}} \widehat{\mathbf{V}}_j \mathbf{u}_j + \mathbf{n}_k \tag{4.4}$$

Note that in order to perform BD, it is only necessary to know the spatial direction of each user's channel, i.e., the subspace spanned by the columns of $\mathbf{H}_k$, and the feedback only needs to convey this information. For this reason, we consider the following quantization scheme: the quantization codebook $\mathcal{C}$ consists of 2^B matrices in $\mathbb{C}^{N_t \times N_r}$ i.e. $(\mathbf{W}_1, \ldots, \mathbf{W}_{2^B})$, where B is the number of feedback bits allocated per user. The quantization of a channel matrix $\mathbf{H}_k$, that is, $\widehat{\mathbf{H}}_k$, is chosen from the codebook $\mathcal{C}$ according to the following rule:

$$\widehat{\mathbf{H}}_k = \underset{\mathbf{W} \in \mathcal{C}}{\arg\min}\ d^2\left(\mathbf{H}_k, \mathbf{W}\right) \tag{4.5}$$

where $d\left(\mathbf{H}_k, \mathbf{W}\right)$ is the distance metric. Here, we consider the *chordal distance* [76]:

$$d\left(\mathbf{H}_k, \mathbf{W}\right) = \sqrt{\sum_{i=1}^{N_r} \sin^2 \theta_i} \tag{4.6}$$

where the θ_i's are the principal angles between the two subspaces spanned by the columns of the matrices $\mathbf{H}_k$ and $\mathbf{W}$ [76]. The choice of this quantity as the metric follows from the need to minimize the error in specifying the subspace spanned by the columns of $\mathbf{H}_k$. As the principal angles depend only on the subspaces spanned by the columns of the matrices, it can be assumed that the elements of $\mathcal{C}$ are unitary matrices (i.e. $\mathbf{W}^{\mathsf{H}}\mathbf{W} = \mathbf{I} \; \forall \; \mathbf{W} \in \mathcal{C}$), without loss of generality. An alternate form for the chordal distance is $d^2\left(\mathbf{H}_k, \mathbf{W}\right) = N_r - \mathrm{tr}\left(\widetilde{\mathbf{H}}_k^{\mathsf{H}}\mathbf{W}\mathbf{W}^{\mathsf{H}}\widetilde{\mathbf{H}}_k\right)$, where $\widetilde{\mathbf{H}}_k$ forms an orthonormal basis for the subspace spanned by $\mathbf{H}_k$. Note that other distance metrics may also be considered, but we do not investigate this further in this work. No channel magnitude information (or CQI) is fed back to the transmitter (since we do not explicitly consider user selection in this chapter).

Since the design of optimal quantization codebooks for the given distance metric is a very difficult problem, we instead study performance averaged over *random* quantization codebooks [77]. The Grassmann manifold is the set of all N_r dimensional subspaces passing through the origin, in an N_t dimensional space. This is denoted by $\mathcal{G}_{N_t,N_r}$. We consider complex Euclidean subspaces in this work. Each of the 2^B unitary matrices making up the random quantization codebook are chosen independently and are uniformly distributed over $\mathcal{G}_{N_t,N_r}$ [78] [79]. We alternatively refer to this uniform distribution as the isotropic distribution in the respective space. A random element drawn from this distribution can be modeled by generating an $N_t \times N_r$ matrix with i.i.d. complex Gaussian elements, and then forming a specific orthonormal basis for the N_r dimensional subspace spanned by the matrix (e.g., through a QR decomposition). The exact elements of the mtraix do not matter, as long as the subspace spanned by the columns of the matrix are the same (so any orthonormal decomposition scheme is valid and will not affect our results).

We analyze the performance averaged over all possible random codebooks. The distortion or error associated with a given codebook $\mathcal{C}$ for the quantization of $\mathbf{H}_k \in \mathbb{C}^{M\times N}$ is defined as:

$$D \triangleq \mathbb{E}\left[d^2(\mathbf{H}_k, \widehat{\mathbf{H}}_k)\right] = \mathbb{E}\left[\min_{\mathbf{W}\in\mathcal{C}} \; d^2(\mathbf{H}_k, \mathbf{W})\right], \tag{4.7}$$

where $\widehat{\mathbf{H}}_k$ is the quantization of $\mathbf{H}_k$. It is shown in [78] that $D \leq \overline{D}$ where,

$$\overline{D} = \frac{\Gamma(\frac{1}{T})}{T}(C_{N_tN_r})^{-\frac{1}{T}}2^{-\frac{B}{T}} + N_r \exp\left[-(2^B C_{N_tN_r})^{1-a}\right], \tag{4.8}$$

for a codebook of size 2^B. Here, $T = N_r(N_t - N_r)$ and $a \in (0,1)$ is a real number between 0 and 1 chosen such that $\left(C_{N_tN_r}2^B\right)^{-\frac{a}{T}} \leq 1$. $C_{N_tN_r}$ is given by $\frac{1}{T!}\prod_{i=1}^{N_r}\frac{(N_t-i)!}{(N_r-i)!}$. The second (exponential) term in (4.8) will be very small compared to the other terms for large B. For systems where $N_r = 2$ or 3, the exponential term may be neglected for most practical cases of interest.

4.2 Analytical Results

In this section, we analyze the rate gap of a MIMO limited feedback-based system with multiple receive antennas per user terminal. We first describe some preliminary mathematical results.

4.2.1 Random Subspace Quantization

In the following theorem, we show that the subspace of the true channel matrix can be decomposed as the weighted sum of the quantized channel and an independent and isotropic quantization error term.

Theorem 4.2.1 *The quantization $\widehat{\mathbf{H}}_k$ of the channel $\mathbf{H}_k$ admits the following decomposition:*

$$\widetilde{\mathbf{H}}_k = \widehat{\mathbf{H}}_k\mathbf{X}_k\mathbf{Y}_k + \mathbf{S}_k\mathbf{Z}_k \tag{4.9}$$

where

1. $\widetilde{\mathbf{H}}_k \in \mathbb{C}^{N_t\times N_r}$ *is an orthonormal basis for the subspace spanned by the columns of* $\mathbf{H}_k$,
2. $\mathbf{X}_k \in \mathbb{C}^{N_r\times N_r}$ *is unitary and distributed uniformly over* $\mathcal{G}_{N_r,N_r}$,
3. $\mathbf{Z}_k \in \mathbb{C}^{N_r\times N_r}$ *is upper triangular with positive diagonal elements, satisfying* $tr(\mathbf{Z}_k^{\mathsf{H}}\mathbf{Z}_k) = d^2\left(\mathbf{H}_k, \widehat{\mathbf{H}}_k\right)$,
4. $\mathbf{Y}_k \in \mathbb{C}^{N_r\times N_r}$ *is upper triangular with positive diagonal elements and satisfies* $\mathbf{Y}_k^{\mathsf{H}}\mathbf{Y}_k = \mathbf{I} - \mathbf{Z}_k^{\mathsf{H}}\mathbf{Z}_k$, *and*
5. $\mathbf{S}_k \in \mathbb{C}^{N_t\times N_r}$ *is an orthonormal basis for an isotropically distributed (complex)* N_r *dimensional plane in the* $(N_t - N_r)$ *dimensional left nullspace of* $\widehat{\mathbf{H}}_k$.

Moreover, the quantities $\mathbf{Y}_k$, $\widehat{\mathbf{H}}_k$ *and* $\mathbf{X}_k$ *are distributed independent of each other, as are the pair* $\mathbf{S}_k$ *and* $\mathbf{Z}_k$.

Proof: See Appendix 4.4.2. □

Hence, we may write the subspace spanned by the channel matrix as a sum of the quantized channel matrix and a term involving the matrix $\mathbf{Z}_k$, which here represents the quantization error. We mention to immediate applications of the above decomposition. It allows us to obtain an upper bound on the rate gap, using techniques similar to those presented in Chapter 2, and also allows us to perform low complexity Monte-Carlo simulations for evaluating the performance of random quantization codebooks, even for very large B. This is a powerful method that can be used to numerically evaluate and study a large number of transmission schemes for multiple receive antennas. We have further described this in Section 4.4.1.

4.2.2 Rate Gap for Digital Feedback

In the case of perfect CSIT and BD, the transmitter has the ability to suppress all interference terms giving a *per user* ergodic rate of [75]:

$$R^{\mathrm{BD}} = \mathbb{E}\left[\log_2\left|\mathbf{I} + \frac{\mathsf{SNR}}{N_t}\mathbf{H}_k^{\mathsf{H}}\mathbf{V}_k\mathbf{V}_k^{\mathsf{H}}\mathbf{H}_k\right|\right] \tag{4.10}$$

where k is any user from $1, \ldots, K$ and equal power allocation is used. The expectation is carried out over the distribution of $\mathbf{H}_k$.

For limited feedback of B bits per user, multiuser interference cannot be completely canceled and this leads to residual interference power. The per-user rate (throughput)

is given by ("BD-DF" stands for Block Diagonalization with Digital Feedback):

$$R^{\text{BD-DF}} = \mathbb{E}\left[\log_2 \frac{\left|\mathbf{I} + \frac{\mathsf{SNR}}{N_t}\sum_{j=1}^{K}\mathbf{H}_k^{\mathsf{H}}\widehat{\mathbf{V}}_j\widehat{\mathbf{V}}_j^{\mathsf{H}}\mathbf{H}_k\right|}{\left|\mathbf{I} + \frac{\mathsf{SNR}}{N_t}\sum_{\substack{j=1\\ j\neq k}}^{K}\mathbf{H}_k^{\mathsf{H}}\widehat{\mathbf{V}}_j\widehat{\mathbf{V}}_j^{\mathsf{H}}\mathbf{H}_k\right|}\right] \tag{4.11}$$

$$= \mathbb{E}\left[\log_2\left|\mathbf{I} + \frac{\mathsf{SNR}}{N_t}\sum_{j=1}^{K}\mathbf{H}_k^{\mathsf{H}}\widehat{\mathbf{V}}_j\widehat{\mathbf{V}}_j^{\mathsf{H}}\mathbf{H}_k\right|\right] - \mathbb{E}\left[\log_2\left|\mathbf{I} + \frac{\mathsf{SNR}}{N_t}\sum_{\substack{j=1\\ j\neq k}}^{K}\mathbf{H}_k^{\mathsf{H}}\widehat{\mathbf{V}}_j\widehat{\mathbf{V}}_j^{\mathsf{H}}\mathbf{H}_k\right|\right] \tag{4.12}$$

where k is any user between 1 and K (since the users are statistically identical) and the expectation is carried out over the channel distribution as well as random codebooks $\mathcal{C}$. Note that $\mathbf{H}_k^{\mathsf{H}}\widehat{\mathbf{V}}_k\widehat{\mathbf{V}}_k^{\mathsf{H}}\mathbf{H}_k$ represents the useful signal component at user k and $\sum_{j=1,j\neq k}^{K}\mathbf{H}_k^{\mathsf{H}}\widehat{\mathbf{V}}_j\widehat{\mathbf{V}}_j^{\mathsf{H}}\mathbf{H}_k$ represents the interference at user k due to all other users. The achievable rate in (4.12) assumes that each user has knowledge of its signal and interference covariance.

Theorem 4.2.2 *The rate gap $R^{BD} - R^{BD\text{-}DF}$ due to limited feedback with respect to perfect CSIT using Block Diagonalization can be bounded from above by:*

$$\overline{\Delta R^{\text{BD-DF}}} = N_r \log_2\left(1 + \frac{\mathsf{SNR}}{N_r}D\right)$$

where D can be tightly bounded from above by $\overline{D}$ from (4.8).

Proof: See Appendix 4.4.3. □

Figure 4.1 depicts the accuracy of the upper bound derived above, for an $N_t = 6, N_r = 2$ system at $\mathsf{SNR} = 20$ dB.

4.2.3 Controlling Feedback Quality

If B is kept fixed and SNR is taken to ∞, it is easy to see that residual interference will eventually overwhelm signal power, and this leads to a bounded rate (i.e., zero

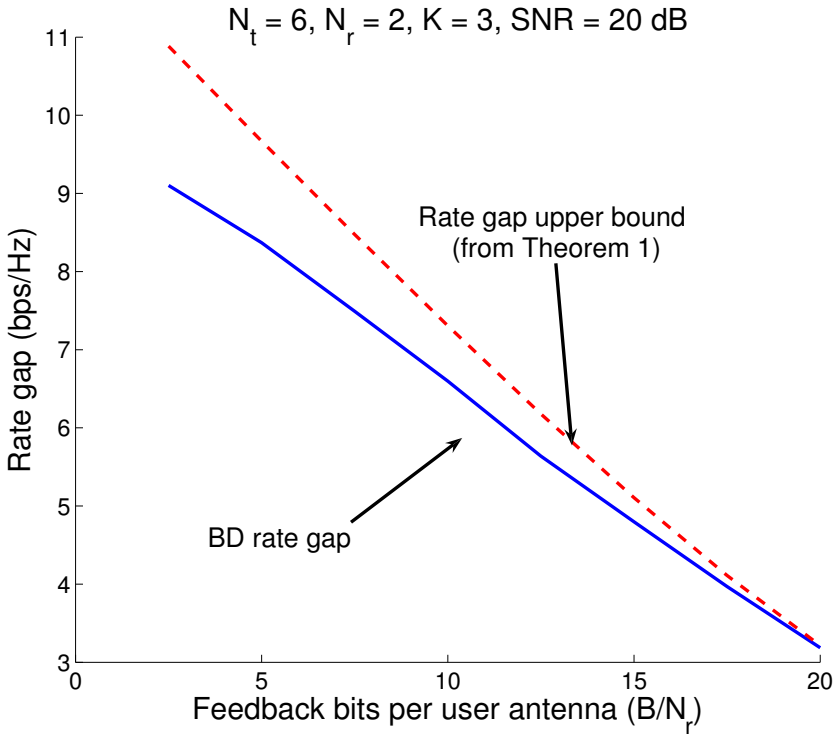

Figure 4.1: Rate gab bound accuracy with two receive antennas

multiplexing gain). Therefore, it is of interest to determine how fast B must grow with SNR in order to prevent this behavior and to maintain a bounded rate loss relative to a perfect CSIT system, that is, how fast B must grow to preserve multiplexing gain and uniformly bound $\overline{\Delta R^{\text{BD-DF}}}$, with respect to SNR.

Corollary 4.2.3 *In order to bound the per-user rate gap by* $\log_2(b) > 0$*, it is sufficient for the number of feedback bits per user to be scaled with SNR as:*

$$B \approx \frac{N(M-N)}{3} P_{dB} - N(M-N)\log_2(N(b^{\frac{1}{N}}-1)) + N(M-N)\log_2\left[\frac{\Gamma(\frac{1}{N(M-N)})}{N(M-N)}\right] - \log_2(C_{N_t N_r}) \tag{4.13}$$

Proof: This expression can be found by equating the upper bound from Theorem 4.2.2 with $\log_2 b$ and solving for B as a function of P. If D is bounded by $\overline{D}$ from (4.8), we

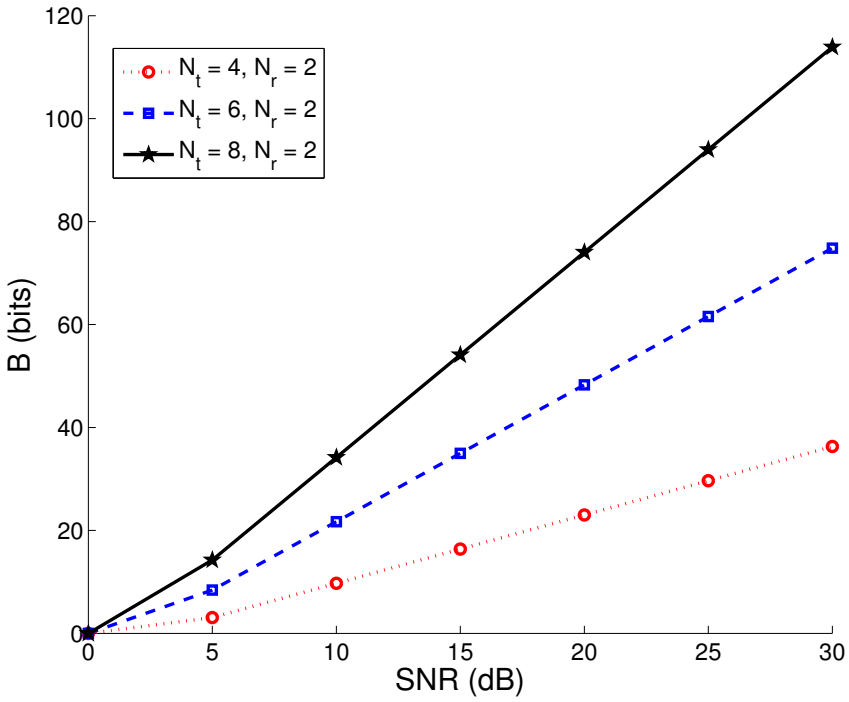

Figure 4.2: Feedback requirement for bounded rate gap with two receive antennas

have that:

$$\log_2 b = N \log_2 \left(1 + \frac{P}{N}\overline{D}\right) \tag{4.14}$$

$$\Rightarrow -\log_2 \overline{D} = \log_2 P - \log_2 \left(N\left(b^{\frac{1}{N}} - 1\right)\right) \tag{4.15}$$

Substituting the value for $\overline{D}$ from (4.8) and solving the above expression numerically for B will yield the number of bits sufficient for a rate loss of no more than $\log_2 b$. We assume that B is large enough to neglect the exponential term in the expression for $\overline{D}$ from (4.8), i.e.,

$$\overline{D} \approx \frac{\Gamma(\frac{1}{T})}{T}(C_{N_t N_r})^{-\frac{1}{T}} 2^{-\frac{B}{T}} \tag{4.16}$$

Note that the $N_r \exp\left[-(2^B C_{N_t N_r})^{1-a}\right]$ term vanishes extremely rapidly with B when compared to the first term (proportional to $2^{-\frac{B}{T}}$), and can be effectively neglected for

moderate to large values of B. By substituting (4.16) in (4.15) and solving for B, (4.13) results. □

Moreover, the total contribution of the term containing the logarithm of the gamma function above is numerically very small compared to the other terms, and can be neglected in all practical scenarios of interest. To maintain a system throughput loss of N_t bps/Hz, which corresponds to an SNR gap of no more than 3 dB with respect to BD with perfect CSIT, it is sufficient to scale the bits as:

$$B \approx \frac{N_r(N_t - N_r)}{3} P_{dB} - \log_2(C'_{N_t N_r}) \tag{4.17}$$

where $C'_{N_t N_r} = N_r^{N_r(M_t - N_r)} C_{N_t N_r}$. Figure 4.2 shows the sufficient number of bits required to maintain this level of performance, when $N_r = 2$ and $N_t = 4, 6$ and 8.

The pre-log factor (i.e. the factor that multiplies the SNR in dB) is $N_r(N_t - N_r)$ rather than $N_t N_r$, the total number of entries in the channel, which matches with the understanding that an N_r dimensional subspace in an N_t dimensional space has a dimensionality of $N_r(N_t - N_r)$ (that is, the subspace can be specified by $N_r(N_t - N_r)$ scalars, which in this case, corresponds to $N_r(N_t - N_r)$ complex numbers).

We present numerical results for $N_r = 2$ and $N_t = 4, 6, 8$ in Figure 4.3, Figure 4.4 and Figure 4.5 respectively, while scaling the bits as per (4.17), i.e. with a target of staying at most 3 dB away (in SNR) from BD with perfect CSIT. As Corollary 4.2.3 only provides the sufficient number of bits, this is a conservative strategy and the actual SNR gaps are found to be 2.65 dB, 2.72 dB and 2.84 dB for $N_t = 4, 6$ and 8, respectively, instead of 3 dB. The results also show that keeping the number of bits fixed will result in a rate gap that increases with SNR. Although our derivations assumed uniform power allocation, the numerical results evaluate optimal power allocation (i.e., waterfilling across effective channel gains), and we see that the analysis presented describes the behavior in this scenario as well.

4.2.4 Comparison with Zero-Forcing with Multiple Receive Antennas

Note that ZF with K users and N_r antennas per user is equivalent to a $KN_r = N_t$ user system, with a single antenna per user (that is, BD reduces to ZF when each user has a single receive antenna). Thus, we can recall results from Chapter 2. Furthermore, an alternative antenna combining method when the users have multiple antennas is

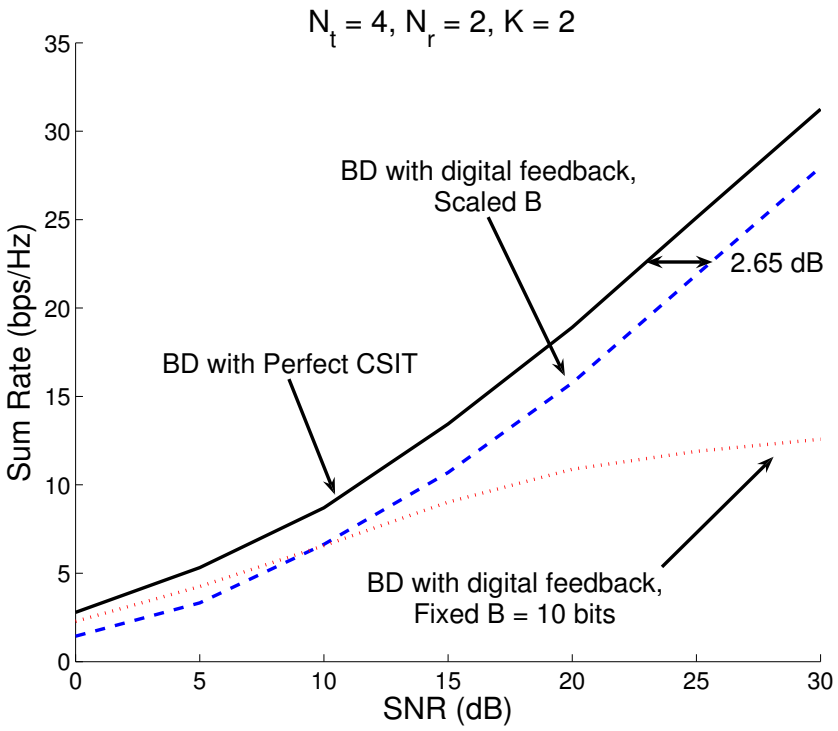

Figure 4.3: Sum rate for $N_t = 4, N_r = 2$

proposed in [45], where each user receives only a single stream of data (as opposed to N_r streams of data with BD), but uses the extra antennas to obtain a very accurate quantization of the effective channel. This effectively allows for a reduction in the feedback load.

We first compare the feedback load required for BD, ZF and antenna combining to achieve the same sum rate. The feedback scaling law for a ZF system is derived in [14] to be:

$$B_{ZF} \approx \frac{(N_t - 1)}{3} P_{dB} \tag{4.18}$$

to maintain an SNR gap of no more than 3 dB with respect to R^{ZF}. In this system, each user with N_r antennas quantizes the direction of the channel vector (i.e. the channel vector normalized to have norm unity) of each of the N_r antennas separately, and feeds this back to the transmitter.

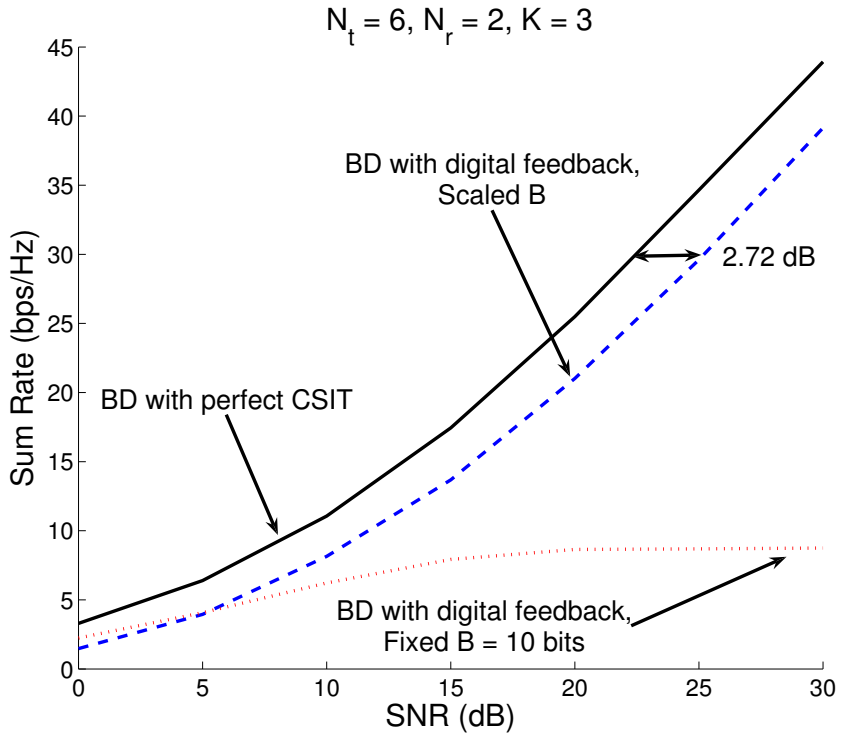

Figure 4.4: Sum rate for $N_t = 4, N_r = 2$

If each UT has N_r antennas and antenna combining is used, the scaling law becomes [45]:

$$B_{AC} \approx \frac{N_t - N_r}{3}\mathsf{SNR}_{\mathrm{dB}} - (N_t - N_r)\log_2 e - \log_2\left(\frac{N_t}{N_t - N_r + 1}\right)^{N_t - N_r} - \log_2 \begin{pmatrix} N_t - 1 \\ N_r - 1 \end{pmatrix} \tag{4.19}$$

to maintain an SNR gap of no more than 3 dB with respect to R^{ZF}.

It is known that with perfect CSIT, BD outperforms ZF because ZF has a more stringent constraint on the input and thus achieves a lower effective SNR (see, for example, [80]). In other words, even though both ZF and BD with perfect CSIT achieve full multiplexing gain, there is a constant rate (or equivalently, SNR) offset between the two strategies as $\mathsf{SNR} \to \infty$, with BD dominating ZF, since ZF can be thought of as a

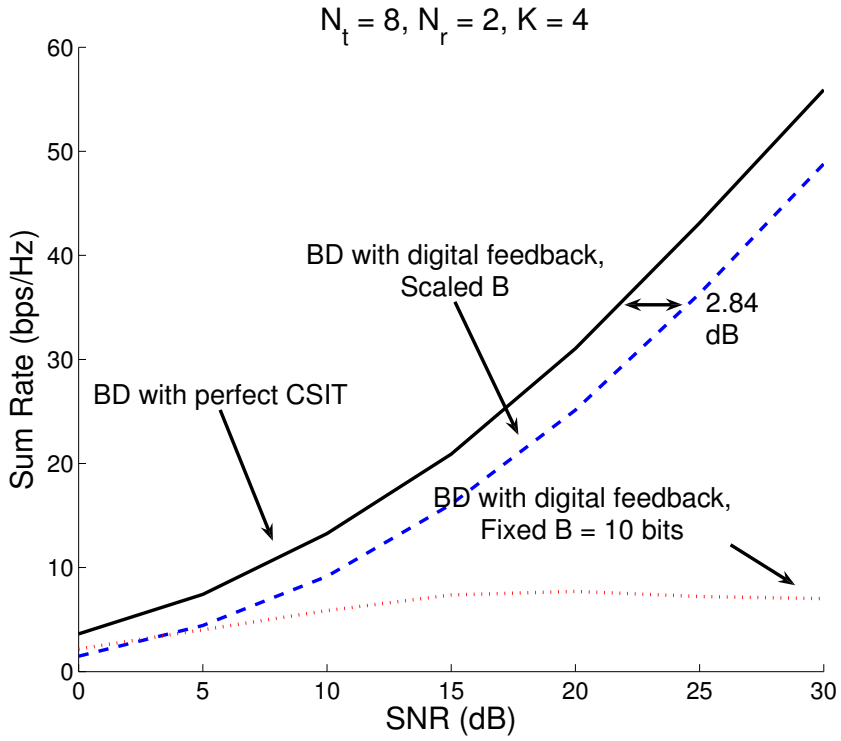

Figure 4.5: Sum rate for $N_t = 8, N_r = 2$

particular form of BD. This offset has been calculated in [80] to be:

$$R_g(P) = K \log_2(e) \sum_{j=1}^{N_r} \frac{N_r - j}{j} \tag{4.20}$$

at high SNR.

Antenna combining does not exploit the multiple receive antennas to receive multiple data streams, and hence antenna combining can ideally only do as well as ZF. Hence, for a fair comparison of the number of bits required for BD, ZF and antenna combining under limited feedback, it is necessary to fix a common target sum rate. By setting $b = 2^{R_g(P)+R}$ in (4.13) where b is as defined in Corollary 4.2.3, $R_g(P)$ is the (per-user) rate gap between BD and ZF (with perfect CSIT) and R is the target (per-user) rate gap for the ZF system, we can compare the *sufficient* number of bits required to achieve

the same sum rate for both strategies. Note that we can only compare feedback loads at a rate that is less than that achieved by ZF, since otherwise we will not get a feasible solution for the required number of bits for ZF and antenna combining.

We can now see the dimensionality advantage of BD (and antenna combining) over ZF in the pre-log factor for the bit scaling law. From (4.17), the pre-log factor for BD is $N_r(N_t - N_r)$ for N_r receive antennas, or $N_t - N_r$ per UT antenna. This is compared to the factor $N_t - 1$ in (4.18). The fact that (4.18) is relative to ZF with CSIT, a lower target rate than BD with CSIT, only reinforces our conclusion. This difference between $N_t - 1$ and $N_t - N_r$ is perhaps due to the fact that the space of N_r dimensional subspaces in an N_t dimensional space has a dimensionality of $N_r(N_t - N_r)$, while the space of N_r one-dimensional subspaces in an N_t dimensional space has dimensionality $N_r(N_t - 1)$. The bit scaling law for antenna combining (4.19) results in the same pre-log factor as BD, but needs N_r times the number of users in the system (i.e. $K = N_t$ where each user as N_r antennas, rather than the $K = N_t/N_r$ for BD).

When the target rate is fixed to be 3 dB (in SNR) away from R^{ZF}, using BD results in a bit savings of 48% for an $N_t = 6, N_r = 2$ system at $\mathsf{SNR} = 15$ dB, and 63% for an $N_t = 9, N_r = 3$ system relative to ZF. The scaling law in Corrolary 4.2.3 is slightly conservative for large b, and the advantage of BD is, in fact, underestimated. Numerical results show that the bit savings possible with BD are even higher.

Table 4.1 compares the *sufficient* number of bits required to achieve the *same target rate*, i.e., 3 dB (in SNR) away from R^{ZF}, when using BD, ZF and antenna combining, respectively, for an $N_t = 6, N_r = 2$ system. ZF and BD have $K = 3$ UTs, while antenna combining has $K = 6$.

Next, we fix the feedback load and compare the throughput of BD, ZF and antenna combining as a function of SNR. Note that even though we assume N_r times more users for antenna combining during comparison, the total feedback load in the system remains fixed. For example, when $N_t = 6$, we compare BD with $N_r = 2, K = 3$ with 5 bits per UT antenna to ZF with $N_r = 1, K = 6$ and antenna combining with $N_r = 2, K = 6$ with 5 bits/user. In all cases, the total feedback load across all users in the system is 30 bits. From Figure 4.6, BD is seen to perform better for this system, even at low SNR. Clearly, the advantage of BD in terms of feedback load to achieve a fixed rate translates to a rate advantage when the feedback load is fixed. A similar plot in Figure 4.7 compares

Table 4.1: Feedback requirement (bits) for different multiple antenna strategies

SNR	Block Diagonalization	Zero Forcing	Antenna Combining
5 dB	1	9	8
10 dB	7	17	15
15 dB	13	25	21
20 dB	20	34	28
25 dB	26	42	35
30 dB	33	50	41

all three strategies at $\mathsf{SNR} = 10$ dB with varying feedback load.

4.2.5 Comparison of Analog and Digital Feedback

We consider here the case when each user k feeds back its channel $\mathbf{H}_k$ by explicitly transmitting the $N_t N_r$ complex coefficients $(\mathbf{H}_k)_{ji}, j = 1, \ldots N_t, i = 1, \ldots, N_r$ over the feedback channel. We assume that the uplink feedback channel is unfaded AWGN with the same SNR as the downlink, i.e., the same model as Section 2.3.2. Each user may transmit each coefficient effectively 'β_{fb}' times on the uplink, resulting in the following matrix being obersved at the BS:

$$\mathbf{G}_k = \sqrt{\beta_{\text{fb}} P}\mathbf{H}_k + \mathbf{N}_k, \tag{4.21}$$

where, $\mathbf{N}_k$ represents the feedback (additive white Gaussian) noise, whose entries are independent and complex Gaussian with variance N_0. As the coefficients of $\mathbf{H}_k$ are independent and complex Gaussian with unit variance, the optimal estimator is the MMSE estimator:

$$\widehat{\mathbf{H}}_k = \frac{\sqrt{\beta_{\text{fb}}}}{1 + \beta_{\text{fb}}\mathsf{SNR}}\mathbf{G}_k, \tag{4.22}$$

where $\widehat{\mathbf{H}}_k$ is the estimate of $\mathbf{H}_k$ formed at the transmitter. It is convenient to express $\mathbf{H}_k$ in terms of the estimate $\widehat{\mathbf{H}}_k$ and estimation noise as follows:

$$\mathbf{H}_k = \widehat{\mathbf{H}}_k + \frac{1}{\sqrt{1 + \beta_{\text{fb}}\mathsf{SNR}}}\mathbf{F}_k, \tag{4.23}$$

where the entries of $\mathbf{F}_k$ are also independent and complex Gaussian with unit variance, and independent of the estimator.

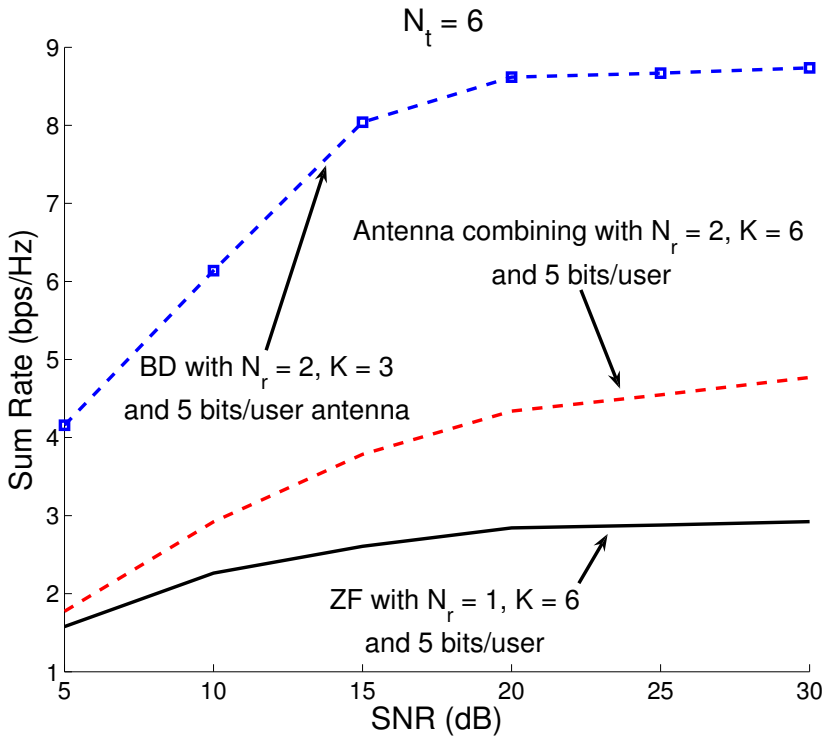

Figure 4.6: Comparison of BD, ZF and antenna combining for various SNR

The beamformers $\{\widehat{\mathbf{V}}_k\}_{k=1}^K$ are selected by treating $\{\widehat{\mathbf{H}}_k\}_{k=1}^K$ as the 'true' set of channels, and following the naive BD procedure. Note that the marginal distribution of the beamformers are the same as in the quantized feedback case, as the addition of independent white Gaussian noise does not affect the isotropic property. As in the case for digital feedback, we compute the quantity:

$$\mathbf{H}_k^{\mathsf{H}}\widehat{\mathbf{V}}_j \quad = \quad \frac{1}{\sqrt{1+\beta_{\mathrm{fb}}P}}\mathbf{F}_k^{\mathsf{H}}\widehat{\mathbf{V}}_j \tag{4.24}$$

for $k \neq j$, which follows from the fact that $\widehat{\mathbf{H}}_k^{\mathsf{H}}\widehat{\mathbf{V}}_j = \mathbf{0}$ for $k \neq j$. Similar to (4.12), we write the rate gap with analog feedback as follows:

$$\Delta R^{\mathrm{BD-AF}} \quad = \quad \mathbb{E}\left[\log_2\left|\mathbf{I}+\frac{\mathsf{SNR}}{N_t}\sum_{j=1}^{K}\mathbf{H}_k^{\mathsf{H}}\widehat{\mathbf{V}}_j\widehat{\mathbf{V}}_j^{\mathsf{H}}\mathbf{H}_k\right|\right] - \mathbb{E}\left[\log_2\left|\mathbf{I}+\frac{\mathsf{SNR}}{N_t}\sum_{\substack{j=1\\ j\neq k}}^{K}\mathbf{H}_k^{\mathsf{H}}\widehat{\mathbf{V}}_j\widehat{\mathbf{V}}_j^{\mathsf{H}}\mathbf{H}_k\right|\right]$$

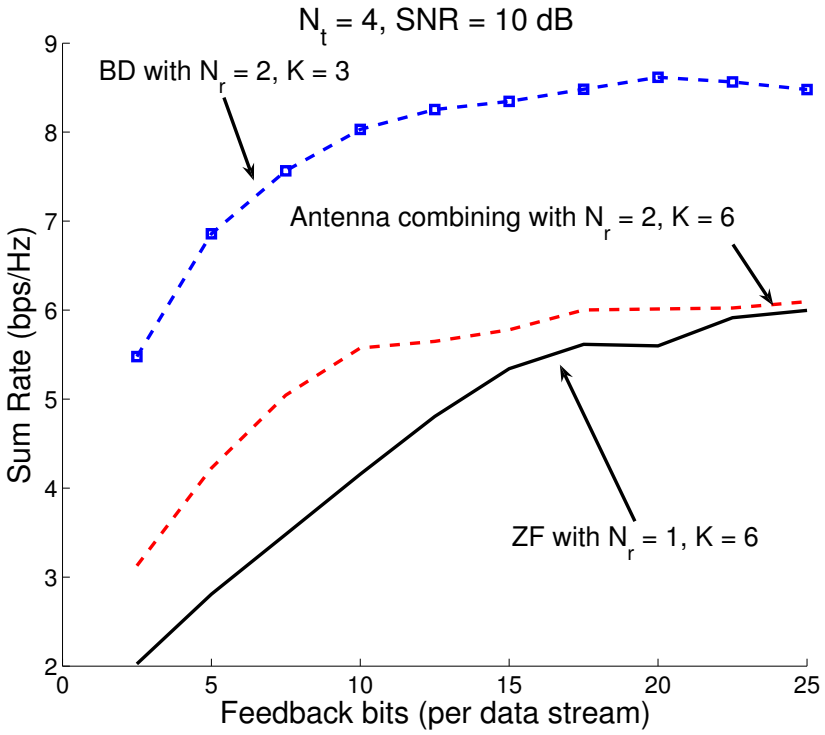

Figure 4.7: Comparison of BD, ZF and antenna combining for various B

Corollary 4.2.4 *The upper bound to the rate gap with BD and analog feedback is given by:*

$$\overline{\Delta R^{BD\text{-}AF}} = N_r \log_2\left(1 + \frac{N_t - N_r}{N_t}\frac{\mathsf{SNR}}{1+\beta_{fb}\mathsf{SNR}}\right) \quad (4.25)$$

$$< N_r \log_2\left(1 + \frac{N_t - N_r}{N_t}\frac{1}{\beta_{fb}}\right) \quad (4.26)$$

Proof: The proof of (4.25) is given in Appendix 4.4.4, and (4.26) is obtained by letting $\mathsf{SNR} \to \infty$ in (4.25). □

In order to compare analog and quantized feedback, we measure the feedback quantity in terms of 'feedback symbols' rather than bits, as we did in Section 2.4. Although analog feedback involves effectively $\beta_{\text{fb}} N_t N_r$ channel uses per UT (assuming that the UTs have orthogonal feedback channels), it also conveys more information that the

quantized case, specifically information regarding the eigenvalues and eigenvector structure, which the 'subspace' information does not capture. Hence, for fair comparison, we equate the $\beta_{\text{fb}} N_t N_r$ analog channel uses to $\beta_{\text{fb}} N_r(N_t - N_r)$ channel symbols in the quantized case (the 'subspace' information may be specified by $N_r(N_t - N_r)$ complex numbers). Under the simplifying assumption that error-free communication at capacity is possible, we set $B = \beta_{\text{fb}} N_r(N_t - N_r) \log_2(1 + \mathsf{SNR})$ for $\beta_{\text{fb}} N_r(N_t - N_r)$ channel uses of the AWGN feedback channel. Using this, we have from Theorem 4.2.2 that:

$$\overline{\Delta R^{\text{BD-AF}}} \quad \leq \quad N_r \log_2 \left(1 + \frac{\mathsf{SNR}}{(1+\mathsf{SNR})^{\beta_{\text{fb}}}} C''_{N_t N_r} \right) \tag{4.27}$$

where D has been bounded from (4.8) (neglecting the exponential term) and

$$C''_{N_t N_r} = \frac{\Gamma\left((N_r(N_t - N_r))^{-1}\right)}{N_r^2 (N_t - N_r)} C_{N_t N_r}^{(N_r(N_t - N_r))^{-1}}. \tag{4.28}$$

Our conclusions are similar to the $N_r = 1$ case considered in Chapter 2. For $\beta_{\text{fb}} \approx 1$, both bounds on the rate gap (i.e. for analog and quantized feedback) behave similarly, and the gap does not vanish as $\mathsf{SNR} \to \infty$. For $\beta_{\text{fb}} > 1$, the rate gap bound decreases rapidly (exponentially fast) for digital feedback, and vanishes entirely as $\mathsf{SNR} \to \infty$. However, for analog feedback, the decrease is relatively slow (i.e. only polynomially fast) and does not vanish as $\mathsf{SNR} \to \infty$. The analysis may also be extended to the case when errors occur with digital feedback, using the same framework presented in Section 2.3.4.

4.3 Summary of Results with Multiple Receive Antennas

Accurate CSIT is clearly important for MIMO broadcast systems in order to maximize the sum rate. When the receiver knows the channel perfectly and instantaneously feeds this information back to the transmitter using a finite number of bits, we have quantified the rate loss and have shown that increasing the number of bits linearly with the system SNR is sufficient to uniformly bound the rate gap. Further, we have established the advantage of BD relative to ZF in terms of feedback load, and the advantage of using digital feedback as opposed to using analog feedback with multiple receive antennas.

4.4 Supplementary Materials and Proofs

4.4.1 Simulating Random Subspace Quantization

The number of bits given by (4.13) can be very large and numerical simulation becomes a computationally complex task, as the chordal distance will have to be calculated for each of the 2^B matrices in the codebook. However, utilizing the statistics of random codebooks, the quantization procedure can be precisely *emulated* without having to do actual quantization. From Theorem 4.2.1, we can repeat the argument by interchanging $\widetilde{\mathbf{H}}_k$ and $\widehat{\mathbf{H}}_k$, to yield the following equivalent decomposition:

$$\widehat{\mathbf{H}}_k = \widetilde{\mathbf{H}}_k \mathbf{X}_k \mathbf{Y}_k + \mathbf{S}_k \mathbf{Z}_k \tag{4.29}$$

which can be used to generate $\widehat{\mathbf{H}}_k$, given $\widetilde{\mathbf{H}}_k$ and a codebook size. $\mathbf{X}_k$ is isotropic and independent of the codebook size, as is $\mathbf{S}_k$ which (in this decomposition) is isotropically distributed in the left nullspace of $\widetilde{\mathbf{H}}_k$. Samples drawn from the distribution of these matrices can thus be generated as samples from the isotropic distribution in their respective spaces.

Moreover, $d^2\left(\widetilde{\mathbf{H}}_k, \widehat{\mathbf{H}}_k\right) = \mathrm{tr}\left(\mathbf{Z}_k^{\mathsf{H}} \mathbf{Z}_k\right)$ is the 1^{st} order statistic from 2^B samples. Here, each sample is drawn from the distribution of the trace of a matrix-variate beta distribution (as described in Appendix 4.4.2). Thus, a sample drawn from the distribution of $\mathrm{tr}\left(\mathbf{Z}_k^{\mathsf{H}} \mathbf{Z}_k\right)$ can be generated by the 'CDF inversion' method, by computing the CDF for a specific M and N. A general expression for the CDF has been computed in closed form in [78], for the case when $d^2\left(\widetilde{\mathbf{H}}_k, \widehat{\mathbf{H}}_k\right) \leq 1$. For moderate to large B and practical values of M, N, this event occurs with extremely high probability, allowing for low complexity CDF inversion. For very small values of B, $d^2\left(\widetilde{\mathbf{H}}_k, \widehat{\mathbf{H}}_k\right)$ may be greater than 1 with appreciable probability, but an exhaustive searching among 2^B possibilities is not a problem in these cases.

From the eigen decomposition $\mathbf{Z}_k^{\mathsf{H}} \mathbf{Z}_k = \mathbf{E}_k \mathbf{D}_k \mathbf{E}_k^{\mathsf{H}}$, as described in Appendix 4.4.3, $\mathbf{E}_k$ can be generated as the eigenvectors of any (complex) Beta$(N_r, N_t - N_r)$ distributed matrix. Further, the distribution of the eigenvalues (i.e., the entries of $\mathbf{D}_k$) *conditioned* on their sum (which is equal to $d^2(\widetilde{\mathbf{H}}_k, \widehat{\mathbf{H}}_k)$), can be computed from their joint distribution [81] ([78] for the complex case). The conditional distribution can be easily computed for small values of N.

In particular, for $N = 2$, if D_1, D_2 are the diagonal elements of $\mathbf{D}_k$ with joint density $f_{D_1,D_2}(d_1, d_2)$, the distribution of D_1 conditioned on $Z = D_1 + D_2 \leq 1$ is given as:

$$F_{D_1|Z}(d_1|z) = \frac{\int_0^z \int_0^{d_1} f_{D_1,D_2}(t_1, t_2 - t_1)\, dt_1 dt_2}{f_Z(z)} \tag{4.30}$$

$$= \frac{\int_0^z \int_0^{d_1} V_{N_t} \frac{(t_2-2t_1)^2(1-t_1)^{N_t-4}}{(1-t_2+t_1)^{4-N_t}}\, dt_1 dt_2}{f_Z(z)} \tag{4.31}$$

where $f_Z(z)$ is the pdf of Z computed to be:

$$f_Z(z) = \frac{z^{2N_t-5}(\Gamma(N_t))^2}{(N_t-1)\Gamma(2N_t-4)} \tag{4.32}$$

for $z \leq 1$. V_{N_t} is a normalizing constant and is given by $V_{N_t} = \frac{1}{2}(N_t-1)(N_t-2)^2(N_t-3)$. For efficient CDF inversion and generation of samples from such a distribution, $F_{D_1|Z}(d_1|z)$ can be computed in closed form for specific values of N_t.

As $\mathbf{Y}_k^{\mathsf{H}}\mathbf{Y}_k = \mathbf{I} - \mathbf{Z}_k\mathbf{Z}_k^{\mathsf{H}}$, $\mathbf{Y}_k$ can be obtained as well. Putting all this together, one is able to randomly generate a realization of the quantized version of $\widetilde{\mathbf{H}}_k$, when random codebooks are used. This prevents the computational complexity from growing with B for numerical results. However, for extremely large B, numerical errors may dominate and care must be taken to maintain numerical precision, as the standard double precision data type available in most software packages will be insufficient (alternatives include using MAPLE or the symbolic toolbox within MATLAB to invert the CDF).

4.4.2 Proof of Theorem 4.2.1

Let $\mathbf{W}$ be any arbitrary matrix in the codebook $\mathcal{C}$. Note that $\mathbf{W}$ is independent of $\widetilde{\mathbf{H}}_k$. We then decompose $\widetilde{\mathbf{H}}_k$ into components that lie in the column space of $\mathbf{W}$ and the left nullspace of $\mathbf{W}$ as follows:

$$\widetilde{\mathbf{H}}_k = \mathbf{W}\mathbf{W}^{\mathsf{H}}\widetilde{\mathbf{H}}_k + \left(\mathbf{I} - \mathbf{W}\mathbf{W}^{\mathsf{H}}\right)\widetilde{\mathbf{H}}_k \tag{4.33}$$

$$= \mathbf{W}\mathbf{W}^{\mathsf{H}}\widetilde{\mathbf{H}}_k + \mathbf{W}^{\perp}(\mathbf{W}^{\perp})^{\mathsf{H}}\widetilde{\mathbf{H}}_k \tag{4.34}$$

where $\mathbf{W}\mathbf{W}^{\mathsf{H}}$ and $\mathbf{W}^{\perp}(\mathbf{W}^{\perp})^{\mathsf{H}} = \mathbf{I}_M - \mathbf{W}\mathbf{W}^{\mathsf{H}}$ are the projection matrices for the column space and left nullspace of $\mathbf{W}$ respectively. $\mathbf{W}^{\perp} \in \mathbb{C}^{N_t \times (N_t - N_r)}$ is chosen such that it forms an orthonormal basis for the left nullsapce of $\mathbf{W}$.

Let the (thin) QR decomposition of $\mathbf{W}\mathbf{W}^{\mathsf{H}}\widetilde{\mathbf{H}}_k$ be $\mathbf{Q}_k\mathbf{A}_k$ where $\mathbf{Q}_k \in \mathbb{C}^{N_t \times N_r}$ forms an orthonormal basis for the same space as $\mathbf{W}$, and $\mathbf{A}_k \in \mathbb{C}^{N_r \times N_r}$ is upper triangular with positive diagonal elements. Further, $\mathbf{Q}_k$ and $\mathbf{A}_k$ are independent, from [82, Theorem 2.3.18] (after verification for the complex case). As $\mathbf{Q}_k$ and $\mathbf{W}$ describe the same subspace, $\mathbf{Q}_k$ may be represented as a rotation of $\mathbf{W}$, i.e., $\mathbf{Q}_k = \mathbf{W}\mathbf{X}_k$ for some unitary matrix $\mathbf{X}_k \in \mathbb{C}^{N_r \times N_r}$.

By isotropy and independence of $\mathbf{W}$ and $\widetilde{\mathbf{H}}_k$, $\mathbf{X}_k$ is also isotropically distributed and is independent of $\mathbf{W}$, which is an arbitrary orthonormal basis. Also note that $\mathbf{W}\mathbf{W}^{\mathsf{H}} = \mathbf{Q}_k\mathbf{Q}_k^{\mathsf{H}}$ and hence $\mathbf{A}_k^{\mathsf{H}}\mathbf{A}_k = \widetilde{\mathbf{H}}_k^{\mathsf{H}}\mathbf{W}\mathbf{W}^{\mathsf{H}}\widetilde{\mathbf{H}}_k$. Thus $\mathrm{tr}\left(\mathbf{A}_k^{\mathsf{H}}\mathbf{A}_k\right) = N_r - d^2\left(\mathbf{W}, \widetilde{\mathbf{H}}_k\right)$.

Note that $\mathbf{W}^{\perp}(\mathbf{W}^{\perp})^{\mathsf{H}}\widetilde{\mathbf{H}}_k$ is the projection of $\widetilde{\mathbf{H}}_k$ onto the left nullspace of $\mathbf{W}$. As $\widetilde{\mathbf{H}}_k$ is isotropically distributed, the projection is also isotropically distributed in the corresponding $N_t - N_r$ dimensional nullspace. Let the (thin) QR decomposition of $\mathbf{W}^{\perp}(\mathbf{W}^{\perp})^{\mathsf{H}}\widetilde{\mathbf{H}}_k$ be $\mathbf{S}_k\mathbf{B}_k$, where $\mathbf{S}_k \in \mathbb{C}^{N_t \times N_r}$ is an orthonormal basis for an isotropically distributed (complex) N_r dimensional plane in the $N_t - N_r$ dimensional left nullspace of $\mathbf{W}$ and $\mathbf{B}_k \in \mathbb{C}^{N_r \times N_r}$ is upper triangular with positive diagonal elements. Similar to the previous case, $\mathbf{S}_k$ and $\mathbf{B}_k$ are independently distributed. It is also straightforward to see that $\mathbf{B}_k^{\mathsf{H}}\mathbf{B}_k = \mathbf{I} - \mathbf{A}_k^{\mathsf{H}}\mathbf{A}_k$ and $\mathrm{tr}\left(\mathbf{B}_k^{\mathsf{H}}\mathbf{B}_k\right) = d^2\left(\mathbf{W}, \widetilde{\mathbf{H}}_k\right)$.

As $\widetilde{\mathbf{H}}_k$ and $\mathbf{W}$ are independent, which has been our assumption thus far in the proof, $\mathbf{B}_k^{\mathsf{H}}\mathbf{B}_k$ is matrix-variate (complex) Beta$(N_r, N_t - N_r)$ distributed [81]. We will now argue that most of the above conclusions remain unchanged, even when the quantization procedure (4.5) is followed.

The quantization procedure amounts to choosing a $\mathbf{B}_k^{\mathsf{H}}\mathbf{B}_k$ such that its trace is the minimum among 2^B choices. Thus, it follows that the quantization procedure only affects $\mathbf{B}_k$ (and $\mathbf{A}_k$, which is the 'inverse' quantization error and is related to $\mathbf{B}_k$ by $\mathbf{A}_k^{\mathsf{H}}\mathbf{A}_k = \mathbf{I} - \mathbf{B}_k^{\mathsf{H}}\mathbf{B}_k$). We use $\mathbf{Y}_k$ and $\mathbf{Z}_k$ to denote the matrices $\mathbf{A}_k$ and $\mathbf{B}_k$ after following the quantization procedure. Hence, even though $\mathbf{Z}_k^{\mathsf{H}}\mathbf{Z}_k$ is not beta distributed, the distribution of the quantities $\mathbf{X}_k$, $\mathbf{S}_k$ and $\mathbf{W}$ remain the same, and are independent of $\mathbf{Z}_k$ (and $\mathbf{Y}_k$). We now use $\widehat{\mathbf{H}}_k$ to denote $\mathbf{W}$ after following the quantization procedure, according to the convention in (4.5).

4.4.3 Proof of Theorem 4.2.2

Theorem 4.2.2 is proved as follows:

$$\begin{aligned}
\Delta R^{\text{BD-DF}} &= R^{\text{BD}} - R^{\text{BD-DF}} \\
&\overset{(a)}{\leq} \mathbb{E}\left[\log_2\left|\mathbf{I} + \frac{\mathsf{SNR}}{N_t}\mathbf{H}_k^{\mathsf{H}}\mathbf{V}_k\mathbf{V}_k^{\mathsf{H}}\mathbf{H}_k\right|\right] - \\
&\quad \mathbb{E}\left[\log_2\left|\mathbf{I} + \frac{\mathsf{SNR}}{N_t}\,\mathbf{H}_k^{\mathsf{H}}\widehat{\mathbf{V}}_k\widehat{\mathbf{V}}_k^{\mathsf{H}}\mathbf{H}_k\right|\right] + \\
&\quad \mathbb{E}\left[\log_2\left|\mathbf{I} + \frac{\mathsf{SNR}}{N_t}\sum_{j=1,j\neq k}^{K}\mathbf{H}_k^{\mathsf{H}}\widehat{\mathbf{V}}_j\widehat{\mathbf{V}}_j^{\mathsf{H}}\mathbf{H}_k\right|\right] \qquad (4.35) \\
&\overset{(b)}{=} \mathbb{E}\left[\log_2\left|\mathbf{I} + \frac{\mathsf{SNR}}{N_t}\sum_{j=1,j\neq k}^{K}\mathbf{H}_k^{\mathsf{H}}\widehat{\mathbf{V}}_j\widehat{\mathbf{V}}_j^{\mathsf{H}}\mathbf{H}_k\right|\right] \qquad (4.36)
\end{aligned}$$

$$\begin{aligned}
&\overset{(c)}{=} \mathbb{E}\left[\log_2\left|\mathbf{I} + \frac{\mathsf{SNR}}{N_t}\widetilde{\mathbf{H}}_k^{\mathsf{H}}\left(\sum_{j\neq k}\widehat{\mathbf{V}}_j\widehat{\mathbf{V}}_j^{\mathsf{H}}\right)\widetilde{\mathbf{H}}_k\boldsymbol{\Lambda}_k\right|\right] \qquad (4.37) \\
&\overset{(d)}{\leq} \log_2\left|\mathbf{I} + \mathsf{SNR}(K-1)\mathbb{E}\left[\widetilde{\mathbf{H}}_k^{\mathsf{H}}\widehat{\mathbf{V}}_j\widehat{\mathbf{V}}_j^{\mathsf{H}}\widetilde{\mathbf{H}}_k\right]\right| \qquad (4.38)
\end{aligned}$$

Here, (a) follows by neglecting the positive semi-definite interference terms in the quantity:

$$\mathbb{E}\left[\log_2\left|\mathbf{I} + \frac{\mathsf{SNR}}{N_t}\sum_{j=1}^{K}\mathbf{H}_k^{\mathsf{H}}\widehat{\mathbf{V}}_j\widehat{\mathbf{V}}_j^{\mathsf{H}}\mathbf{H}_k\right|\right].$$

By the BD procedure, both $\mathbf{V}_k$ and $\widehat{\mathbf{V}}_k$ are distributed isotropically, and are chosen independent of $\mathbf{H}_k$, which means the first two terms in (4.35) are identical and thus gives (b). We write $\mathbf{H}_k\mathbf{H}_k^{\mathsf{H}} = \widetilde{\mathbf{H}}_k\boldsymbol{\Lambda}_k\widetilde{\mathbf{H}}_k^{\mathsf{H}}$, where $\widetilde{\mathbf{H}}_k \in \mathbb{C}^{N_t\times N_r}$ forms an orthonormal basis for the subspace spanned be the columns of $\mathbf{H}_k$ and $\boldsymbol{\Lambda}_k = \text{diag}[\lambda_1, \ldots, \lambda_{N_r}]$ are the N_r non-zero, unordered eigenvalues of $\mathbf{H}_k\mathbf{H}_k^{\mathsf{H}}$ ($\mathbf{H}_k$ is of rank N_r and diagonalizable with probability 1). Both the density function of $\mathbf{H}_k$ (which is matrix-variate complex Normal distributed) [82] and the Jacobian of the singular value decomposition transformation of a matrix [83] can be separated into a product of functions of $\widetilde{\mathbf{H}}_k$ and $\boldsymbol{\Lambda}_k$ alone. Thus, $\widetilde{\mathbf{H}_k}$ and $\boldsymbol{\Lambda}_k$ are independent and $\mathbb{E}[\boldsymbol{\Lambda}_k] = N_t\mathbf{I}$. Step (c) follows using this and the

fact that $|\mathbf{I}+\mathbf{AB}| = |\mathbf{I}+\mathbf{BA}|$, for matrices $\mathbf{A}$ and $\mathbf{B}$. Next, (d) follows from Jensen's inequality due to the concavity of $\log|\cdot|$. Note that $\mathbb{E}[\mathbf{\Lambda}_k] = N_t\mathbf{I}$.

$\mathbb{E}\left[\widetilde{\mathbf{H}}_k^{\mathsf{H}}\left(\widehat{\mathbf{V}}_j\widehat{\mathbf{V}}_j^{\mathsf{H}}\right)\widetilde{\mathbf{H}}_k\right]$ is computed as follows. First, we compute

$$\begin{aligned}\widetilde{\mathbf{H}}_k^{\mathsf{H}}\widehat{\mathbf{V}}_j &= \mathbf{Y}_k^{\mathsf{H}}\mathbf{X}_k^{\mathsf{H}}\widehat{\mathbf{H}}_k^{\mathsf{H}}\widehat{\mathbf{V}}_j + \mathbf{Z}_k^{\mathsf{H}}\mathbf{S}_k^{\mathsf{H}}\widehat{\mathbf{V}}_j &(4.39)\\ &= \mathbf{Z}_k^{\mathsf{H}}\mathbf{S}_k^{\mathsf{H}}\widehat{\mathbf{V}}_j &(4.40)\end{aligned}$$

for $k \neq j$, which follows from Theorem 4.2.1 and the fact that $\widehat{\mathbf{H}}_k^{\mathsf{H}}\widehat{\mathbf{V}}_j = \mathbf{0}\ \forall k \neq j$, by the BD procedure. Therefore,

$$\begin{aligned}\mathbb{E}\left[\widetilde{\mathbf{H}}_k^{\mathsf{H}}\widehat{\mathbf{V}}_j\widehat{\mathbf{V}}_j^{\mathsf{H}}\widetilde{\mathbf{H}}_k\right] &= \mathbb{E}\left[\mathbf{Z}_k^{\mathsf{H}}\left(\mathbf{S}_k^{\mathsf{H}}\widehat{\mathbf{V}}_j\widehat{\mathbf{V}}_j^{\mathsf{H}}\mathbf{S}_k\right)\mathbf{Z}_k\right] &(4.41)\\ &\overset{(e)}{=} \frac{N_r}{N_t-N_r}\mathbb{E}\left[\mathbf{Z}_k^{\mathsf{H}}\mathbf{Z}_k\right] &(4.42)\\ &\overset{(f)}{=} \frac{D}{N_r}\frac{N_r}{N_t-N_r} &(4.43)\end{aligned}$$

Here, (e) follows from the fact that $\widehat{\mathbf{V}}_j$ (which is just isotropically distributed in the left nullspace of $\widehat{\mathbf{H}}_k$) and $\mathbf{Z}_k$ are independent, as are $\mathbf{S}_k$ and $\mathbf{Z}_k$ from Theorem 4.2.1. Further, $\mathbf{S}_k$ is also isotropically and distributed in the left nullspace of $\widehat{\mathbf{H}}_k$, and is independent of $\widehat{\mathbf{V}}_k$. Thus $\widehat{\mathbf{V}}_j^{\mathsf{H}}\mathbf{S}_k\mathbf{S}_k^{\mathsf{H}}\widehat{\mathbf{V}}_j$ is matrix-variate Beta(N_r, N_t-2N_r) distributed [82], and $\mathbb{E}\left[\mathbf{Z}_k^{\mathsf{H}}\left(\mathbf{S}_k^{\mathsf{H}}\widehat{\mathbf{V}}_j\widehat{\mathbf{V}}_j^{\mathsf{H}}\mathbf{S}_k\right)\mathbf{Z}_k\right] = \frac{N_r}{N_t-N_r}\mathbb{E}\left[\mathbf{Z}_k^{\mathsf{H}}\mathbf{Z}_k\right]$, by [82, Theorem 5.3.12] and [82, Theorem 5.3.19] (after verification for the complex case).

Let $\mathbf{E}_k\mathbf{D}_k\mathbf{E}_k^{\mathsf{H}}$ be the eigen decomposition of $\mathbf{Z}_k^{\mathsf{H}}\mathbf{Z}_k$, where $\mathbf{E}_k \in \mathbb{C}^{N_r\times N_r}$ is orthonormal and $\mathbf{D}_k \in \mathbb{C}^{N_r\times N_r}$ is diagonal, with strictly positive elements along the diagonal. If an arbitrary matrix in the codebook $\mathcal{C}$ is selected as the quantization, $\mathbf{Z}_k^{\mathsf{H}}\mathbf{Z}_k$ is matrix-variate (complex) Beta(N_r, N_t-N_r) distributed (as described in Appendix 4.4.2), and $\mathbb{E}\left[\mathbf{Z}_k^{\mathsf{H}}\mathbf{Z}_k\right]$ is a multiple of the identity matrix. Both the density function of this distribution [82] and the Jacobian of the eigen decomposition transformation for a matrix [83] can be separated into a product of functions of $\mathbf{E}_k$ and $\mathbf{D}_k$ alone, and these are hence independently distributed.

For the actual quantization matrix, after following the procedure in (4.5), only the distribution of the diagonal matrix $\mathbf{D}_k$ is affected, and the distribution of $\mathbf{E}_k$ remains unchanged and independent of $\mathbf{D}_k$. Thus, we have that $\mathbb{E}\left[\mathbf{Z}_k^{\mathsf{H}}\mathbf{Z}_k\right] = \rho\mathbf{I}$ for some constant ρ, even after following the quantization procedure. This can also be concluded by

observing that $\mathbf{Z}_k^{\mathsf{H}}\mathbf{Z}_k$ is invariant to unitary rotations. In terms of the trace of the matrix, we have $\rho = \frac{\mathbb{E}[\mathrm{tr}(\mathbf{Z}_k\mathbf{Z}_k^{\mathsf{H}})]}{N_r} = \frac{D}{N_r}$, and (f) follows.

Substituting (4.43) in (4.38), we have:

$$\overline{\Delta R^{\text{BD-DF}}} \;=\; N_r \;\log_2\left(1+\frac{\mathsf{SNR}}{N_r}D\right) \tag{4.44}$$

4.4.4 Proof of Equation 4.25

$\Delta R^{\text{BD}-\text{AF}} = R^{\text{BD}} - R\text{BD} - \text{AF}$

$$\begin{aligned}
&\overset{(a)}{\leq} \;\mathbb{E}\left[\log_2\left|\mathbf{I}+\frac{\mathsf{SNR}}{N_t}\mathbf{H}_k^{\mathsf{H}}\mathbf{V}_k\mathbf{V}_k^{\mathsf{H}}\mathbf{H}_k\right|\right] - \\
&\qquad \mathbb{E}\left[\log_2\left|\mathbf{I}+\frac{\mathsf{SNR}}{N_t}\mathbf{H}_k^{\mathsf{H}}\widehat{\mathbf{V}}_k\widehat{\mathbf{V}}_k^{\mathsf{H}}\mathbf{H}_k\right|\right] + \\
&\qquad \mathbb{E}\left[\log_2\left|\mathbf{I}+\frac{\mathsf{SNR}}{N_t}\sum_{j=1,j\neq k}^{K}\mathbf{H}_k^{\mathsf{H}}\widehat{\mathbf{V}}_j\widehat{\mathbf{V}}_j^{\mathsf{H}}\mathbf{H}_k\right|\right] && (4.45)\\
&\overset{(b)}{=} \;\mathbb{E}\left[\log_2\left|\mathbf{I}+\frac{\mathsf{SNR}}{N_t}\sum_{j=1,j\neq k}^{K}\mathbf{H}_k^{\mathsf{H}}\widehat{\mathbf{V}}_j\widehat{\mathbf{V}}_j^{\mathsf{H}}\mathbf{H}_k\right|\right] && (4.46)\\
&\overset{(c)}{=} \;\mathbb{E}\left[\log_2\left|\mathbf{I}+\frac{\mathsf{SNR}}{N_t}\frac{1}{1+\beta_{\text{fb}}\mathsf{SNR}}\sum_{\substack{j=1\\j\neq k}}^{K}\mathbf{F}_k^{\mathsf{H}}\widehat{\mathbf{V}}_j\widehat{\mathbf{V}}_j^{\mathsf{H}}\mathbf{F}_k\right|\right] && (4.47)\\
&\overset{(d)}{\leq} \;\log_2\left|\mathbf{I}+\frac{\mathsf{SNR}(K-1)}{N_t(1+\beta_{\text{fb}}\mathsf{SNR})}\mathbb{E}\left[\mathbf{F}_k^{\mathsf{H}}\widehat{\mathbf{V}}_j\widehat{\mathbf{V}}_j^{\mathsf{H}}\mathbf{F}_k\right]\right| && (4.48)\\
&\overset{(e)}{=} \;\log_2\left|\mathbf{I}+\frac{\mathsf{SNR}(K-1)}{N_t}\frac{1}{1+\beta\mathsf{SNR}}N_r\mathbf{I}\right| && (4.49)\\
&= \;N_r\;\log_2\left(1+\frac{N_t-N_r}{N_t}\frac{\mathsf{SNR}}{1+\beta_{\text{fb}}\mathsf{SNR}}\right) && (4.50)
\end{aligned}$$

Here, (a) and (b) have the same justification as in the proof of Theorem 4.2.2 (in Appendix 4.4.3), (c) follows from (4.24), and (d) is obtained by applying Jensens inequality. By Gaussianity of $\mathbf{F}_k$ and independence of $\mathbf{F}_k$ and $\widehat{\mathbf{V}}_j$, $j \neq k$, $\mathbf{F}_k^{\mathsf{H}}\widehat{\mathbf{V}}_j$ is matrix-variate complex Gaussian distributed with i.i.d. elements, and $\mathbb{E}\left[\mathbf{F}_k^{\mathsf{H}}\widehat{\mathbf{V}}_j\widehat{\mathbf{V}}_j^{\mathsf{H}}\mathbf{F}_k\right] = N_r\mathbf{I}$, which results in (e).

Chapter 5

Multihop Ad Hoc Networks with Multiple Antennas

In the preceeding chapters, we considered the situation involving a fixed transmitter (BS) which directly communicates with the receivers. This is referred to as a "single-hop" situation, that is, there is a direct link between the transmitter and receiver, or the transmitter and receiver are physically close together. In contrast, we can consider the situation where a number of transmitters and receivers are present in an "ad hoc" fashion, and each transmitter intends to communicate to a receiver a large distance away. This implies that the message to the intended receiver will need to be carried by intermediate relays. This is referred to as a "multi-hop" situation. The problem of efficiently using multiple antennas under a multi-hop setting is still not well understood, and in this chapter, we determine efficient multiple-antenna techniques to maximize end-to-end performance in MIMO multi-hop ad hoc networks.

There are broadly two relevant multiple-antenna techniques in this setting: (a) aggressive interference cancellation, and (b) aggressive spatial multiplexing. When the transmitter sends a single data stream, the receiver can use its multiple antennas to cancel some of the nearby interferers, thereby reducing the interference and allowing for a higher spatial reuse factor, i.e., allowing for more transmitting nodes to exist per unit area. On the other hand, when the transmitter uses spatial multiplexing to send

multiple data streams, the receiver uses its multiple antennas to decode the transmitted multiple data streams, and cannot cancel nearby interferers. This leads to a large per-hop rate due to the multiple data streams, but a lower spatial reuse factor, due to high interference. Thus, there is a tradeoff between these two approaches, and the goal of this chapter is to determine the point on this tradeoff that maximizes the end-to-end performance.

Prior work for single-hop networks have shown that when the transmitting node sends a single data stream, the system throughput scales only logarithmically with the number of antennas if the spatial reuse factor is kept fixed [84], and linearly if the spatial reuse is optimally chosen [85]. Further, it is shown in [86] that single stream transmission is preferable to multiple stream transmission when sub-optimal receive filters are used.

In this chapter, we would like to investigate if similar gains are possible for the multi-hop setting, and analyze the effect of nodes transmitting multiple data streams. Particularly, we are interested in quantifying end-to-end performance with blind opportunistic routing, and would like to determine the optimal multi-antenna approach. We focus on an "open-loop" system, in contrast to the feedback-based systems considered in preceding chapters. This is relevant due the fact that the network structure is constantly changing in this scenario, and there might not be sufficient time to train and feed back the channel state. We assume that the transmitters have no channel state information, that is no CSIT, but the receivers have obtained a perfect estimate of their channels, that is, perfect CSIR.

5.1 System Model and Performance Metric

We consider a set Φ of an infinite number of nodes located according to a 2D homogeneous Poisson point process (PPP), with density λ m^{-2}. We assume that the network is well synchronized (for example, by local atomic clocks or with timing information extracted from a positioning system), and consider a slotted transmission protocol such that in every time slot, each node independently decides to be a transmitter with probability p or a receiver with probability $1-p$. Therefore, the set of transmitters Φ^t and the set of receivers Φ^r form independent PPPs with density λp and $\lambda(1-p)$, respectively. We assume that for each time slot, Φ^t and Φ^r assume a new realization drawn from

their respective PPPs.

5.1.1 Routing Protocol

We consider a blind geographic opportunistic routing system, where each node is aware of its own geographic location and each packet is labeled with geographic coordinates of the final destination. Specifically, routing is carried out as follows:

- In each time slot, the transmitter broadcasts its packet without any prior knowledge of its neighbors.
- Every receiver successfully decoding the packet feeds back an ACK message, which includes the receiver location information. We further assume that this feedback information is received perfectly by the transmitter.
- The transmitter extracts the location information of the receiver and calculates the forward progress (to the final destination which is very far away) each successful receiver can provide.
- The transmitter then sends a message to the receiver which offers the most progress selecting it as a relay[1] .

The above routing process is illustrated in Figure 5.1, which depicts the progress with respect to TX0. The dashed link denotes the acknowledgment link, and the solid link represents the chosen link.

5.1.2 Channel Model

We consider a spatial multiplexing system in a Rayleigh fading channel with distance based path-loss with exponent $\alpha > 2$, where each node is equipped with N antennas: each transmitter transmits N_t ($1 \leq N_t \leq N$) independent data streams through different antennas at each time slot, while receivers are assumed to fully utilize all N antennas. We also assume an interference limited environment, so that the effect of thermal noise is negligible.

[1] As discussed in [87], the receiver offering the most progress is also the receiver closest to the final destination in a network where the final destination is very far away.

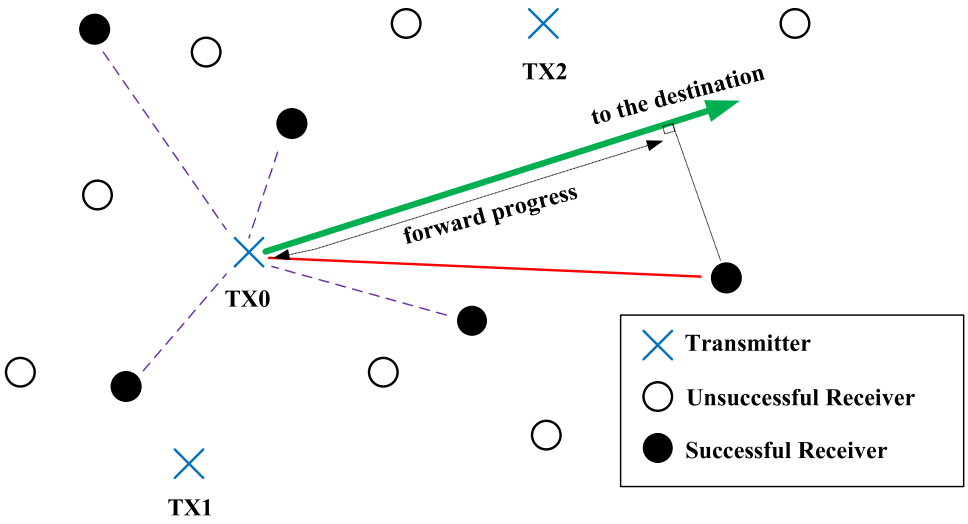

Figure 5.1: Illustration of opportunistic routing and forward progress

For a homogeneous PPP, we can focus on a typical transmitter at the origin, from the perspective of which all the other transmitting nodes form an independent homogeneous PPP with intensity λp. Without loss of generality, we assume that the final destination is located an infinite distance away from the typical transmitter along the positive X-axis. For notational convenience, $X_i \in \Phi^r$ $(i \in \mathbb{Z}^+)$ is used to denote the location of the i-th closest receiver from the origin. With respect to any receiver, D_j and $\mathbf{H}_j$ $(j \in \mathbb{Z}^+ \cup 0)$ are used to denote the distance to the j-th transmitter and the corresponding fading channel matrix (the typical transmitter is indexed by 0). The entries of the fading matrix are assumed to be i.i.d. Rayleigh with zero mean and variance one, remain constant for each time slot, and vary independently from slot to slot.

Then the $N \times 1$ received signal vector at the i-th closest receiver on the k-th stream is given by

$$\mathbf{y}_{i,k} = D_0^{-\alpha/2}\mathbf{h}_{0,k}x_{0,k} + D_0^{-\alpha/2}\sum_{q=1,q\neq k}^{N_t}\mathbf{h}_{0,q}x_{0,q} + \sum_{j\in\mathbb{Z}^+} D_j^{-\alpha/2}\sum_{q=1}^{N_t}\mathbf{h}_{j,q}x_{j,q}, \tag{5.1}$$

where $x_{j,q}$ is the unit-power symbol sent on the q-th stream of the j-th transmitter, and

$\mathbf{h}_{j,q}$ is the q-th column of $\mathbf{H}_j$.

We assume that each receiver uses a linear MMSE filter. Thus, given any D_0, the signal-to-interference ratio (SIR) at receiver i for stream k is expressed as

$$\mathrm{SIR}_{i,k} = D_0^{-\alpha} \cdot \mathbf{h}_{0,k}^{\dagger} \mathbf{R}_{i,k}^{-1} \mathbf{h}_{0,k}, \tag{5.2}$$

where

$$\mathbf{R}_{i,k} = D_0^{-\alpha} \sum_{q=1, q\neq k}^{N_t} \mathbf{h}_{0,q} \mathbf{h}_{0,q}^{\dagger} + \sum_{j \in \mathbb{Z}^+} D_j^{-\alpha} \mathbf{H}_j \mathbf{H}_j^{\dagger} \tag{5.3}$$

represents the color of the interference. Therefore, for decoding stream k from the typical transmitter 0, we assume that the receiver knows the channel matrix $\mathbf{H}_0$, as well as the interference covariance matrix $\mathbf{R}_{i,k}$ perfectly.

Further, we assume that the transmitter gets a separate ACK for each stream, from each receiver that successfully decodes it. The transmitter can therefore potentially select different relays for different streams. Receiver i applies an MMSE filter to decode stream k independent of the other streams, and hence $\mathrm{SIR}_{i,1}, \mathrm{SIR}_{i,2}, \ldots, \mathrm{SIR}_{i,N_t}$ are all statistically identical[2] . We will therefore focus only on per-stream performance, and henceforth drop the second subscript.

We use β to denote the SIR threshold for successful per-stream communication, so that a stream is successfully decoded by receiver i if and only if $\mathrm{SIR}_i > \beta$. The probability that the receiver at position X_i successfully decodes a stream from the transmitter at the origin is given as:

$$p_s(|X|) \;=\; \mathbb{P}^{\Phi^t}\left[\mathrm{SIR}_i \geq \beta\right]. \tag{5.4}$$

Assuming the same rate is used for every stream, the per-hop rate is thus $N_t \log_2(1+\beta)$.

5.1.3 Performance Metric

Under the opportunistic routing scheme, we use $d(\lambda, p, N_t, N, \beta)$ to denote the expected distance or *expected forward progress* a packet from a transmitter travels (toward the

[2] This holds under the assumption that each relay node is fully back-logged and there is no limit on the number of ACK's that a receiver can feed back.

final destination), with node density λ, transmit probability p, N_t streams per transmitter, N antennas per node, and an SIR threshold β. $d(\lambda, p, N_t, N, \beta)$ is defined as:

$$\mathbb{E}^{\Phi,\mathbf{H}}\left[\max_{X_i \in \Phi^r}\left(\mathbf{1}(\mathrm{SIR}_i > \beta|\Phi^t) \cdot |X_i|\left(\cos(\angle X_i)\right)^+\right)\right], \tag{5.5}$$

where the expression inside the max(·) function directly comes from the relay selection process of the opportunistic routing protocol, $\mathbf{1}(\cdot)$ represents the indicator function, and $\angle X_i$ is the phase angle of $X_i \in \mathbb{R}^2$ ($-\pi < \angle X_i < \pi$). The $(\cdot)^+$ function is equal to the argument if the argument is positive, and is zero otherwise, i.e., we only consider the case when the relay offers positive progress.

Further, we use progress-rate-density (PRD) in a multi-hop setting, which is defined as follows:

$$\mathrm{PRD} \triangleq \lambda p \cdot d(\lambda, p, N_t, N, \beta) \cdot N_t \log_2(1+\beta), \tag{5.6}$$

and is the product of the spatial transmit density λp, the expected forward progress d, and the per-hop rate $N_t \log_2(1+\beta)$. This can be related to the end-to-end rate when the final destination is a finite distance L meters away from the source as follows: from [87], at most $\lambda p \cdot d(\lambda, p, N_t, N, \beta) \cdot N_t/L$ packets can originate from each node per slot, and the end-to-end rate is at most $\lambda p \cdot d(\lambda, p, N_t, N, \beta) \cdot N_t \log_2(1+\beta)/L = \mathrm{PRD}/L$.

A large p results in higher density of transmitters (and high spatial reuse), but also a larger density of interferers, and there is a tradeoff between the two. We are interested in maximizing end-to-end performance by optimizing p, as follows:

$$p^\star = \arg\max_{0<p<1} \lambda p \cdot d(\lambda, p, N_t, N, \beta) \cdot N_t \log_2(1+\beta). \tag{5.7}$$

Note that this is an offline optimization, i.e., p is not varied dynamically from time slot to time slot. We generally find that it is far more important to maximize PRD over p rather than β, and consider only the optimization (5.7) in this work.

5.2 Single Stream Transmission

We first consider the case of $N_t = 1$, i.e., each transmitter necessarily transmits only a single stream of data. Prior work has established that spatial reuse can be increased

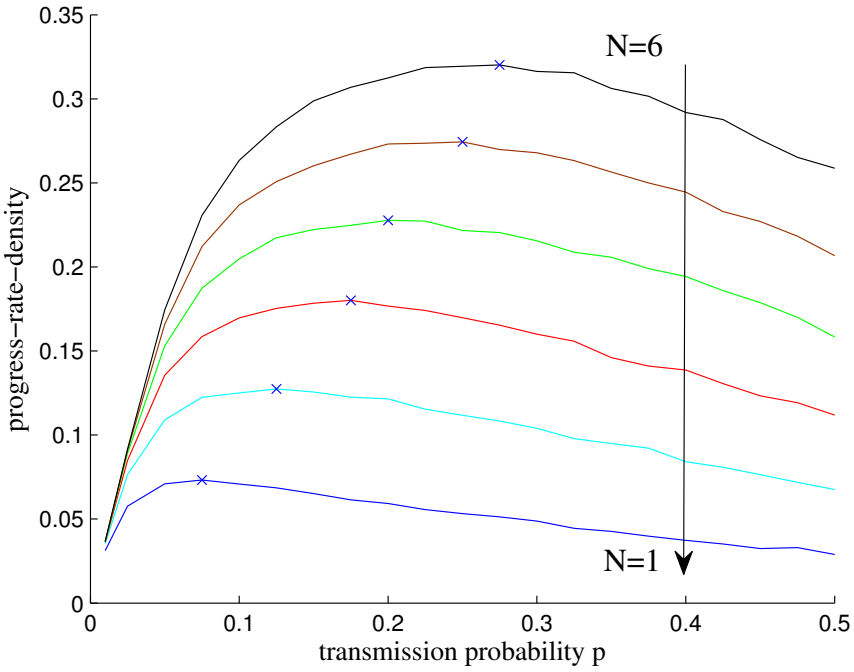

Figure 5.2: Single-stream PRD vs. transmission density

linearly with the number of receive antennas N in the single-hop transmission capacity model, and the goal here is to see if similar gains can be achieved in a multi-hop setting.

Figure 5.2 depicts the progress-rate-density vs. p, for various values of N, and the corresponding optimal p for each value of N is marked. We notice that when p is small, increasing p also increases PRD, as more spatial reuse makes up for the slight decrease in the expected forward progress; however when p is beyond a certain point (i.e., the optimal transmission probability p^*), increasing p reduces PRD as the sharp decrease of progress cannot be compensated by more simultaneous transmissions. Next, for optimal operating point, we make the following two important observations:

- The optimal transmission probability increases with N.
- The optimal PRD increases roughly linearly with N.

These turn out to be the key behavior patterns of single stream transmission, and the

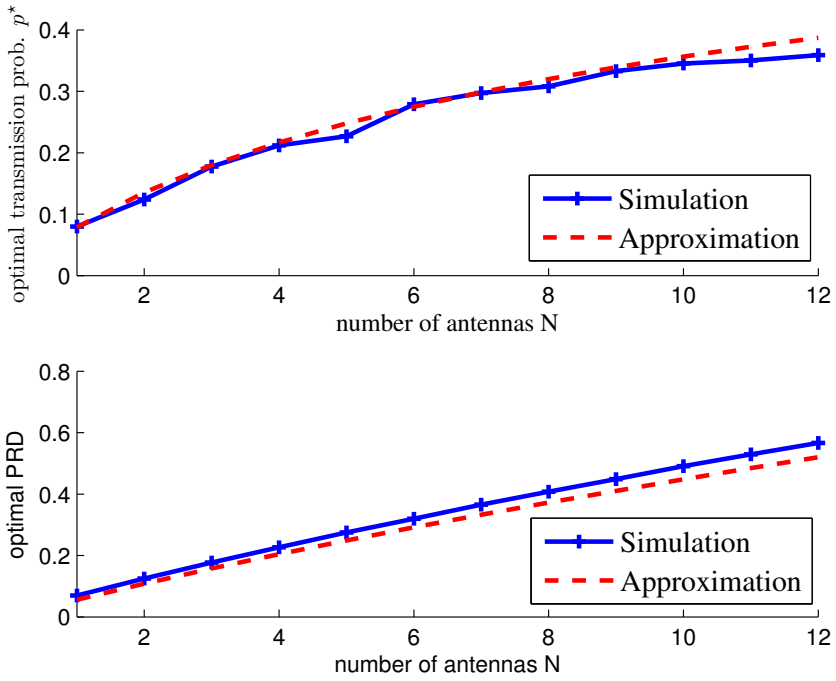

Figure 5.3: Optimal single-stream transmission density and the optimized PRD

remainder of this section is devoted to explaining these observations analytically.

To better understand single stream transmission in a multi-hop setting, we require an effective characterization of PRD. Unfortunately, to the best of authors' knowledge, no closed-form expression of PRD can be found. In [87], an analytical lower bound to PRD is presented, but that bound fails to accurately capture the behavior of the optimal transmission probability. However, more accurate results can be obtained by using the SIR-cell based approximation introduced in [88], the key idea of which is briefly explained as follows: to model the effect of interference, assume any receiver within a particular region (i.e., the SIR cell) around a transmitter can decode the packet successfully, and then select the receiver which provides the most progress in the region as the next forwarder.

To get a tractable approximation, a square region with the area equal to the mean of

the SIR cell is used (because fading causes the SIR cell[3] to vary across time slots). The area of the square, denoted by v_0, is computed by integrating the point-wise success probability over all space. According to [89], when the single stream transmission is implemented, the point-wise success probability for a MMSE receiver at distance $|X|$ from the transmitter is

$$p_s(|X|) = \Gamma(N, \pi|X|^2\lambda p\beta^{\frac{2}{\alpha}}/G(\alpha))/\Gamma(N), \tag{5.8}$$

where $\Gamma(\cdot)$ is the gamma function, $\Gamma(\cdot,\cdot)$ is the upper incomplete gamma function, and

$$G(\alpha) = \alpha\left(2\Gamma\left(2/\alpha\right)\Gamma\left(1-2/\alpha\right)\right)^{-1}. \tag{5.9}$$

Thus, by integrating (5.8) over $\mathbb{R}^2$, we get

$$v_0 = \int_{X\in\mathbb{R}^2} p_s(|X|)dX = \frac{N}{\lambda p}\cdot\frac{G(\alpha)}{\beta^{\frac{2}{\alpha}}}. \tag{5.10}$$

Notice as p increases, the SIR cell shrinks because there are more simultaneous transmissions, and thus more interference.

The approximated expected forward progress, denoted by $\tilde{d}$, is the expected maximum progress of the receivers within the SIR cell. Considering the receivers follow a PPP with intensity lambda $(1-p)$, and thus $\tilde{d}$ is [88]:

$$\tilde{d} = \frac{\sqrt{v_0}}{2}\left(\frac{e^{-c}-(1-c)}{c}\right), \tag{5.11}$$

where $c = \lambda(1-p)v_0/2$ is the average number of receivers in the half-square. The $(e^{-c}-(1-c))/c$ term decreases as p increases, and captures fact that the receiver density $\lambda(1-p)$ is decreasing in p. For large N or small p, this term is nearly unity and thus we can safely ignore it:

$$\tilde{d} \approx \hat{d} = \frac{\sqrt{v_0}}{2} \sim \mathrm{O}\left(\sqrt{N/p}\right). \tag{5.12}$$

Now we can further approximate PRD with $N_t = 1$ as $\log_2(1+\beta)\cdot\lambda p\cdot\hat{d}$. From (5.12), this implies:

$$\mathrm{PRD} \;\approx\; \log_2(1+\beta)\cdot\sqrt{Np}\cdot\sqrt{\lambda G(\alpha)/(4\beta^{\frac{2}{\alpha}})}. \tag{5.13}$$

[3] The SIR cell is well defined in the absence of fading with $N_t = 1$. In the presence of fading, although the SIR cell is not well defined, the mean cell area is still representative of the decoding area.

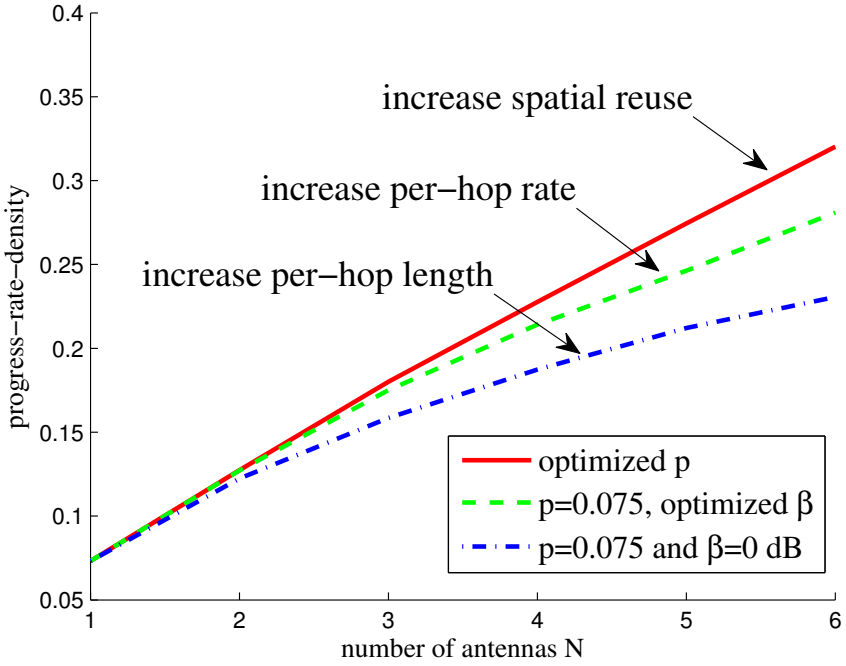

Figure 5.4: Single-stream PRD with (a) optimized p, (b) optimized β, (c) fixed p, β.

Therefore, if the transmission probability p is kept constant, PRD scales roughly on the order of $\sqrt{N}$, since the per-hop length increases roughly on the order of $\sqrt{N}$ (as seen in (5.12)).

On the other hand, as long as p increases linearly with N, PRD also increases roughly linearly with N. However, we cannot increase p without limit, as the PPP of receivers has an intensity of $\lambda(1-p)$ which decreases with p, and hence there will not be sufficient receivers for large p. Hence, we see that single stream multi-hop transmission exhibits limited linear scaling, i.e., linear scaling for moderate N.

In Figure 5.3, the optimal transmission probability $p^\star$ and the p-optimized PRD are plotted against the number of antennas N, for both Monte Carlo simulation and the v_0-approximation[4] . We see that the v_0-approximation is reasonably accurate in

[4] For the v_0 approximation, we use (5.11) to compute the approximated PRD, and then optimize it over p.

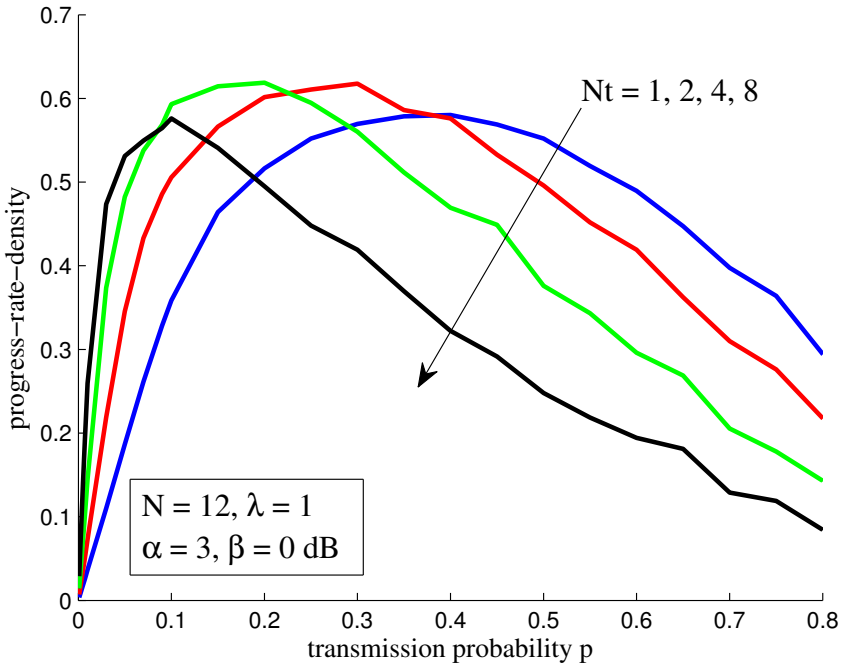

Figure 5.5: Multi-stream PRD vs. transmission density for various values of N_t

the sense of capturing the optimal operating point. The first subfigure shows that p^* increases roughly linearly with N for small N (here, $N < 4$), but loses linearity when N continues to grow. Further, the second subfigure shows that the optimized PRD is roughly linear with the number of antennas within the selected range of N.

In Figure 5.4, PRD is plotted against N for three different schemes: (a) increasing spatial reuse (optimizing p), (b) increasing per-hop rate (fixing p and optimizing β), and (c) increasing per-hop length (fixing both p and β, in which case the per-hop length increases with N). According to (5.13), both (b) and (c) result in PRD $\sim \mathbf{O}(\sqrt{N})$ only, and thus we should aggressively increase the spatial reuse (i.e., increase p) rather than the per-hop rate or length.

5.3 Multiple Stream Transmission

We now consider the case when $1 < N_t \leq N$, and each transmitter transmits N_t streams of data simultaneously. As we perform routing (and forwarder selection) on a per-stream basis, the multi-stream setting is quite similar to the single-stream setting with the exception of two differences in the interference structure:

1. Each interferer transmits N_t streams, and hence nearby interferers contribute greatly to the total interference.

2. There is self interference at each receiver from other streams from the same transmitter.

Both of these appear to discourage multiple stream transmission, however we will see that multiple stream transmission can still be preferable in a multi-hop setting.

As described before, the SIR values and the success probabilities for each stream at a particular receiver are all identically distributed. A closed from expression of $p_s(|X|)$ for multi stream transmission is derived in [90], but the expression is complicated and does not allow for tractable computation of PRD. We instead derive a lower bound on the expected distance and hence on PRD, which is summarized in Theorem 5.3.1.

Theorem 5.3.1 *The expected distance $d(\lambda, p, \eta N, N, \beta)$ with multiple stream transmission and separate acknowledgments per stream can be bounded from below by $\underline{d}$, given by:*

$$\frac{1}{2\pi\sqrt{\pi(1-p)\lambda\Gamma(i)}}\left[\Gamma\left(i+\frac{1}{2}\right)-\frac{\eta\beta\Gamma\left(i+\frac{\alpha+1}{2}\right)C_\alpha}{1-\eta(K+1)}\right]$$

and

$$C_\alpha \;=\; \left(\frac{p}{1-p}\right)^{-\frac{\alpha}{2}}\left(K-\left\lceil\frac{\alpha}{2}\right\rceil\right)^{1-\frac{\alpha}{2}}\left(\frac{\alpha}{2}-1\right)^{-1}. \tag{5.14}$$

Here, $K \geq \lceil \alpha/2 - 1 \rceil, i \geq 1,\ K, i \in \mathbb{Z}^+$, and $\eta \;=\; N_t/N \;<\; 1/(K+1)$.

The bound $\underline{d}$ is also a lower bound on the expected distance when the transmitter restricts itself to selecting only the i^{th} ($i \geq 1$) nearest receiver (in the right half-plane) as a relay.

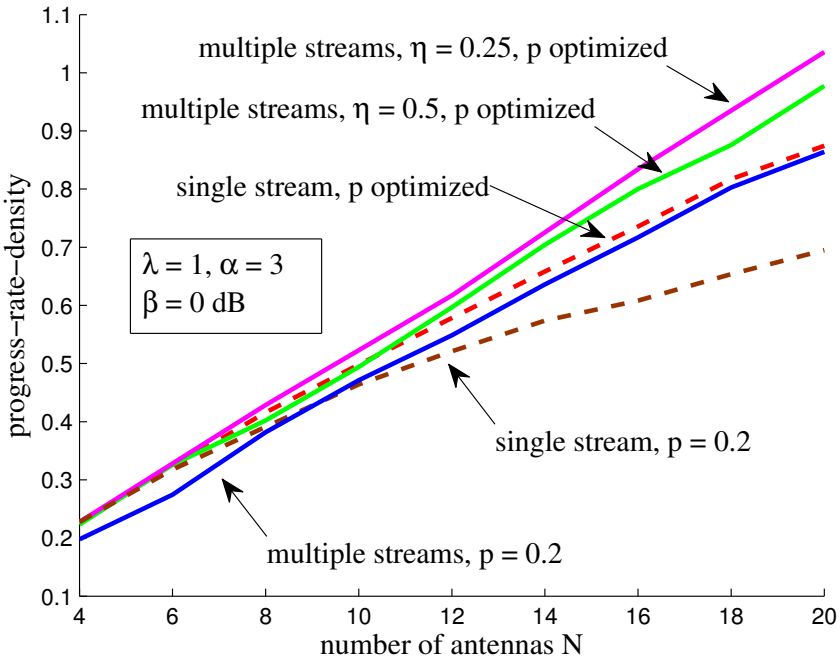

Figure 5.6: Multi-stream and single-steam PRD vs. N for various settings

Proof: See Section 5.5.2. □

Direct application of Theorem 5.3.1 allows us conclude that the PRD is bounded from below by $\lambda p \cdot \underline{d} \cdot \eta N \log_2(1+\beta)$. Thus, for any choice of $i \geq 1$, and β, p, K and λ held constant, taking $N \to \infty$ while keeping $\eta = N_t/N < 1/(K+1)$ fixed, the above PRD lower bound increases linearly with N. Note that $\underline{d}$ does not depend on N, and so the hop distance is $O(1)$ while the per-hop rate is $O(N)$ (using spatial multiplexing). Hence, the PRD with transmission of multiple streams increases linearly with the number of antennas, even when spatial reuse p is kept fixed, which is in contrast to the limited linear scaling of the single stream case. Note that setting $i = 1$ corresponds to nearest neighbor routing, and we find that the progress-rate-density still increases linearly with antennas in this setting.

Figure 5.5 depicts the progress-rate density vs. p for $N_t = 1$ (single stream transmission), as well as $N_t = 2, 4$ and 8 (multiple stream transmission), for $N = 12, \lambda = 1$,

$\alpha = 3$ and $\beta = 0$ dB. We see that multiple stream transmission can slightly out-perform single stream transmission. However, it is important to note that when $N_t = 1$, the optimal transmission probability p^* is usually much larger than when $N_t > 1$, which is consistent with the observation in Section 5.2. In other words, we expect a much lower transmission probability, and hence much lower spatial reuse when $N_t > 1$. The system compensates with a high degree of spatial multiplexing of N_t streams per transmitter. In fact, we have from Theorem 5.3.1, that p can be held constant, and still have the progress-rate-density increase linearly with N, which is in contrast to the single stream transmission case.

Figure 5.6 compares multiple and single stream transmission schemes, both when p is held constant and when p is optimized. When p is fixed, as described in Section 5.2, we see that the progress-rate-density with single stream transmission increases only sub-linearly with N, as opposed to multiple stream transmission. When p is optimized to maximize the progress-rate-density, there is large improvement in performance, even for $N_t > 1$, and we find that the performance with $N_t > 1$ can be greater than $N_t = 1$ for large N. For small or moderate values of N however, $N_t = 1$ can still be very competitive. Thus we see that for moderate N, the performance of single stream transmission with high spatial reuse is comparable to multiple stream transmission at low spatial reuse, and multiple stream transmission performs increasingly better as N increases.

5.4 Summary of Results for MIMO Ad Hoc Networks

In open-loop multi-hop MIMO ad hoc networks, we find that the progress-rate-density for single stream communication is maximized by increasing transmission probability (spatial reuse), and is generally competitive when compared to multiple stream communication, for moderate number of antennas. For large number of antennas, single stream communication has limited performance as the spatial reuse cannot be increased without limit. However, the progress-rate-density with multiple stream communication increases linearly, even for fixed reuse and nearest-neighbor routing, by increasing the number of data streams via spatial multiplexing.

5.5 Supplementary Materials and Proofs

5.5.1 Simulation of Multihop MIMO Ad Hoc Networks

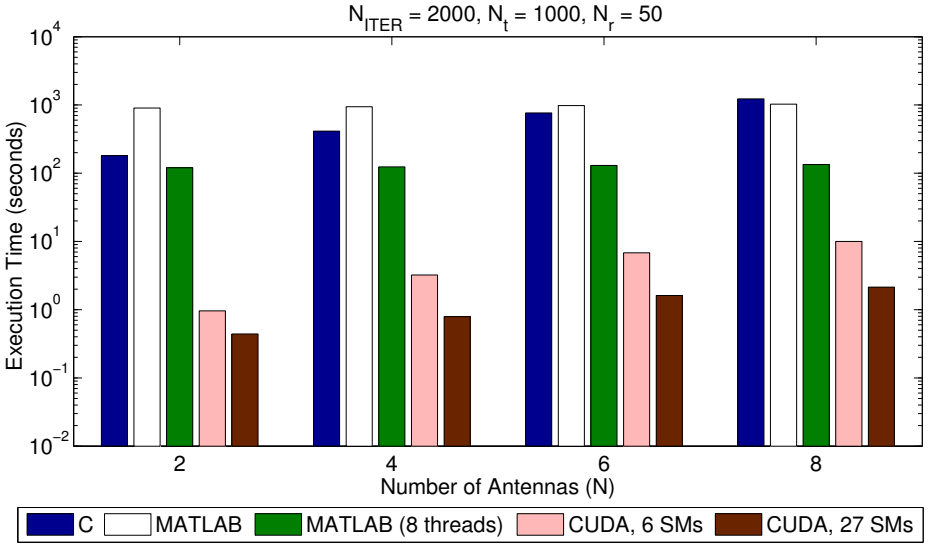

Figure 5.7: C, MATLAB and CUDA GPU simulations of MIMO ad hoc networks

Numerical simulations for investigating investigating large ad hoc networks with many antennas, especially to verify asymptotic results, can be computationally intensive and extremely slow. Although there are several multi-layer network simulators currently available for the CPU, the problems we are interested in investigating in this work require only PHY level simulations, which can yield efficient implementations. Since the numerical results largely depend on Monte-Carlo simulations, which involves computation for i.i.d. random draws from some random distribution over a large number of iterations, the simulator can be decoupled and parallelized readily, and can greatly benefit from taking advantage of low-cost Graphics Processing Unit (GPU) hardware, specifically nVidia's Compute Unified Device Architecture (CUDA)[91].

CUDA offers a unified framework to develop parallel executed programs, including plugins for MATLAB. Figure 5.7 compares the execution time with efficiently written C code, MATLAB code, MATLAB with the parallel computing toolbox using an 8-core

CPU, and 2 different GPUs, with 6 and 27 streaming multiprocessors (SM) respectively. N_{ITER} refers to the number of Monte-Carlo iterations, which is selected to be 2000 for purposes of comparison. Note that only about another order of magnitude in N_{ITER} is feasible for realistic execution times with MATLAB and C implementations, thus limiting the accuracy numerical results.

The choice of two GPUs, both with the CUDA 1.2 architecture, but with different number of multiprocessors, is made to depict the scalability of the GPU implementation. We find that there is potentially an improvement of 2-3 orders of magnitude with an efficient CUDA implementation, with some degree of scalability as well (that is, using more SMs results in a proportionally decreased execution time, showing that the implementation is not bottlenecked by memory). This results in the ability to evaluate ad network scenarios in a matter of few minutes to an hour, as opposed to several days with MATLAB or C, and achieve a reasonable degree of accuracy to verify and investigate analytical results.

We did observe that brute-force C code is marginally more efficient for small matrices when compared to MATLAB, while MATLAB is more efficient for larger matrices, but this is likely to be highly dependent on the particular implementation of matrix algorithms used. A CUDA implementation does require rewriting any simulation code which can be time consuming, but we find that modest reductions in simulation time is also possible using the MATLAB parallel computing toolbox, which requires minimal restructuring of Monte-Carlo implementations that are already in MATLAB or C.

The large reduction in execution time with GPUs is mainly due to two factors: the GPU's ability to perform many parallel computations simultaneously for decoupled problems such as Monte-Carlo simulations, and the ability to exploit psuedo-random number generating algorithms to avoid a memory bottleneck. We will elaborate on the second factor here, since it is an interesting aspect not typically relevant in most conventional parallel computation problems. Large ad hoc networks with many data streams/antennas essentially require a large number of random numbers to be generated and stored, which then requires frequent transactions between the local cache memory of the processing hardware (CPU or GPU), and the random access memory (RAM, or in the case of the GPU, video RAM). Methods to pipeline fetching of data and minimize the impact of memory access overhead times are well known, and we will not discuss these

further here. However, we find that while simulating large MIMO networks the number of memory transactions can equal or exceed the number of floating-point computations that need to be performed, effectively creating an *inevitable* memory bottleneck.

Since all random numbers in computer-based Monte-Carlo simulations are generated based on a deterministic psuedo-random number algorithm, such deterministic procedures can be executed locally at SMs or cores to acquire data when needed, transacting only a minimum amount with the RAM. Thus, the bulk of the data required is generated locally (that is, using the local cache), and i.i.d. properties of the random numbers can be maintained by initializing and sharing only the "seeds" required by the random number generator, resulting in significantly reduced memory overhead. This effectively trades in increased number of computations for reduced memory overhead, which is relevant in situations that are limited by the memory access speed (which is the case for many MIMO ad hoc network regimes we investigated in this work).

The scalability of such a scheme is not without limits. For example, the size of the local cache mamory will eventually decide the largest number of random variables that can be generated locally, which could limit the largest value of N or N_r possible with this technique. A more detailed discussion of Monte-Carlo simulations on GPUs is beyond the scope of this work.

5.5.2 Proof of Theorem 5.3.1

We derive a lower bound to PRD with the MMSE receiver using the partial zero-forcing (P-ZF) receiver, as described in [92], which lends itself more easily to analysis. Specifically, we consider a P-ZF receiver where the K nearest interferers are canceled out by the receiver. Further, the receiver also cancels out any self-interference caused by the other streams received from the same transmitter. Note that in practice however, the MMSE is a linear receiver and has less stringent channel information requirements than the P-ZF receiver (which requires the channels of the K nearest interferers), and will hence be preferable.

We also require that $N \geq N_t + KN_t$, so that each receiver, while receiving a particular stream from the transmitter, can cancel out N_t streams from K interferers, and $N_t - 1$

streams from the transmitter. Further, we have that:

$$\begin{aligned} d(\lambda, p, N_t, N, \beta) &\overset{(a)}{\geq} \mathbb{E}\left[\max_{i\geq 1} |X_i| \cos(\angle X_i) p_s(|X_i|)\right] \\ &\overset{(b)}{\geq} \max_{i\geq 1} \mathbb{E}[\cos(\angle X_i)] \mathbb{E}\left[|X_i| p_s(|X_i|)\right] \end{aligned}$$

for a receiver at position X_i, where (a) is obtained from [87], and (b) is obtained by moving the $\max(\cdot)$ operation outside the expectation, and then noting that the angle and magnitude of X_i are independently distributed. Note that for the homogeneous PPP, $\mathbb{E}[\cos(\angle X_i)]$ is distributed uniformly and independent of i. We will restrict ourselves to receivers in the left half-plane, and hence $\mathbb{E}[\cos(\angle X_i)] = 1/(2\pi)$ in this region.

To bound $\mathbb{E}\left[|X_i| p_s(|X_i|)\right]$, we derive a lower bound to $p_s(|X_i|)$ using the P-ZF receiver:

$$p_s(|X_i|) \geq 1 - \frac{|X_i|^\alpha \beta N_t (\pi\lambda p)^{\frac{\alpha}{2}} \left(K - \left\lceil \frac{\alpha}{2} \right\rceil\right)^{1-\frac{\alpha}{2}}}{\left(\frac{\alpha}{2} - 1\right)(N - N_t(K+1))}.$$

The bound is derived for $N_t = 1$ in [92]. The above is an extension of this to $N_t > 1$, and is proved using the same techniques. Note that this bound exists only when $K \geq \lceil \alpha/2 - 1 \rceil$ and $N_t \leq N_r/(K+1)$. These provide the restrictions on the number of streams and antennas.

Substituting the above bound in $\mathbb{E}\left[|X_i| p_s(|X_i|)\right]$ and computing its expectation with respect to $|X_i|$, we obtain a lower bound to $d(\lambda, p, N_t, N, \beta)$. Using

$$\text{PRD} = N_t \lambda p \log_2(1 + \beta) d(\lambda, p, N_t, N, \beta), \tag{5.15}$$

we obtain the desired result.

Chapter 6

Extensions and Future Work

We would like to note that some practically relevant extensions of the results in Chapter 2 have been presented. In particular, the rate gap analysis is extended to the case of MIMO Orthogonal Frequency Division Multiplexing (OFDM) with frequency-correlated fading in [46], the optimal allocation of training and feedback resources is considered in [36, 37, 38], explicit coding schemes for the CSIT digital feedback MIMO-MAC channel are presented in [47], and comparisons between single-user and multi-user MIMO (based on the bounds developed here and related approximations) are performed in [93].

Practical wireless systems will undergo fading that can be correlated spatially, temporally, and may also have a line-of-sight component. We have considered i.i.d. Rayleigh and line-of-sight channels in our work, but the particularities of various fading models can be exploited to reduce feedback loads. Practical techniques that exploit the structure of the fading model are of interest, both in cellular systems as well as ad hoc systems.

In terms of channel correlation across time and frequency, we note that [94] studies a tradeoff closely related to the one we considered in Chapter 3, in the context of a frequency-selective channel: should each user quantize its entire frequency response or only a small portion of the frequency response (i.e., quantize only a single resource block)? The first option corresponds to coarse CSI (even though frequency-domain correlation is exploited) but a large user population, while the second corresponds to accurate CSI but fewer users per resource block. Consistent with our results, the second option is seen to provide a considerably larger sum rate than the first. We suspect the

same holds true in the context of temporal correlation, where the comparison is between a user quantizing its channel across many continuous blocks (possibly exploiting the correlation of the channel by using a differential quantization scheme) and a user finely quantizing its current channel at only a few limited time instants.

The Block Diagonalization scheme we considered in Chapter 4 is just one of many linear precoding techniques that can be used on the MIMO broadcast channel with multiple user antennas (for e.g., see coordinated beamforming [95] and Multiuser Eigenmode Transmission [96]). It remains to be seen which of these perform best in a limited feedback setting and also when multiuser diversity/user selection is considered.

Finally, we note that the advantages of multiple antennas in MIMO ad hoc networks (which we investigated in Chapter 5) as well as cellular downlink systems will require acquisition of CSI at the transmitter and/or receiver nodes. This is a daunting task for both an ad hoc network with uncoordinated transmissions, as well as a cellular system, when there are a large number of antennas. Hence, it is of interest to analyze practical methods of CSI acquisition in MIMO ad hoc networks, quantify the effect on performance, and hence establish practical limits on how well multiple antennas can be exploited.

References

[1] M.Costa. Writing on dirty paper. *IEEE Trans. on Inform. Theory*, 29:439–441, May 1983.

[2] G. Caire and S. Shamai. On the achievable throughput of a multiantenna Gaussian broadcast channel. *IEEE Trans. on Inform. Theory*, 49(7):1691–1706, 2003.

[3] S. Vishwanath, N. Jindal, and A. Goldsmith. Duality, achievable rates, and sum-rate capacity of Gaussian MIMO broadcast channels. *IEEE Trans. on Inform. Theory*, 49(10):2658–2668, 2003.

[4] P. Viswanath and D.N.C. Tse. Sum capacity of the vector Gaussian broadcast channel and uplink-downlink duality. *IEEE Trans. on Inform. Theory*, 49(8):1912–1921, 2003.

[5] W. Yu and J.M. Cioffi. Sum capacity of Gaussian vector broadcast channels. *IEEE Trans. on Inform. Theory*, 50(9):1875–1892, 2004.

[6] H. Weingarten, Y. Steinberg, and S. Shamai. The capacity region of the Gaussian multiple-input multiple-output broadcast channel. *IEEE Trans. on Inform. Theory*, 52(9):3936 – 3964, September 2006.

[7] N. Jindal and A. Goldsmith. Dirty paper coding vs. TDMA for MIMO broadcast channels. *IEEE Trans. Inform. Theory*, 51(5):1783–1794, May 2005.

[8] D. Gesbert, M. Kountouris, Jr. R. W. Heath, C. B. Chae, and T. Salzer. From single user to multiuser communications: shifting the MIMO paradigm. *IEEE Sig. Proc. Magazine*, 2007.

[9] T. Yoo and A. Goldsmith. On the optimality of multiantenna broadcast scheduling using zero-forcing beamforming. *IEEE J. on Select. Areas in Commun.*, 24(3):528–541, 2006.

[10] G. Dimic and ND Sidiropoulos. On downlink beamforming with greedy user selection: performance analysis and a simple new algorithm. *IEEE Trans. on Sig. Proc.*, 53(10):3857–3868, 2005.

[11] G. Caire, N. Jindal, M. Kobayashi, and N. Ravindran. Quantized vs. analog feedback for the mimo broadcast channel: A comparison between zero-forcing based achievable rates. In *Proc. IEEE Int. Symp. on Inform. Theory*, pages 2046–2050. IEEE, 2007.

[12] G. Caire, N. Jindal, M. Kobayashi, and N. Ravindran. Achievable throughput of mimo downlink beamforming with limited channel information. In *Proc. IEEE Personal, Indoor and Mobile Radio Commun. Symp.*, pages 1–5. IEEE, 2007.

[13] G. Caire, N. Jindal, M. Kobayashi, and N. Ravindran. Multiuser mimo achievable rates with downlink training and channel state feedback. *IEEE Trans. on Inform. Theory*, 56(6):2845–2866, 2010.

[14] N. Jindal. MIMO Broadcast Channels with Finite Rate Feedback. *IEEE J. Select. Areas Commun.*, 2006, cs.IT/0603065.

[15] P. Ding, D. Love, and M. Zoltowski. Multiple antenna broadcast channels with partial and limited feedback. *IEEE Trans. on Sig. Proc.*, 55(7):3417–3428, 2007.

[16] K. Huang, R.W. Heath, and J.G. Andrews. Space division multiple access with a sum feedback rate constraint. *IEEE Trans. on Sig. Proc.*, 55(7 Part 2):3879–3891, 2007, cs.IT/0609030.

[17] M. Sharif and B. Hassibi. On the capacity of MIMO broadcast channels with partial side information. *IEEE Trans. on Inform. Theory*, 51(2):506–522, 2005.

[18] M. Kountouris, D. Gesbert, and T. Salzer. Enhanced multiuser random beamforming: dealing with the not so large number of users case. *IEEE J. on Select. Areas in Commun.*, 26(8):1536–1545, 2008.

[19] A. Narula, M. J. Lopez, M. D. Trott, G. W. Wornell, M. Inc, and M. A. Mansfield. Efficient use of side information in multiple-antenna data transmission over fading channels. *IEEE J. Select. Areas Commun.*, 16(8):1423–1436, 1998.

[20] DJ Love, RW Heath Jr, and T. Strohmer. Grassmannian beamforming for multiple-input multiple-output wireless systems. *IEEE Trans. on Inform. Theory*, 49(10):2735–2747, 2003.

[21] KK Mukkavilli, A. Sabharwal, E. Erkip, and B. Aazhang. On beamforming with finite rate feedback in multiple-antenna systems. *IEEE Trans. on Inform. Theory*, 49(10):2562–2579, 2003.

[22] S. Srinivasa and Syed A. Jafar. The optimality of transmit beamforming: a unified view. *IEEE Trans. on Inform. Theory*, 53(4):1558–1564, April 2007.

[23] S.A. Jafar and S. Srinivasa. On the optimality of beamforming with quantized feedback. *Communications, IEEE Transactions on*, 55(12):2288–2302, 2007.

[24] C. K. Au-Yeung and D. J. Love. On the performance of random vector quantization limited feedback beamforming in a MISO system. *IEEE Trans. Wireless Comm.*, 6:458 – 462, February 2007.

[25] A. D. Dabbagh and D. J. Love. Feedback rate-capacity loss tradeoff for limited feedback MIMO systems. *IEEE Trans. on Inform. Theory*, 52(5):2190–2202, May 2006.

[26] T.L. Marzetta. How much training is required for multiuser MIMO? *Signals, Systems and Computers, Fortieth Asilomar Conf. on*, pages 359–363, 2006.

[27] TL Marzetta and BM Hochwald. Fast transfer of channel state information in wireless systems. *IEEE Tran. on Signal Proc.*, 54(4):1268–1278, 2006.

[28] A.F. Dana, M. Sharif, and B. Hassibi. On the capacity region of multi-antenna Gaussian broadcast channels with estimation error. In *IEEE Int. Symp. on Inform. Theory*, July 2006.

[29] M. Kobayashi and G. Caire. Joint beamforming and scheduling for a multi-antenna downlink with imperfect transmitter channel knowledge. *IEEE J. Select. Areas Commun.*, 25(7), 2007.

[30] M. Médard. Channel capacity in wireless wommunications of perfect and imperfect knowledge of the channel. *IEEE Trans. on Inform. Theory*, 46(3):933–946, May 2000.

[31] A. Lapidoth and S. Shamai. Fading channels: how perfect need "perfect" side information" be? *IEEE Trans. on Inform. Theory*, 48(5):1118–1134, 2002.

[32] B. Hassibi and B. Hochwald. How much training is needed in multiple-antenna wireless links? *IEEE Trans. on Inform. Theory*, 49(4):951–963, 2003.

[33] A. Lapidoth, S. Shamai, and M.A. Wigger. On the capacity of fading MIMO broadcast channels with imperfect transmitter side-information. In *Proc. 43rd Ann. Allerton Conf. on Commun., Control, and Computing*, 2005, cs.IT/0605079.

[34] G. Caire, N. Jindal, and S. Shamai. On the Required Accuracy of Transmitter Channel State Information in Multiple Antenna Broadcast Channels. In *Conf. Rec. 41st Asilomar Conf. on Sig., Sys., and Computers*, pages 287–291, 2007.

[35] E. Biglieri, J. Proakis, S. Shamai, and D. di Elettronica. Fading channels: information-theoretic and communications aspects. *IEEE Trans. on Inform. Theory*, 44(6):2619–2692, 1998.

[36] M. Kobayashi, G. Caire, and N. Jindal. How much training and feedback are needed in mimo broadcast channels? In *Proc. IEEE Int. Symp. on Inform. Theory*, pages 2663–2667. IEEE, 2008, cs.IT/0905.3689.

[37] M. Kobayashi, G. Caire, and N. Jindal. Optimized training and feedback for MIMO dwnlink channels. In *Proc. IEEE Inform. Theory Workshop*, 2008.

[38] M. Kobayashi, N. Jindal, and G. Caire. Training and feedback optimization for multiuser mimo downlink. *IEEE Trans. on Commun.*, 59(8):2228–2240, 2011.

[39] A.Bayesteh and A.K.Khandani. An efficient method for user selection in MIMO broadcast channels. *Proc. Conf. on Inform. Sciences, and Sys.*, March 2005.

[40] M.S. Alouini and AJ Goldsmith. Capacity of Rayleigh fading channels under different adaptive transmission and diversity-combining techniques. *IEEE Trans. on Vehic. Tech.*, 48(4):1165–1181, 1999.

[41] M. Abramowitz and I. A. Stegun. *Handbook of Mathematical Functions with Formulas, Graphs, and Mathematical Tables*. Dover, New York, 1964.

[42] H.V. Poor. *An introduction to signal detection and estimation*. Springer-Verlag New York, Inc. New York, NY, USA, 1994.

[43] T.A. Thomas, K.L. Baum, and P. Sartori. Obtaining channel knowledge for closed-loop multi-stream broadband MIMO-OFDM communications using direct channel feedback. In *Proc. IEEE Glob. Telecom. Conf.*, volume 6, November 2005.

[44] D.Samardzija and N.Mandayam. Unquantized and uncoded channel state information feedback on wireless channels. *Proc. of IEEE WCNC*, March 2005.

[45] N. Jindal. Antenna combining for the MIMO downlink channel. *IEEE Trans. Wireless Comm.*, 7(10):3834–3844, 2008, cs.IT/0704.1308.

[46] H. Shirani-Mehr and G. Caire. Channel state feedback schemes for multiuser mimo-ofdm downlink. *IEEE Trans. on Commun.*, 57(9):2713–2723, 2009.

[47] K. Raj Kumar and G. Caire. Channel state feedback over the MIMO-MAC. In *IEEE Int. Symp. on Inform. Theory, ISIT09*, Seoul (Korea), June 2009.

[48] A. Goldsmith. *Wireless Communications*. Cambridge University Press, 2005.

[49] M.Gastpar, B.Rimoldi, and M.Vetterli. To code, or not to code : Lossy source-channel communication revisited. *IEEE Trans. on Inform. Theory*, 49, May 2003.

[50] T. Yoo, N. Jindal, and A. Goldsmith. Multi-antenna downlink channels with limited feedback and user selection. *IEEE J. Select. Areas Commun.*, 25:1478–1491, 2007.

[51] N. Ravindran, N. Jindal, and H.C. Huang. Beamforming with finite rate feedback for los mimo downlink channels. In *Proc. IEEE Glob. Telecom. Conf.*, pages 4200–4204. IEEE, 2007.

[52] I. S. Gradshteyn and I. M. Ryzhik. *Table of Integrals, Series, and Products*. Academic, fifth edition, 1994.

[53] C. B. Peel, B. M. Hochwald, and A. L. Swindlehurst. A vector-perturbation technique for near-capacity multiantenna multiuser communication Part I: Channel inversion and regularization. *IEEE Trans. on Commun.*, 53:195–202, 2005.

[54] S.P. Boyd and L. Vandenberghe. *Convex Optimization*. Cambridge University Press, 2004.

[55] N. Ravindran and N. Jindal. Multi-user diversity vs. accurate channel feedback for mimo broadcast channels. In *Proc. IEEE Int. Conf. on Commun.*, pages 3684–3688. IEEE, 2008.

[56] N. Ravindran and N. Jindal. Multi-user diversity vs. accurate channel feedback for MIMO broadcast channels. *To appear: IEEE Trans. Wireless Comm.*, 2012, cs.IT/0710.1336.

[57] MATLAB code comparing multiuser diversity and accurate CSI for a fixed feedback budget. `http://www.ece.umn.edu/users/nihar/mud_csi_code.html`.

[58] J.S. Kim, H. Kim, C.S. Park, and K.B. Lee. On the performance of multiuser MIMO systems in WCDMA/HSDPA: Beamforming, feedback and user diversity. *IEICE Trans. on Commun.*, 89(8):2161–2169, 2006.

[59] K. Huang, J.G. Andrews, and R.W. Heath. Performance of Orthogonal Beamforming for SDMA with Limited Feedback. *IEEE Trans. on Vehic. Tech.*, 58(1):152–164, 2009, cs.IT/0606121.

[60] R. Zakhour and D. Gesbert. A two-stage approach to feedback design in MU-MIMO channels with limited channel state information. In *Proc. IEEE Personal, Indoor and Mobile Radio Commun. Symp.*, pages 111–115, 2008.

[61] C. Swannack, G.W. Wornell, and E. Uysal-Biyikoglu. MIMO Broadcast Scheduling with Quantized Channel State Information. In *Proc. IEEE Int. Symp. on Inform. Theory*, pages 1788–1792, 2006.

[62] R. Agarwal, C.S. Hwang, and J. Cioffi. Scalable feedback protocol for achieving sum-capacity of the MIMO BC with finite feedback. *Stanford Technical Report*, 2006.

[63] A. Bayesteh and A.K. Khandani. On the User Selection for MIMO Broadcast Channels. *IEEE Trans. on Inform. Theory*, 54(3):1086–1107, 2008.

[64] D. Gesbert and M.S. Alouini. How much feedback is multi-user diversity really worth? In *Proc. IEEE Int. Conf. on Commun.*, volume 1, 2004.

[65] N. Jindal. MIMO broadcast channels with finite rate feedback. *IEEE Trans. on Inform. Theory*, 52(11):5045–5059, November 2006.

[66] P. Viswanath, DNC Tse, and R. Laroia. Opportunistic beamforming using dumb antennas. *IEEE Trans. on Inform. Theory*, 48(6):1277–1294, 2002.

[67] T. Yoo, N. Jindal, and A. Goldsmith. Multi-antenna downlink channels with limited feedback and user selection. *IEEE J. on Select. Areas in Commun.*, 25(7):1478–1491, 2007.

[68] R.M. Corless, G.H. Gonnet, D.E.G. Hare, D.J. Jeffrey, and D.E. Knuth. On the LambertW function. *Adv. in Comput. Math.*, 5(1):329–359, 1996.

[69] I.H. Kim, S.Y. Park, D.J. Love, and S.J. Kim. Improved multiuser MIMO unitary precoding using partial channel state information and insights from the Riemannian manifold. *IEEE Trans. on Wireless Commun.*, 8(8):4014–4023, 2009.

[70] H.A. David and HN Nagaraja. *Order statistics*. Wiley-Interscience, 2004.

[71] S. Zhou, Z. Wang, and G.B. Giannakis. Performance Analysis for Transmit-Beamforming with Finite-Rate Feedback. In *Proc. Conf. on Inform. Sciences, and Sys.*, 2004.

[72] N. Ravindran and N. Jindal. Mimo broadcast channels with block diagonalization and finite rate feedback. In *Proc. IEEE Conf. on Acoustics, Speech and Signal Proc.*, volume 3, pages III–13. IEEE, 2007.

[73] N. Ravindran and N. Jindal. Limited feedback-based block diagonalization for the mimo broadcast channel. *Selected Areas in Communications, IEEE Journal on*, 26(8):1473–1482, 2008.

[74] L. U. Choi and R. D. Murch. A transmit preprocessing technique for multiuser MIMO systems using a decomposition approach. *IEEE Trans. on Wireless Commun.*, 3(1):20–24, 2004.

[75] Q. H. Spencer, A. L. Swindlehurst, and M. Haardt. Zero-forcing methods for downlink spatial multiplexing in multiuser MIMO channels. *IEEE Trans. on Signal Proc.*, 52(2):461–471, 2004.

[76] J. H. Conway, R. H. Hardin, and N. J. A. Sloane. Packing lines, planes, etc.: Packings in Grassmannian space. *Exper. Math.*, 5:139–159, 1996.

[77] W. Santipach and ML Honig. Asymptotic capacity of beamforming with limited feedback. *Proc. of International Symp. on Inform. Theory*, 2004.

[78] W. Dai, Y. Liu, and B. Rider. Quantization bounds on grassmann manifolds and applications in MIMO systems. *IEEE Tran. on Inform. Theory*, 2008, cs.IT/0603039.

[79] B. Hochwald and T. Marzetta. Capacity of mobile multiple-antenna communicaiton link in Ralyeigh flat fading. *IEEE Trans. Inform. Theory*, 45(1):139–157, January 1999.

[80] J. Lee and N. Jindal. High SNR analysis for MIMO broadcast channels: Dirty paper coding vs. linear precoding. *IEEE Tran. on Inform. Theory*, 2007.

[81] R.J. Muirhead. *Aspects of multivariate statistical theory*. Wiley New York, 1982.

[82] A.K. Gupta and DK Nagar. *Matrix variate distributions*. Chapman & Hall/CRC, 2000.

[83] A. Edelman and N.R. Rao. Random matrix theory. *Acta Numerica*, 14:233–297, 2005.

[84] S. Govindasamy, D.W. Bliss, and D.H. Staelin. Spectral efficiency in single-hop ad-hoc wireless networks with interference using adaptive antenna arrays. *Selected Areas in Communications, IEEE Journal on*, 25(7):1358–1369, 2007.

[85] N. Jindal, J.G. Andrews, and S. Weber. Multi-antenna communication in ad hoc networks: Achieving mimo gains with simo transmission. *IEEE Trans. on Commun.*, 59(2):529–540, 2011.

[86] R. Vaze and RW Heath. Transmission capacity of ad-hoc networks with multiple antennas using transmit stream adaptation and interference cancelation. In *Conf. Record of the Forty-Third Asilomar Conf. on Sig., Sys. and Compu.*, pages 1709–1713, 2009.

[87] F. Baccelli, B. Blaszczyszyn, and P. Muhlethaler. An Aloha protocol for multihop mobile wireless networks. *IEEE Trans. Inform. Th.*, 52(2):421–436, 2006.

[88] J. Blomer and N. Jindal. Opportunistic routing in ad hoc networks: How many relays should there be? what rate should nodes use? In *Proc. IEEE Glob. Telecom. Conf.*, pages 1–5. IEEE, 2010.

[89] O. B. S. Ali, C. Cardinal, and F. Gagnon. Performance of optimum combining in a Poisson field of interferers and Rayleigh fading channels. *IEEE Trans. Wireless Commun.*, 9(8):2461–2467, 2010.

[90] R.H.Y. Louie, M.R. McKay, and I.B. Collings. Open-loop spatial multiplexing and diversity communications in ad hoc networks. *Information Theory, IEEE Transactions on*, 57(1):317–344, 2011.

[91] Compute unified device architecture programming guide. `http://goo.gl/nga9S`.

[92] R. H. Y. Louie, R. M. McKay, N. Jindal, and I. B. Collings. Spatial multiplexing with MMSE receivers: Single-stream optimality in ad hoc networks. *arXiv1003.3056*, 2010.

[93] J. Zhang, R.W. Heath, M. Kountouris, and J.G. Andrews. Mode switching for the multi-antenna broadcast channel based on delay and channel quantization. *EURASIP J. on Adv. in Sig. Proc.*, 2009:1–15, 2009.

[94] M. Trivellato, S. Tomasin, and N. Benvenuto. On channel quantization and feedback strategies for multiuser mimo-ofdm downlink systems. *IEEE Trans. Commun.*, 57(9):2645–2654, 2009.

[95] C.B. Chae, D. Mazzarese, and R.W. Heath. Coordinated Beamforming for Multiuser MIMO Systems with Limited Feedforward. *Proc. Asilomar Conf. on Signals, Systems and Computers*, pages 1511–1515, 2006.

[96] F. Boccardi and H. Huang. A Near-Optimum Technique using Linear Precoding for the MIMO Broadcast Channel. 3, 2007.